Spring 2001

Evaluation of 135- and 150-degree sliding hip screws

Kelly Blayne Crittenden

INFORMATION TO USERS

This manuscript has been reproduced from the microfilm master. UMI films the text directly from the original or copy submitted. Thus, some thesis and dissertation copies are in typewriter face, while others may be from any type of computer printer.

The quality of this reproduction is dependent upon the quality of the copy submitted. Broken or indistinct print, colored or poor quality illustrations and photographs, print bleedthrough, substandard margins, and improper alignment can adversely affect reproduction.

In the unlikely event that the author did not send UMI a complete manuscript and there are missing pages, these will be noted. Also, if unauthorized copyright material had to be removed, a note will indicate the deletion.

Oversize materials (e.g., maps, drawings, charts) are reproduced by sectioning the original, beginning at the upper left-hand corner and continuing from left to right in equal sections with small overlaps. Each original is also photographed in one exposure and is included in reduced form at the back of the book.

Photographs included in the original manuscript have been reproduced xerographically in this copy. Higher quality 6" x 9" black and white photographic prints are available for any photographs or illustrations appearing in this copy for an additional charge. Contact UMI directly to order.

UMI®

Bell & Howell Information and Learning
300 North Zeeb Road, Ann Arbor, MI 48106-1346 USA
800-521-0600

NOTE TO USERS

This reproduction is the best copy available.

UMI

EVALUATION OF 135- AND 150-DEGREE SLIDING HIP SCREWS

by

Kelly Crittenden, B.S.

A Dissertation Presented in Partial Fulfillment
of the Requirements for the Degree
Doctor of Philosophy

COLLEGE OF ENGINEERING AND SCIENCE
LOUISIANA TECH UNIVERSITY

May 2001

LOUISIANA TECH UNIVERSITY

THE GRADUATE SCHOOL

May 18, 2001
Date

We hereby recommend that the dissertation prepared under our supervision by Kelly Crittenden entitled Evaluation of 135- and 150-Degree Sliding Hip Screws be accepted in partial fulfillment of the requirements for the Degree of Doctor of Philosophy

Supervisor of Dissertation Research

Head of Department

Biomedical Engineering
Department

Recommendation concurred in:

Advisory Committee

Approved:

Director of Graduate Studies

Approved:

Director of the Graduate School

Dean of the College

GS Form 13
2/97

ABSTRACT

Sliding hip screws are routinely used to repair Garden III femoral neck fractures. This research seeks to better understand the influence of the hip screw angle on the performance of the fixation. The mechanics of fractured femurs repaired with 135- and 150-degree sliding fixation devices are explored using experimental, finite element, and analytical modeling. The experimental study involves testing of both intact and fixated femurs; the finite element work centers on two-dimensional models of intact and fixated femurs; and the analytical modeling explores the forces, moments and stresses in the fixation. The analytical model predicts that the screw will serve as a hinge point leading to compressive contact forces across the fracture faces below the screw. The peak stresses I the screw are seen to be a function of the installation position of the screw on the fracture plane. Screw are seen to have lower stresses when they are installed low on the fracture plane, especially in the case of the 150-degree screw. The experimental and finite element results both predict that the 150-degree fixation will be stiffer than the 135-dgree fixation. The finite element calculations are verified by comparison with the experimental results.

APPROVAL FOR SCHOLARLY DISSEMINATION

The author grants to the Prescott Memorial Library of Louisiana Tech University the right to reproduce, by appropriate methods, upon request, any or all portions of this Dissertation. It is understood that "proper request" consists of the agreement, on the part of the requesting party, that said reproduction is for his personal use and that subsequent reproduction will not occur without written approval of the author of this Dissertation. Further, any portions of the Dissertation used in books, papers, and other works must be appropriately referenced to this Dissertation.

Finally, the author of this Dissertation reserves the right to publish freely, in the literature, at any time, any or all portions of this Dissertation.

Author Kelly Cutler

Date 5/18/01

GS Form 14
2/97

DEDICATION

In memory of my father, David Crittenden.

TABLE OF CONTENTS

LIST OF TABLES

LIST OF FIGURES

ACKNOWLEDGEMENTS

The author wishes to thank the members of his advisory committee, Dr. David Hall, Dr. Debi Mukherjee, Dr. Stan Napper, Dr. Raja Nassar, and Dr. Roy Schubert. Without the guidance from these men, this dissertation would not have been possible. In addition, the author thanks Ray Mayeux and Al Ogden for their assistance throughout the study, especially during the experimental testing phase. Additional thanks goes to BioMet for the use of two of their variable angle hip screws during the experimental testing. The author's thanks goes to Robert Lauve, the BioMet representative, and Solomon H. Chaim, MD for their assistance in the installation of the fixation devices for the experimental tests.

Above all others, the author thanks his Lord and Savior, Jesus Christ, Who never left his side during any of the trials and tribulations he has faced over the years.

CHAPTER 1

INTRODUCTION

Hip fracture refers to the fracture of the proximal femur anywhere from the femoral head down to the first five centimeters of the subtrochanteric area (Winkley, 1998). The focus of this research is on modeling two particular methods of fixation of hip fractures involving the femoral neck. The two fixation methods under investigation in this study are fixation by the use of a 135-degree sliding hip screw and fixation by a 150-degree sliding hip screw.

Hip fractures most often occur in elderly people, with almost half of all hip fractures occur after the age of 80. In addition, nearly 75 percent of all hip fractures occur in women. One in six women aged 80 years or more will suffer a hip fracture (World Health Organization Study Group, 1994.) The chance of hip fracture doubles with every decade after 50 years of age (Zuckerman, 1996). There are several reasons that hip fractures are more common in the elderly. As a person ages, the bone mineral density tends to decrease leaving a softer, more easily broken bone. In addition, the bone mineral density may have been lowered through a disease state such as osteoporosis.

Most hip fractures occur as a result of trauma, such as a fall or automobile accident. Stress fractures, without trauma, are uncommon and usually occur in

osteoporotic elderly or in extremely active individuals such as endurance athletes or military recruits (Egol et al., 1998).

According to the UK National Osteoporosis Society, patients with femoral neck fractures occupy 20% of all orthopedic beds at any given time (UK National Osteoporosis Society, 1994.) In the United States of America, there are approximately 250,000 cases of hip fracture each year. It is predicted that by the year 2040 the USA's annual cost of hip fracture related medical care will be $16 billion. In that same year there are predicted to be 512,000 cases of hip fracture in the United States alone (Cummings et. al., 1990).

The sliding hip screw is a popular device for fixation of fractures of the femoral neck. This device consists of a single large screw and a sideplate that holds the screw at a predetermined angle. The screw is installed into a predrilled pilot hole in the femur. Then the sideplate is attached to the shaft of the femur with up to four bone screws. The barrel of the sideplate and the screw are usually grooved in a manner that prevents rotation of the screw within the barrel of the sideplate. However, the screw is allowed to slide along its axis in the barrel of the sideplate. The sliding action of this type of fixation is thought to increase stability by allowing the fracture to be further reduced by impaction of the fragment onto the femur.

It is theorized that a 150-degree screw and sideplate will provide a better fixation than a 135-degree setup. The resultant force applied to the femoral head has previously been determined to be at approximately a 20-degree angle from the vertical axis of the femoral shaft. Therefore, the axis of a 150-degree screw will be more inline with the applied resultant force than a screw at a 135-degree angle. By aligning the axis of the screw closer to the line of action of the applied load, better conditions for sliding of the

screw in the barrel of the sideplate will exist. As a result of improved sliding, more of the stress will be carried by the fractured bone, which is thought to increase the fracture healing rate and therefore the healing rate (Carter et. al., 1998; Claes et. al., 1998.)

The downside to using a 150-degree screw is the difficulty in installing them. Without clear evidence that 150-degree screws are superior in femoral neck fracture fixation, the easier-to-install 135-degree screws will continue to be more popular. This study seeks to better understand the complex interactions between bone, load, and screw by analytically studying the mechanics of the fixation systems and by building finite element models of these two screw arrangements. With this new information, a more informed decision can be made on which screw angle would be a better choice in femoral neck fracture fixation.

There have been many studies involving hip implants and femoral fixation devices. However, there are few, if any, finite element studies of sliding hip screws at this time. Therefore, a more detailed analysis of the stresses and deflections under typical loading conditions for this type of fixation is necessary in order to have a better understanding of the advantages and disadvantages of screw angle in sliding hip screw fixation.

This research seeks to characterize the performance of 135- and 150-degree sliding hip screws through analytical study and finite element modeling. The analytical methods used in the study were chosen for their ability to describe the major stresses in the fixation. The finite element method was chosen because it is capable of representing the highly irregular geometry of the femur, the properties of the cortical and cancellous bone, and the complex bone-to-bone, metal-to-bone, and metal-to-metal surface contact conditions that evolve as a repaired femur is loaded. No closed form analytical or

experimental technique is available that can completely predict the stresses, contact pressures, and displacements that are necessary to understand the effect of fixation angle on the integrity of the repair.

Three analytical models were developed to describe the forces and stresses in the fixated femur. These three models were based on the kinematics of the fixation, static equations, and equations for beams on elastic foundations. The analytical models provide greater insight into the locations and magnitudes of the stresses in the fixation as a result of the position of the screw.

Three two-dimensional and two three-dimensional finite element models were completed. The two-dimensional finite element models represented an intact femur, a femur with a 135-degree compression screw installed and a femur with a 150-degree compression screw installed. These two-dimensional models serve as the basis for many of the conclusions drawn from this work. The three-dimensional models, whose geometry is based on a CT scan of a femur, provide a basis for verifying that the trends of the stress distributions and repair stiffness predicted by the two-dimensional models are reasonable. The three-dimensional models of the intact femur presented here also document a method by which an accurate model of a bone can be constructed.

The analytical models and experimental study support the validity of the finite element models. This work, coupled with existing experimental and analytical research, provides new information on which a more informed decision can be made for selecting the fixation angle for femoral neck fracture repairs.

Hypothesis

Based on the sliding characteristics and loading conditions of a Garden III, Pauwel's Type 3 fractured femur fixated with a sliding hip screw, a 150-degree fixation will provide a more stable fixation than a 135-degree fixation.

CHAPTER 2

LITERATURE REVIEW

The focus of this dissertation is on modeling the stresses and deflections of fractured femurs that have been fixed with sliding hip screws. This chapter gives background information dealing with the properties of the femur, hip fracture, fracture healing, repair techniques, and modeling of the femur.

Properties of the Femur

It is important to understand the anatomy and properties of the femur to analyze the data from this study properly. The relevant anatomy of the femur will be discussed along with properties such as the different bone types found in the femur and the femoral geometry. Other bone related factors such as fracture healing will be covered, and the material properties of the femur will be given. These properties will be used in the formation of the analytical and finite element models presented in this study. The focus of this study is on femoral neck fractures; therefore, the properties and anatomy will be focused accordingly.

Anatomy of the Femur

The femur is the long bone of the upper leg. A typical long bone is divided into three regions. These regions are labeled epiphysial and diaphysial regions, with the third region being the metphysial region. The epiphyses are the ends of the bone and the diaphysis is the shaft of the bone. An epiphysial region contains the cancellous, or spongy, bone and red marrow. The metaphysial region is the region of transition between the epiphysis and diaphysis. Cancellous bone is a three-dimensional web-like network of bony tissue. The diaphysis is made of compact bone and contains yellow marrow. The compact bone is arranged in concentric layers. The diaphysis has a hollow center; the hollow portion is termed the medullary cavity. Yellow marrow fills the medullary cavity in an adult. A detailed diagram of a typical long bone is shown in **Figure 2.1**. Also shown in **Figure 2.1** are the periosteum and endosteum; these are the outer and inner layers of the diaphysis, respectively. The femoral head and neck are the focus of this study. Both the femoral head and neck are part of the proximal epiphysis and metaphysis of the femur. This proximal portion of the femur is also part of the hip joint.

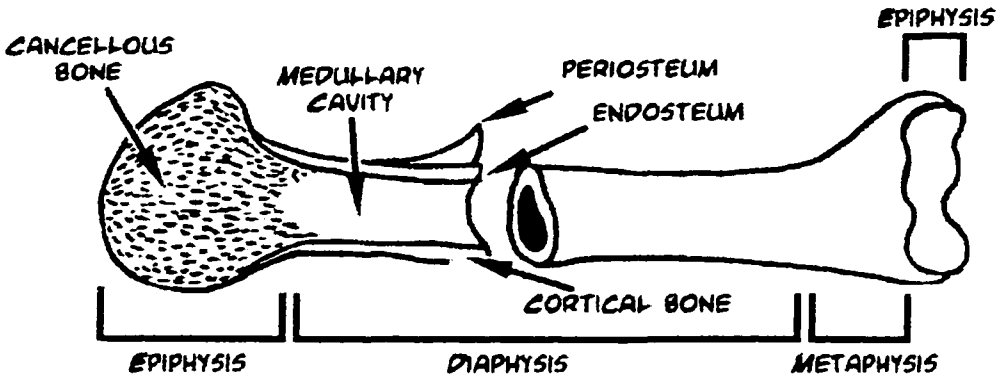

Figure 2.1 - Diagram of a typical long bone.

The hip joint is a ball-and-socket type joint consisting of the femur and the acetabulum. The femoral head constitutes the ball and the acetabulum is the socket. A diagram of a hip joint is shown in **Figure 2.2**. The hip joint is where the weight from the axial skeleton is transmitted to the lower limbs when in a standing position. Under severe loading conditions, such as stair climbing, forces applied to the femoral head can range up to eight times the body of weight of the individual. These forces are transmitted to the axially loaded portion of the femur through the femoral head and neck. The superior portion of the femur can be divided into four regions. These regions are the femoral head, the femoral neck, the intertrochanteric region and the subtrochanteric region. **Figure 2.2** shows these regions of the upper femur.

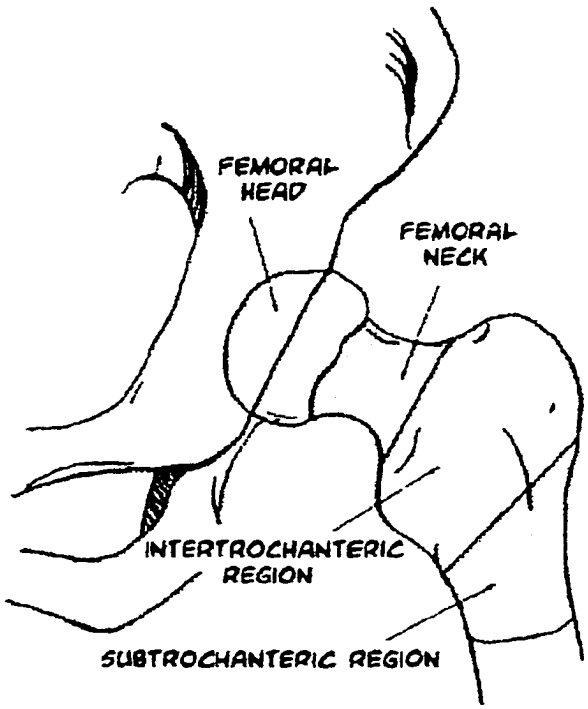

Figure 2.2 - Diagram of a human hip joint.

The femoral neck is angled medially approximately 130-degrees and anteriorly about 15-degrees (Harty, 1982). However, there is a range of approximately ten degrees for the angle of the normal femoral neck. The diameter of the femoral neck is only about three-quarters of the diameter of the femoral head. This reduction in diameter from the head to the neck allows for a greater range of motion before the femoral neck contacts the acetabular labrum.

Bone Types of the Femur

The human femur contains two distinct types of bone. These two bone types are referred to as either cancellous or compact bone. Cancellous bone is also known as spongy bone because of its soft and porous qualities. Cancellous bone is located in the

epiphyses of the femur. Cancellous bone consists of three-dimensional branches of bony trabeculae. The trabeculae are denser in locations that coincide with the forces experienced during the load bearing process. The differing densities of trabeculae produce noticeable patterns when x-rayed. The main groupings of the trabecular patterns are: principal compressive, secondary compressive, principal tensile, and the greater trochanter group. Sometimes a secondary tensile group is also included. The trabecular pattern groups are shown in **Figure 2.3**. It is these trabecular patterns that were used by Singh and associates (Singh, et al., 1970) to determine bone quality. However, determining bone quality by this method is very subjective. Depending on the quality of the bone being x-rayed some of the patterns will be less noticeable. A bone of lower quality such as an osteoporotic bone will have less pronounced trabecular patterns.

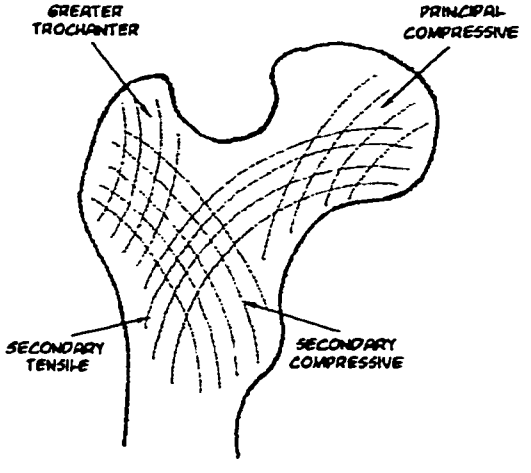

Figure 2.3 - Trabecular patterns in the proximal femur.

Compact, or cortical, bone is denser than cancellous bone. The diaphysis of long bones is made of this type of bone. Also, the epiphyses are surrounded by a thin layer of compact bone. Compact bone is made of many osteons. An osteon is a set of concentric layers of bone. A single concentric layer is termed a lamellae. At the center of each

osteon is a canal referred to as a Haversian canal. A network of these canals runs throughout the cortical bone. Contained in the Haversian canals are the blood vessels used for supplying the surrounding bone. **Figure 2.4** shows a typical cross section of compact bone including the osteons and Haversian canals.

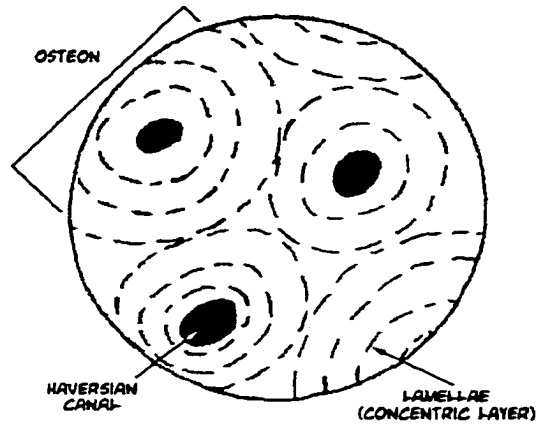

Figure 2.4 - Cross section of compact bone.

Material Properties

In order to model the femur accurately, the material properties of the different bone types that make up the femur have to be properly defined. Nonosteoporotic cancellous bone has a Young's modulus of approximately 1,000 MPa while compact bone has a Young's modulus of approximately 17,000 MPa. Both cancellous and compact bone have a Poisson's ratio of 0.33. **Figure 2.5** clearly shows the areas of compact bone and cancellous bone in a transverse section of the proximal femur. The areas of cancellous bone and cortical bone shown in **Figure 2.5** are unique for each femur, but these general regions are constant. The outer layer of compact bone, or cortex,

varies in thickness. The medial cortex of the femur may be greater than 7mm thick (Albright, et. al. 1978). The cortex of the femoral head is very thin, less than 1 mm in places and acts like a shell containing the lattice of cancellous bone in the femoral head.

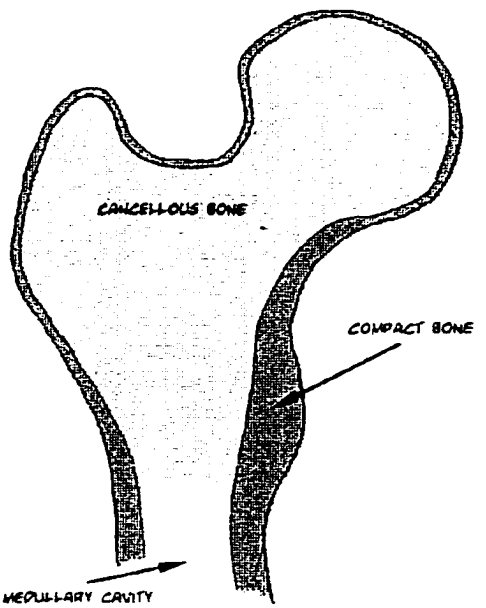

Figure 2.5 - Diagram showing the relative locations of compact and cancellous bone in the proximal femur.

The trabecular patterning of the cancellous bone in the femoral head causes the center of the femoral head to be the strongest area of the head. Refer back to **Figure 2.3** to see the overlapping trabecular patterns in the femoral head. However, the same is not true for the center of the femoral neck. The trabecular patterns in the neck cause the inferior portion of the neck to be stronger than the center. Also, there is a shelf or calcar of cortical bone near the lesser trochanter. This shelf can be seen in **Figure 2.5** as an increase in the thickness of the cortical bone in the inferior portion of the femoral neck.

This combination of calcar and increased bone strength in the center of the femoral head and inferior portion of the femoral neck dictate the optimum location for a fixation screw.

There are a few more material properties of bone worth mentioning. Bone is stronger in compression than in tension. Bones are not often loaded in a pure tensile situation. Tension does occur as a result of bending moments in bones. Also, bone does not have an endurance limit as many materials do and operates near its fatigue limit on a daily basis (Egol, et. al., 1998). Even operating near its fatigue limit, bones do not normally fail in fatigue, although it is possible. Bone fractures are usually the result of trauma. Microcracks sometimes occur in bone; however, they will heal if not unduly stressed over a period of time.

A very interesting property of bone is its ability to remodel itself as a result of changing loading conditions. Bone will become stronger in areas of high stress and weaker in areas of low stress. The constant remodeling of bone tends to increase bone density in areas of high stress and decrease bone density in area of low stress. This type of bone remodeling is referred to as Wolfe's law. This is an important property to consider in fixation device design. If the device carries too much of the load that would normally be carried by the bone, the bone will become weaker.

Blood Supply

Since bone is a living tissue, it requires blood to continue to live. The blood supply to portions of a bone is often interrupted in a fracture. The major blood supply of the femoral head runs along the femoral neck and may be interrupted by a femoral neck fracture (Albright, et. al., 1978). Therefore, it is important to understand the blood supply

of the proximal femur. A serious concern in the repair of femoral neck fractures is avascular necrosis of the proximal fragment. Avascular necrosis refers to the death of cells brought on by the lack of blood flow to the cells. This concern arises from the location of the blood supply of the femoral head. In compact bone, the arteries and veins travel in tiny canals throughout the bone. These canals are termed Haversian canals as mentioned earlier. In cancellous bone, the blood travels in the hollow spaces created by the porous trabeculae.

The blood supply for long bones arises from several sources. Among these sources are the principal nutrient artery, the metaphyseal arteries, and the periosteal arteries (Rhinelander, 1973). These vessels mainly supply the diaphyseal cortex region of the bone. The installation of the sideplate may interfere with these vessels. However, the vessels supplying the femoral head are of greater concern.

The Synovial joints, such as the hip joint, have a rich blood supply derived from surrounding vessels (Harty, 1982). These surrounding vessels converge to form arterial articular circles. Three such circles surround the hip joint. The major vessels to the femoral head and neck come from one of these rings located at the base of the femoral neck. The foveal artery also supplies portions of the femoral head. The most important of the supply vessels to the femoral head and neck is the medial circumflex artery. This artery ascends the femur to the trochanteric anastomosis where it joins the superior gluteal vessels. **Figure 2.6** is a diagram of the major blood supply vessels to the femoral head and neck. Both the trauma of the fracture and the invasive nature of the implant can cause disruption of these blood supply vessels. If the supply of blood to the femoral head is not adequately restored, the cells will begin to die and the fixation will eventually fail.

Therefore, it is necessary to not only stabilize the fracture, but to do it in such as way that minimizes the disruption of blood flow.

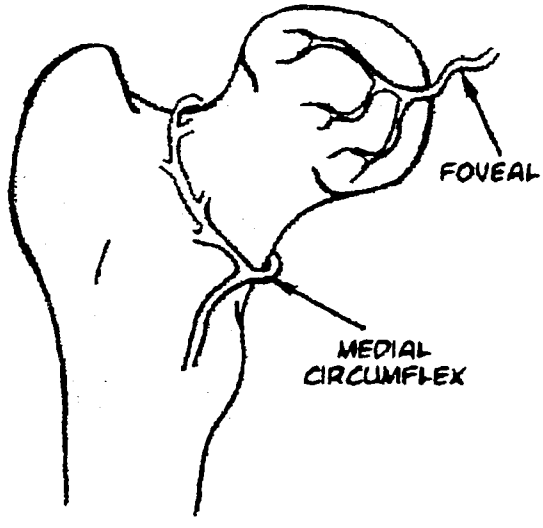

Figure 2.6 - Blood supply of the proximal femur.

Hip Fracture

Hip fracture refers to the fracture of the proximal femur anywhere from the head down to the first five centimeters of the subtrochanteric area (Winkley, 1998). Hip fracture generally occurs in the elderly patient, almost half of hip fractures occur after the age of 80. In addition, nearly 75 percent of hip fractures occur in women. The chance of hip fracture doubles with every decade after 50 years of age (Zuckerman, 1996). There are several reasons that hip fractures are more common in the elderly. As we age, the bone mineral density tends to decrease leaving a softer, more easily broken bone. In addition, the bone mineral density may have been lowered through a disease state such as

osteoporosis. Most hip fractures occur as a result of trauma, such as a fall or automobile accident. Stress fractures, without trauma, are uncommon and usually occur in osteoporotic elderly or in young active individuals such as endurance athletes or military recruits (Egol, et al. 1998). In the United States of America, there are approximately 250,000 cases of hip fracture each year. By the year 2040 it is predicted that the annual cost of hip fracture related medical care will be $16 billion and that there will be 512,000 cases of hip fracture in the United States alone (Cummings et. al. 1990).

Classification of Hip Fractures

The focus of this study is on fractures of the femoral neck. These fractures, especially displaced fractures, often lead to avascular necrosis of the femoral head if not dealt with quickly. There are many different techniques for treatment of hip fractures. In 1974, Tronzo identified over 100 different methods for fixation of a fractured femoral neck (Tronzo, 1974). Three of the current treatment plans are fixation with multiple screws, fixation with a dynamic hip screw, and hip replacement (Weinrobe, et. al., 1998). The type of surgery used to repair the fractured femur is based on the fracture characteristics, the assessment of the patient and the personal preferance of the surgeon. The fracture characteristics include the location of the fracture, bone quality, displacement and comminution. The patient assessment consists of the patient's sex, age, level of function before the injury and comorbidities.

Hip replacement allows for quicker mobility of the patient. However, loss of the natural joint may lead to complications. These complications may result in additional surgeries to correct the joint. Internal fixation, either by multiple screws or by a dynamic

hip screw, does retain the natural hip joint, but can also experience failure. In a study of 2,251 patients with internally fixed hip fractures, 12 percent had redisplacement of the fracture, 11 percent had nonunion, and 12 percent had segmental collapse (Holmberg, et. al. 1987). Generally, patients under the age of 65 should always be considered for some type of fixation (Bray, 1997). Patients over the age of 85 are most often treated with hemiarthroplasty because of their high rate of nonunion (Chua, et al. 1997). The group of patients between 65 and 85 years of age is treated based on the surgeon's knowledge of the patient and techniques involved.

There are several classification systems for femoral neck fractures. One of the simplest ways to classify femoral neck fractures is as a displaced or as a nondisplaced fracture. This is the simplest classification. A displaced fracture is one in which the bone has been partially or completely broken and the fragment is no longer in an anatomically natural position. Another subdivision of fractures is based on the location of the fracture. A fracture can be either intracapsular or intertrochanteric. An intracapsular fracture occurs inside the capsule of the hip joint and is more common than the intertrochanteric fracture. There are several other classification schemes. Two such systems are the Graden Classification system and Pauwel's Classification system.

Garden Classification System. The Garden classification system breaks down the fracture into four types. The four levels of the Garden system are based on the severity of the displacement of the fracture. These four types are listed in **Table 2.1**.

Table 2.1 - The Garden classification system for femoral neck fractures.

Garden Classification	Description
Garden I	Stress fracture or incomplete fracture
Garden II	Impacted fracture
Garden III	Complete fracture with partial displacement
Garden IV	Complete fracture with total displacement

As **Table 2.1** shows, the Garden classification divides femoral neck fractures based on the severity of the fracture. Fractures in this classification range from Garden I, the least severe fractures, to Garden IV, the most severe fractures. Garden I fractures can be handled without surgery in some cases, but the Garden II, III, and IV normally require surgery. **Figure 2.7** shows a diagrammatical representation of the four Garden classifications.

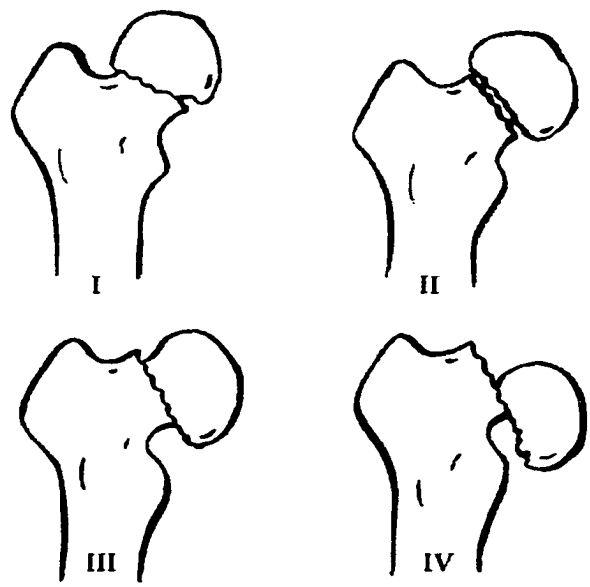

Figure 2.7 - Diagrammatic representation of the Garden classification system for femoral neck fractures.

Garden I Fractures

Garden I fractures, the stress or nondisplaced fractures, are the least severe of the four types of hip fractures in the Garden classification system. This type of fracture is stable and can bear the patient's weight soon after surgery, if surgery is required. When surgery is involved, it is normally a percutaneous lateral approach. First, two to four guide pins are inserted across the fracture. Next, a cannulated drill is used to cut the holes through the outer cortex for the screws. Finally, cannulated screws are used to hold the fractured neck in place as it heals.

Garden II Fractures

The impacted, Garden II, fracture is usually treated with surgery. Impacted fractures are complete nondisplaced fractures. There are those who believe that impacted fractures are treatable without surgery (Raaymakers, 1996). Raaymakers reports that he and a colleague have used a nonoperative treatment in 200 patients. The approach allowed early mobility (up to one week in bed) and partial load bearing. In his study, Raaymakers states that only 19 percent of the patients required surgery because of secondary instability. Complications arise from the difficulty in determining an impacted fracture from a nondisplaced or minimally displaced fracture. Also, some surgeons consider unrestricted load bearing is essential for optimization of postoperative rehabilitation (Zuckerman and Rosenberg, 1996).

Garden III Fractures

Garden III fractures are complete fractures with partial displacement. These fractures are usually treated with internal fixation in the younger patient and with some type of prosthetic replacement in the elderly patient. If the displacement is large enough, there is a possibility for avascular necrosis. Garden III fractures are the focus of this

paper as they are the most common femoral neck fractures repaired by internal fixation methods.

Garden IV Fractures

These fractures are the worst fractures in the Garden classification. Garden IV fractures are complete fractures with total displacement. Generally, Fractures in which the femoral head had been completely separated from the neck will not heal if reduced by internal fixation. The vascular supply to the femoral head has usually been severed and this will lead to avascular necrosis of the femoral head. However, it is still desirable to attempt fixation in younger patients. Elderly patients require prosthetic replacement of the superior portion of the femur.

Pauwel's Classification. Another classification scheme considers the angle of the fracture. The Pauwel's classification suggests that as the angle of the fracture line becomes more vertical, the more likely nonunion or delayed union would be (Bray, 1997). Pauwel's classification of femoral neck fractures divides the fractures into three groups. The three groups are Typel, Type 2 and Type 3. The angle of the fracture is measured from the horizontal tangent of the femoral head. Type 1 fractures occur at a 30-degree angle, Type 2 at 50-degrees, and Type 3 at 70-degrees. **Figure 2.8** is a diagram of the three types of fractures in the Pauwel's classification. In this study a Pauwel's Type 3 fracture has been modeled. This is the most common fracture angle for a Garden III fracture.

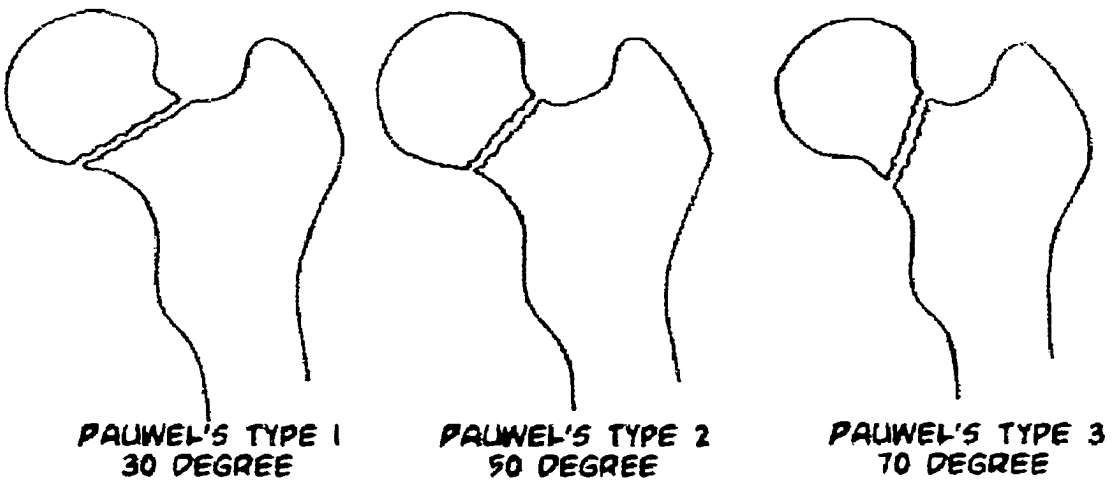

Figure 2.8 - Pauwel's classification for femoral neck fracture.

Bone Quality

Along with classifying the severity of a fracture and the angle of the fracture line, Bone quality must be assessed in order to prescribe the appropriate treatment plan. Bone quality plays a very important role in the eventual success or failure of a fracture repair. The bone density must be strong enough to hold the screws that are holding the fracture stable during the healing process.

Osteoporosis and other bone degenerating diseases can reduce bone quality drastically. Other factors thought to influence bone density range from high blood presure (Cauley, 1999) to sex hormones (Bonjour, 1997) to prolonged exposure to cadmium (Fagard, 1999.) Other factors such as the use of caffeine, tabacco and steroids have also been associated with a decrease in bone density (Ullom-Minnich, 1999.) With so many factors capable of affecting the quality of bone, it is very important to consider the bone quality when treating a femoral neck fracture.

Singh Index. In an effort to classify bone quality, Singh and associates describe radiographic trabecular pattern changes that can be used to grade the degree of osteoporosis (Singh, 1970). The Singh index is based on the amount of trabecular patterns that show up on x-rays of the bone in question. A bone with more visible trabecular patterning will have a higher Sing index number, with a Singh index of six being the highest. Others have disputed the accuracy of the Singh index, but it can still be used to determine between poor and good bone quality (Bray, 1997).

DEXA Scan. Another technique for determining bone quality is by using DEXA bone densitometry. DEXA was used in this study rather than the Singh index. DEXA stands for Dual Energy X-ray Absorptiometer. Two x-rays of different energies are used distinguish between bone and soft tissue. This method gives a very accurate measurement of bone density at the exposed sites. This method is much less subjective in nature than the Singh index and was the preferred method for determining bone quality in this study.

Fracture Healing

Since this study is concerned with femoral neck fractures, it is important to understand the basic fracture healing process. This understanding will help to evaluate the results of this study in order to qualify the performance of the devices being studied. The goal of the fracture fixation device is to provide the optimum environment for healing of the fracture. One of the most important jobs of the device is to hold the fracture site stable while the fracture heals.

Any type of bodily injury will initially result in inflammation and edema of the affected tissue (Peacock and Van Winkle, 1970.) The fracture healing process can be broken down into three overlapping phases (Cater, et. al., 1998.) The first phase is marked by the rapid proliferation of *pluripotential* tissue at the fracture site forming the fracture callus. The second stage involves the endocholdral ossification of the cartilage formed at the fracture site. The final stage is the remodeling of the endochondral boned formed in phase two.

During the first phase, the callus is formed. Fibroblasts and primitive mesenchymal cells with osteogenic potential begin to migrate to the fracture site. These cells are responsible for creating the fibrous matrix called the callus. The callus first forms a short distance from the fracture and continues to grow until it encompasses the fracture.

The second phase of the fracture healing process results in the callus transforming into bone tissue. Some of the callus, usually the innermost layer, will be transformed directly into bone. As the rest of the callus grows away from its blood supply, it will be changed into cartilage. The cartilage will then be slowly transformed into bone be the process known as endochondral ossification.

The third and final stage in the healing process involves the remodeling of the new bone. This remodeling process is based on Wolff's law. The excess bone will be resorbed as it is not carrying a significant portion of the stresses in the bone. Where there is a large stress in the bone, the bone will be strengthened. This stage is where a poorly designed fixation device can cause problems. If the device is not allowing the bone to carry any of the load, the bone will eventually become extremely weak, relying entirely on the fixation device.

There are many factors that affect this healing process. Kenwright and Gardner lists these factors as: the severity of the initial injury, the strain magnitude, the strain rate, and the stresses applied to the tissues. Also, the nature of the loading factors in to the healing process (Kenwright and Gardner, 1998.) Another important aspect of fracture healing is the reduction of the fracture. In a study by Claes and colleagues, it was found that increasing the interfragmentory gap delayed the healing process and that increasing interfragmentory movement stimulated callus formation but not tissue quality (Claes, et. al., 1998.) It was their hypothesis that gap size and the amount of strain and hydrostatic pressure along the fracture are the fundamental mechanical factors in bone fracture healing.

Repair Techniques

As mentioned earlier, there are many techniques used for the repair of hip fractures. Of primary interest in this paper are internal fixation methods. These repair techniques include nails, side-plated nails, sliding devices, screws, and pins (Albright, et. al. 1978). In the early days of fracture repair an ordinary iron nail was sometimes used to fix a fracture site. In 1931 Smith-Peterson described a nail specifically designed for hip fracture fixation. However, nails can often back out of the femoral head or even break. To prevent the nail from backing out of the head, a side plate was added that attached to the femoral shaft and to the nail head. Now that the nail was held in place another problem arose. If the femoral head became impacted onto the femoral neck, the nail would penetrate the head into the acetabulum.

To lessen the possibility of penetration of the nail into the acetabulum, sliding devices were developed. Since the nail can telescope, a sliding device allows the fracture to impact without the danger of penetration. The problem with a sliding device is that it can become jammed if the bending forces on it are too great. If a sliding device can not slide it is no better than a fixed device.

With displaced fractures it may be necessary to use screws to compress the fracture site. As the fracture site is compressed, the friction on the fracture surface resists rotation and shear to an extent. Pins are also used to fix hip fractures. Threaded pins can be used instead of screws or nails. Pins do not compress the fracture, but they do help avoid possible penetration into the acetabulum. The most common devices in use today are the simple bone screw and the sideplated sliding screw.

Bone Screws

Bone screws are used to treat many types of fractures. A typical bone screw has very coarse threads to better hold the bone. Bone screws can be either cannulated or non-cannulated. The purpose of these screws is to hold the fragments of a fractured bone in close contact with each other as they mend. Bone screws have been used in several different configurations over the years to treat femoral neck fractures. It is possible to use a single large screw such as the Graves screw or up to four smaller screws such as the Richard's screw in the fixation of hip fractures. When a single screw is used, it is common to use a side plate as well.

It is intuitively noted that multiple screws will resist rotation better than a single screw. However, with multiple screw techniques, placement of the screws becomes more

critical as there is a limited amount of space in the femur in which to place them. One of the most influential factors in the placement of the screws is the angle of insertion. As the screw angle becomes more horizontal, more of the load is transferred to the screws in the form of bending.

There are several properties affecting the performance of a screw. Some of these factors are pitch, major diameter, minor diameter, thread depth, and thread length. The pitch of a screw refers to the distance between two consecutive threads. The major diameter of a screw is the outer most diameter including the threads. The minor diameter of a screw is the diameter excluding the threads. The thread depth is the difference in major and minor diameters. The thread length refers to the length of the screw that is threaded. **Figure 2.9** is a diagram of a typical bone screw showing these screw characteristics.

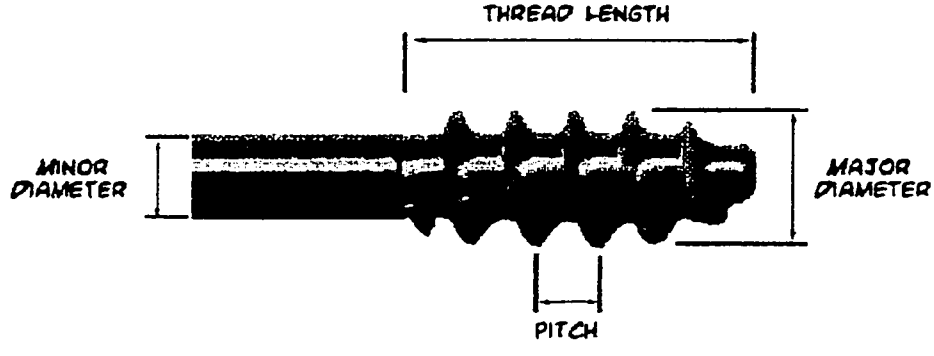

Figure 2.9 - Typical bone screw with features labeled.

Screws can be either fine or coarse threaded. Finer threaded screws generally have a greater pullout strength than coarse threaded screws because of their greater thread surface area. However, fine threaded screws do not perform so well in bone, particularly

because of the relative softness of bone. When dealing with the cancellous bone in femoral head, a coarse threaded screw will have a greater holding strength than a fine threaded screw.

Another factor affecting the performance of screws is tapping. Tapping refers to cutting threads in the screw hole before inserting the screw. Normally tapping is advantageous; however, with cancellous bone, tapping reduces the pullout strength of the screw (Chapman, et. al., 1996). The study done by Chapman and colleagues showed an average reduction of eight percent in pullout strength from tapping.

Cancellous and Cortical Screws

Cancellous screws are different from cortical screws, which are used in harder compact bone. Cortical screws are used to hold the sideplate on to the shaft of the femur. However, since the femoral head is primarily soft cancellous bone, cancellous screws are used to fix any fracture at this site. A cancellous screw is usually designed to have a larger thread depth and decreased thread cross-sectional thickness compared to a cortical screw (Perren, et al., 1992). The threads of a cancellous screw will compress the surrounding trabeculae as it is inserted into the femoral head. Cancellous screws are often used in groups of three to fix femoral neck fractures. However, placing three cancellous screws in such close proximity can be difficult.

Cannulated Cancellous Screws

To aid in the placement of screws, cannulated screws have been developed. Cannulated screws have the same properties as non-cannulated screws but have a hole

through their centerline. To install a cannulated screw a guide wire is inserted into the bone and a cannulated drill is used to cut a pilot hole for the screw. The screw is then placed over the guide wire and screwed into the fracture. This allows for more control over the placement of the screws. Nearly all types of screws in modern hip fracture repair are cannulated.

There are a few drawbacks to using cannulated screws. Since cannulated screws have a hole through their center, they are not as strong as a similarly sized non-cannulated screw of the same material. In addition, the hole prevents cannulated screws from having a large thread depth because the minor diameter has to be larger to accommodate the hole. Compared to a similar cannulated screw a non-cannulated cancellous screw will have approximately 20 percent higher pullout strength (Chapman, et al., 1996).

Sliding SidePlated Screws

Another type of screw in use today in is the sliding sideplated screw. This type of screw is similar to a single large cannulated screw. However, the sliding screw is accompanied by a sideplate that serves to hold the screw in place while allowing it to slide along its axis. The sideplate is attached to the shaft of the femur with several cortical screws, usually no more than four. The sideplate has a barrel that the sliding screw fits in. The barrel of the sideplate is usually grooved in such a way that the sliding screw can not rotate. This design allows the fragment to impact onto the rest of the femur, providing for a better reduction of the fracture. As the fragment impacts, the fracture becomes more stable as the area of bone in contact with bone increases. The screw

provides resistance to valgus and varus movement of the femoral head. Also anteversion and retroversion are resisted by the screw. **Figure 2.10** shows a diagram of a sliding screw and sideplate.

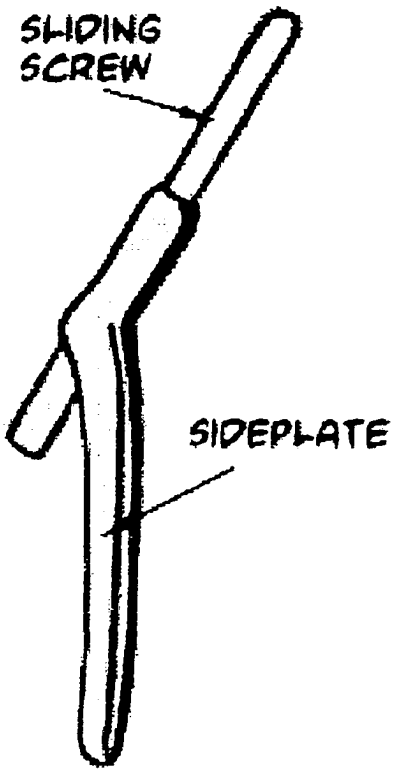

Figure 2.10 - Sliding sideplated hip screw.

Modeling of Hip Fracture

Mathematical models are necessary to predict the success or failure of an internal fixation device before the device is actually used in a clinical situation. Human trials are one of the last steps in the evolution of an implanted device. As early as 1917 theoretical

beam models were being made of the human femur (Koch, 1917.) The simplest stress analysis of the proximal femur involves only a joint reaction force applied to the femoral head and boundary forces applied at mid-shaft. Occasionally an abductor muscle force is added to the joint reaction force for a more complete model. The joint reaction force has been theoretically (Paul, 1967) and experimentally (Davy, et. al. 1988) established. In order to fully model the stress distribution in the femur it would be necessary to include the influence of the major muscle groups associated with the femur. These three major muscle groups are the abductors, the iliopsoas, and the iliotibial tract. However, the contributions of the muscles that are attached to the femur are not entirely known.

Without the addition of the major muscle groups attached to the proximal femur, the models of the femur predict a bending stress distribution in the femoral shaft. There is some debate whether or not the femoral shaft is actually under bending stress or if the shaft is under a more compressive stress. It has been noted that the shape of a transverse section of the femoral shaft does not agree with a femur in bending, but rather with a femur in compression. For instance, a transverse section of a femoral shaft shows a relatively circular cross sectional area with a fairly constant cortex thickness (Taylor, et. al. 1996). Wolff's law states that bone will remodel itself to equalize the stress levels in the bone. Therefore, by Wolff's law, a bending stress distribution in the femur would create a cross section that was elliptical or with varying cortex thickness or a combination of both. In a study by Taylor and colleagues, the hypothesis that the femur is loaded primarily in compression was tested. The group found that based upon a finite element model and a radiological study, the load distribution in the femur was mainly compressive, at least for an one-legged stance position (Taylor, et. al., 1996).

Analytical Models

For centuries, analytical modeling has been a useful tool for many types of research and design. An analytical model uses equations based on scientific theories and laws. An analytical model can be a single equation or a series of equations. Analytical models provide researchers with the means necessary to design and construct many devices. Also, an analytical model can be used as a research tool to describe a complex system. In this type of study, analytical models can be used to predict stresses, strains, and displacements in the femur and in the screw.

The first analytical models used to study stress in the human femur were reported in 1867 when Meyer investigated the stresses in the proximal femur (Meyer, 1867). Julius Wolff and J. C. Koch were also early investigators of the femur. Wolff is credited with the observation that bone is reshaped in response to the forces acting on it (Wolf, 1870.) Koch developed a description of the architecture of the femur based on femoral cross sections. Koch determined centers of gravity and moments of inertia for the cross sections. (Koch, 1917.)

In the late 1960's, Toridis used a three-dimensional analysis to study the stresses in the femur (Toridis, 1969). In his model, Toridis used three-dimensional straight beam theory with forces applied by the body weight and some muscles. The three-dimensional model allowed Toridis to investigate twisting moments that were not included in the two-dimensional models. However, this model was isotropic so it was not completely accurate for a bone-based model.

Rybicki and colleagues studied the effect of muscle forces on the femur in the one-legged stance phase (Rybicki, et al., 1972). The data from Koch's study of femur

architecture was used in this study. Rybicki used elementary beam theory along with a two-dimensional finite element model. The researches concluded that while elementary beam theory was acceptable for the femoral shaft, it was unacceptable for the ends of the femur. The complex geometry of the epiphyses requires a more complex modeling procedure.

In an effort to account for the different phases of bone in the femur, Carter and Vasu used a composite beam approach (Carter and Vasu, 1981). They studied the effect of axial loading, bending, and twisting on the femur. Carter and Vasu assumed that the strain was continuous across contact surfaces of the two regions representing compact and spongy bone. From this assumption they reduced the model to an equivalent beam of one material. They produced the one material model by reducing the cross section of the lighter material by the ratio of the elastic moduli of the two original materials.

In studies done by Huiskes and his colleagues, stresses on the femur were calculated from beam theory and compared to results from strain gages located at 100 points on their test femur. The beam theory model was based on assumptions that the femur was isotopic and linearly elastic. The researchers concluded that differences between their calculated results and their strain gage results were from the simplifications necessary in their model (Huiskes, 1981; 1982; 1984.)

Raftopoulos and Qassem offered a three-dimensional curved beam approach in 1987 (Raftopoulos and Qassem, 1987.) They use two models in their study. The first model is a three-dimensional isotropic curved beam. The second model is a three-dimensional anisotropic composite beam approach, in which the cancellous bone is surrounded by the cortical bone. They feel that the curved beam approach produces more accurate results than a straight beam approach because the curvature of the longitudinal

axis of the proximal femur is relatively large compared to that of the femoral shaft. Raftopoulos and Qassem conclude that three-dimensional curved beam analysis of the femur is valuable to designers of orthopedic devices.

Another type of analytical model was proposed by Cristofilini and associates (Cristofolini; et. al, 1996.) Their model was a reverse model based on data sets from 43 loading cases. This model describes the state of strain with a few synthetic indices. Their model can also be used to explain the state of strain and to predict the strain distribution under different loading conditions. They based their models on five bone related characteristics. However, this model is only useful in the diaphysial region of the femur.

Finite Element Method

As computing power has increased over the years, finite element (FE) modeling has become the research tool of choice for many scientists. Finite element modeling has been used to predict such things as stresses in the femur, fracture loads, and bone remodeling. The popularity of FE analysis (FEA) stems from its relative ease of use and detailed results.

The Finite Element Method (FEM) divides a model into many small sections called elements. Loads can be applied to the model along with boundary conditions and from this, each element can be solved. The elements can be solved to find stresses, strains, displacements, temperature and a host of similar things. The solution for each element is based on the solutions of all the surrounding elements and any external constraints.

There are two basic types of FE models. The simplest way to divide FE models is into two-and three-dimensional models. Two-dimensional FE models do have somewhat of a three-dimensional aspect to them; they usually have a thickness associated with them. Two-dimensional elements represent a small, "finite", area of the model. Similarly, three-dimensional elements represent a small volume of the model. Both two- and three-dimensional models are used in this study. There are also several other specialized types of elements such as spring, spar, and contact elements along with many others. The particular elements used in the models in this study will be discussed later.

The construction of any FE model is a slow process. Generally, three-dimensional models are used in the study of femurs. When three-dimensional models are necessary, manual model generation is extremely arduous. Another difficulty in modeling bone tissue is the use of nonhomogeneous material properties. The nonhomogeneous properties were found to have a significant effect on the results of the model (Hayes, et. al., 1982). In an effort to decrease the time needed for model generation and to include the nonhomogeneous material properties, several automated FE approaches have been developed. These automated FE methods are capable of generating three-dimensional models from successive CT scans. Another benefit of using CT scans to produce FE models is the ability to provide bone density data from the scans along with the shape of the bone.

After constructing the model of the desired object, it is necessary to mesh the model. The mesh the most important part of a FE model. The mesh is made up of the individual elements that will be solved in the solution process. A poor mesh with large or distorted elements will produce unreliable results. Mesh creation is often the most time consuming part of the FEM.

It is possible to generate a FE mesh automatically from computed tomography (CT) scans. Automatic mesh generation allows the researcher the ability to model each bone individually. This ability is necessary in the orthopedic arena because of the amount of variation between individuals. However, these automatically generated models must be carefully validated before using them. It is always necessary to validate any FE model. Without validation of the model, the data generated from it can be incorrect. Validation consists of increasing and decreasing the element count to determine the proper number of elements that will balance accuracy with computing time. Also, it is important to compare the model's results to experimental and analytical results.

The elements used in a FE mesh greatly affect the use of the mesh. Elements are made of nodes. The nodes of an element represent points where the elements are connected to the surrounding elements. Some elements have nodes only at their vertices others elements may have additional nodes in between their vertices. Generally the more nodes in a model the more accurate it will be. Of course, element size and shape is important as well. Some common three-dimensional element shapes are brick, tetrahedral and more recently the voxel.

A tetrahedral element is a solid element with four triangular sides. The simplest tetrahedral element has four nodes, one at each vertex. This type of element is useful for meshing complex geometry such as femoral geometry. Tetrahedrals are easier to arrange into complex shapes. A simple tetrahedral element is shown in **Figure 2.11**.

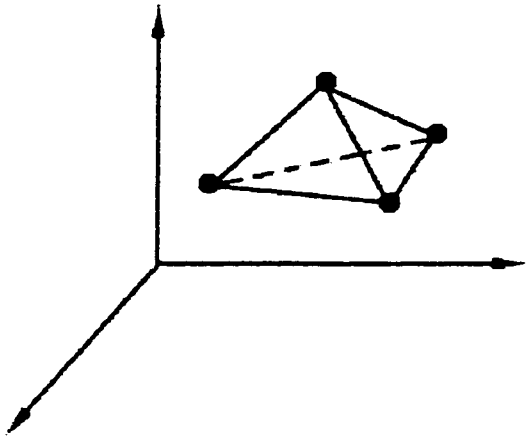

Figure 2.11 - Diagram of a simple tetrahedral element with four nodes.

Brick elements, or hexahedral elements, are slightly more complicated than tetrahedral elements. The simplest brick element contains eight nodes and is shaped like a brick. Brick elements are better suited for meshing regular geometries. When trying to mesh complex geometry with brick elements, there are often shape failures in the elements or there are so many elements that solving the model consumes too much time. **Figure 2.12** shows a simple brick element. It should be noted that just because it is called a brick element it is not necessarily brick shaped. The opposite sides are not required to be parallel or equally sized.

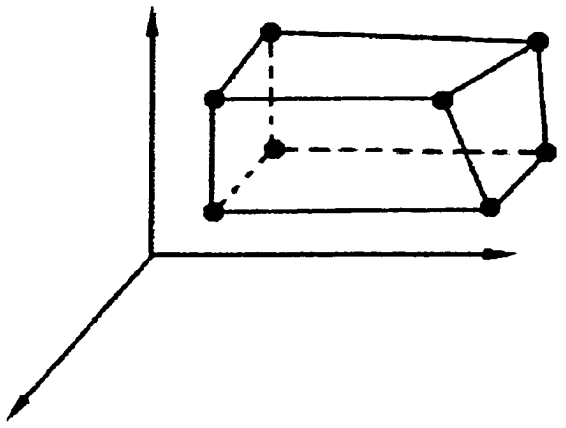

Figure 2.12 - Diagram of a simple brick element with eight nodes.

A voxel is much like a brick element except that each side of the element is equal in length and each element is the same size. A voxel based mesh is suited for large range interior geometric and density-distribution variations (Keyak, 1990). However, this method would not serve well for surface effects or for bone-implant interfaces. On the other hand, a mesh made of parabolic tetrahedrons is capable of surface measurements and bone-implant interfaces while still allowing for some density variations throughout the material (Merz, 1996). There are other factors to choosing elements such as the number of nodes per element and isotropic versus anisotopic elements and linear versus nonlinear elements. This type of element has been primarily used by J. H. Keyak and associates in femur research.

The first FE models for orthopedics began showing up in 1972. Brekelmans and colleagues termed it the 'new method to analyze mechanical behavior of skeletal parts. (Brekelmans; et. al., 1972.) These early efforts were not so much directed at a specific problem, but rather were used to show the usefulness of the FE method. These models used two-dimensional plane-stress elements of uniform thickness. Rybicki and associates

tried to account for the irregular thickness of the proximal femur by varying the Young's moduli of the elements. The results were compared to two-dimensional beam analysis and only matched in the diaphysisal region (Rybicki; et. al., 1972.)

One of the early three-dimensional finite element models was produced by Scholten (Scholten, 1975.) This model had approximately 10,000 degrees of freedom. This model was also one of the first to report the extensive use of convergence tests. The data generated by models such as this generally agreed with data from mathematical models in the shaft area of the femur, but did not compare favorably in the proximal femur.

As researchers became more familiar with the use of the FE method, the models began to focus on more problem solving goals. Among these goals was fracture fixation. One of the early fracture fixation studies was conducted by Rybicki and Simonen (Rybicki and Simonen, 1977.) In this analysis a two-dimensional FE model of an oblique fracture fixed with bone plates was shown. Stresses were evaluated for different conditions such as pretension in the plate, screw orientation, and loading.

In 1990, Keyak and colleagues introduced an automatic method for generating FE meshes (Keyak, et. al., 1990.) In this method, cubic elements of a user-specified size are generated directly form data from CT scans of the bone in question. Material properties for each cubic element were assigned based on the CT data. Some user intervention was required in the generation of the femoral geometry; however, the elements were generated automatically. Convergence tests were made much easier with the automatic mesh generation. In a follow up study, the model was verified to accurately characterize the strains on the surface of the diaphysis and neck of the femur (Keyak, et. al., 1993.)

Taylor and associates used FEA to study the effect of the muscle groups attached to the femur (Taylor, et. al., 1996). The Taylor group determined that it is possible for a femur to be loaded primarily in compression instead of the traditionally assumed bending. The model used in this study was based on 44 transverse CT scans of a dry cadaveric femur. The scans were at 20 mm intervals from the distal end of the femur to the mid-diaphysis. Then the interval was decreased to 10 mm until the lesser trochanter was reached, from there the interval was further reduced to 5 mm for the remaining scans. A three-dimensional FE model was constructed based on the CT scans. The model consisted of approximately 2500 six- and eight-noded elements.

In a more recent study by Keyak and colleagues, automated FEA was used to predict fracture loads in matched pairs of human cadaveric femurs (Keyak, et. al., 1997). CT scans of the femurs were used to generate FE meshes for each femur. In each pair of femurs, one of the femurs was loaded in a stance position and the other was loaded in a fall position. The FE models of the femurs were loaded similarly. The fracture strength of the femurs was predicted with the FE and measured with the actual femurs. Significant relationships were found between the predicted and measured values. For the pooled data r equaled 0.87. The FE models in this study consisted of 6,876 – 19,151 nodes and 5,152 – 15,552 elements depending on the size of the femur. The elements were linear eight-noded cube shaped elements measuring three millimeters on each side.

More closely related to the scope of this study is research done by Wang and associates(Wang, et. al., 1999.) A FE model of a gamma nail was constructed for the purpose of investigating stresses in the gamma nail during use. Both femoral neck and subtrochanteric fractures were studied. The model was constructed using ANSYS 5.3 and has approximately 29800 degrees of freedom. Three areas of bone were defined with

their own elastic moduli. Cortical bone was given an elastic moduli of 17 GPa, while two different areas of cancellous bone were given moduli of 1.3 and 0.32 GPa. The titanium implant was also modeled and given a separate elastic moduli. The model was made of eight-noded brick, four-noded tetrahedral, and point-to-surface contact elements. Linear elements were used in conjunction with the contact elements, as this was the extent of the capability of the FE analysis software. There were some loading conditions studied in which the model did not converge to a solution as the system was structurally unstable. These conditions could have been modified to force a solution; however, the model would have become unrealistic.

Relative Experimental Tests Conducted at LSUMC

Two additional experimental studies will be reported here. These studies were both done in the BioMechanics laboratory of LSUHSC. The data from these studies will be used to help support the validity of the analytical models and the finite element study contained in the current study.

Screw Angle in Femoral Neck Fracture Fixation

Lynn (Lynn, 1995) conducted experiments at the LSUHSC similar to those of the current study. Both studies used only the proximal half of the femur, cut a mid-shaft. Also, the loading conditions were similar with the load being applied to the femoral head while the femur was held at a 20-degree angle from vertical. In Lynn's test, eight pairs of femurs were used. The femurs were loaded in an intact state and the deflection at the point of the force application was recorded. After the intact testing, the femurs were

artificially fractured to simulate a Garden III, Pauwel's type 3 fracture and a 135- or 150-degree fixation device was installed. During the fixation tests, the femurs were loaded until failure and the displacement at the point of force application was recorded. While the experimental procedure was similar to the procedure of the current tests, there were notable differences.

The main difference between this study and the current study is the use of embalmed femurs in Lynn's study. There are also several other differences between the studies. Among the differences are the use of a 222 N (50 lb) preload and only a single run per femur. **Table 2.2** shows a side-by-side comparison of the similarities and differences between the two studies.

Table 2.2 - Comparison of the similarities and differences between Lynn's previous study and the current study.

Lynn's Study	Current Study
222 Newton Preload	No Preload
Embalmed Femurs	Fresh Frozen Femurs
Eight Pair of Femurs	One Pair of Femurs
Load Applied at 20-degrees	Load Applied at 20-degrees
Single Run per Femur	Multiple runs per Femur
Loaded to Failure	Loaded to 1350 Newtons
INSTRON Force and Displacement Measured	INSTRON Force and Displacement Measured, Along with Two Other Displacements
Intact, 135-degree, and 150-degree tests	Intact, 135-degree, and 150-degree tests

By using the more plentiful embalmed femurs in the previous study, a better statistical analysis can be performed. However, the embalming process changed the material properties of the femurs. Embalmed femurs are weaker than their fresh frozen counterparts. Therefore, the results of this study will be normalized for comparison with

the current study. The normalized trends should still be similar between the two studies, but the absolute values will be different.

The results of Lynn's experimental tests of sixteen human cadaveric femurs showed that femurs fixed with 150-degre screws failed at a lower load than femurs fixed with 135-degree screws. However, the current study does not consider the load at failure but rather considers the performance of the femurs over a smaller load range. The load range considered in the present study is from 0 to 1,350 N. Only the results that correspond to the load range in the current study will be used. **Table 2.3** lists the intact and fixated stiffness values calculated from the displacement data from Lynn's study. The first eight bones listed in **Table 2.3** were fitted with the 135-degree device while the second eight were fitted with the 150-degree device.

Table 2.3 - Stiffnesses calculated from the Intact and fixated femurs in Lynn's study (Lynn, 1995).

Bone Number	Intact Stiffness (N/mm)	Fixated Stiffness (N/mm)
L868 (135)	181.96	182.03
L808	134.04	144.24
R811	180.69	263.74
R888	308.23	162.13
L799	239.36	202.59
L831	201.18	168.12
L863	144.49	200.26
R875	207.19	116.57
R868 (150)	212.57	110.6
R808	134.39	125.33
L811	129.46	205.04
L888	199.23	94.88
R799	119.56	200.54
R831	174.8	99.12
R863	198.98	320.1
L875	99.18	193.81

Intact Deflections of Fresh Frozen Femurs

The second study that will be used to help validate the accuracy of the finite element models in the current study was performed by Karastinos (Karastinos, 2001.) Karastinos' study was conducted between February and March of 2001 in the BioMechanics laboratory at LSUHSC. The focus of Karastinos' study was not femoral neck fracture, but intact testing of fresh frozen femurs was part of the study and it is this data that will be useful for FE validation.

There is one significant difference concerning the data from Karastinos' study. The femurs in Karastinos' study were whole femurs whereas the femurs in the current study are cut at midshaft. In order to be able to use Karastinos' data for validation, the two-dimensional finite element model was modified to include a whole shaft. It will be this modified finite element model that will be used to compare the stiffness with the stiffness calculated from Karastinos' data.

The femurs in Karastinos' study were held at a 20-degree angle with a load applied to the femoral head, just as in the current study. This procedure is comparable to the procedure used in the current study. The intact axial stiffness values that were calculated from Karastinos' data are shown in **Table 2.4**.

Table 2.4 - Intact axial stiffness values calculated from Karastinos' study of sixteen fresh frozen femurs (Karastinos, 2001).

Bone Number	Intact Stiffness N/mm
1798 L	570.9
1995 R	636
1821L	929.8
1821R	514.8
1831L	573
1831R	755.4
1833L	662.8
1833R	968.3
1866L	874.3
1866R	526.4
1877L	1339.2
1877R	752.3
1898 L	848.1
1898 R	670.1
1903 L	559.1
1903 R	624.4

Discussion of the Literature

The anatomy and complex geometry of the femur has been discussed. The complexity of the geometry of the proximal femur almost excludes simple analytical models from accurately describing the interactions between bone and fixation device. The two different phases of bone, cortical and cancellous, have been defined and their material properties listed. For a typical femur, cortical bone has a modulus of elasticity of 17,000 MPa. Cancellous bone is typical assigned a modulus of elasticity of 1,000 MPa. Both bone types have a Poisson's ratio of 0.33.

The importance of restoring the blood supply to the femoral head fragment has been given. The living portions of bone rely on a constant blood supply just as any other tissue. If, after a fracture, this blood supply is not restored the unsupplied portion of the

bone will die. It is important for the fixation device to not interfere with this blood supply while at the same time allowing it to be restored.

There are two main classification systems for femoral neck fractures. The Garden classification system uses the severity of the displacement of the fracture as the basis for classification. Pauwel's classification system uses the angle of the fracture as its criteria. In this study, Garden Type III fractures with a Pauwel Type 3 fracture angle are modeled.

In order for a fixation device to succeed, the bone must be of a certain quality. Generally, bone quality decreases with age. The Singh Index and the DEXA Scan were mentioned as possible measurements of bone quality. In this study, bone quality could not be considered because of the unavailability of surplus cadaveric femurs. However, in a clinical fixation, the bone quality would be an important factor in determining what fixation technique to use.

The fracture healing process was also described. Fracture healing can be broken down into three basic steps. The first step in the fracture healing process is the formation of the callus around the fracture site. During the second phase, the callus is transformed into bone tissue. The final stage of the bone healing process is the remodeling of the newly formed bone.

Current femoral neck fracture techniques can be divided into two basic groups. One group uses several small screws to fix the fracture and the other group relies on a single large screw. In this study, a single large sliding screw is used with the angle of insertion of the screw being the primary focus of the investigation. Different angles of insertion will produce different stresses in the fixation screws and in the bone fragments.

In an attempt to quantify the performance of fixation devices, researchers have relied upon analytical and finite element models. The models are often models of the

proximal femur with a resultant force applied to the femoral head. Most of the current femur models are finite element models. The FEM is better suited to representing the complex geometry of the proximal femur than any other modeling method. However, there are relevant analytical models that can shed understanding on the mechanics of fixated femurs.

A typical modern FE model of the proximal femur will contain from 6,000 to 30,000 elements depending on the size and resoultion of the model. The elements most commonly used in the models are linear four-noded tetrahedral and eight-noded hexahedral elements. Higher order elements can predict more accurate results with fewer elements; however, due to the limits of the FE software package and computers available for use in this study, only the four- and eight-noded elements are used in the three-dimensional analysis. The two-dimensional models contain six-noded triangular elements of varying thickness to represent the different areas of bone.

Finally, two relevant studies conducted at the LSUHSC were discussed. The similarities and differences between these studies and the current study were presented along with the data from the studies. The data from these previous studies will be helpful in validating the finite element models of the current study.

This research will focus on the mechanics of 135- and 150-degree sliding screws for fixating Garden III, Pauwel Type 3 femoral neck fractures. The performance of the devices will be evaluated through examination of the forces, displacements, and stresses in the bone and screw, as well as the stiffness of the fixated femurs. Experimental, analytical and finite element modeling techniques will be employed.

CHAPTER 3

EXPERIMENTAL METHODS

Introduction

The purpose of experimental testing is to provide a general understanding of how an actual femur reacts to a given load. By comparing the results from experimental testing of an intact femur with the results from repaired femurs, the effect(s) of the repairs can be quantified. Experimental testing can provide data for verification of models while at the same time adding to the general scientific knowledge base. The experimental tests help to prove or disprove the usefulness of the other analysis. If similar trends are noticed among the experimental, analytical, and finite element studies, then the data produced by them will be useful.

The irregular geometry of bones provides a complex challenge to the researcher studying them. No two bones are identical, not even paired bones from the same person. Each bone will have its own unique structural geometry, and material properties vary widely and change with position in a bone. However, by using the proper baseline testing procedure the data can be normalized so that it can be appropriately compared. Highly accurate numerical matches between one bone and another or between experiments and analytical models are unlikely due to geometry and material property variation.

The experimental section of this dissertation attempts to quantify the deflection of a fixated femur under a given loading condition. This load condition represents an one-legged stance position in which the resultant force applied to the femur is given by a concentrated load on the femoral head. The load is applied to a point on the femoral head at a 20-degree angle from the vertical.

Materials and Methods

This section will cover the various materials and methods used in the experimental portion of this study. The testing was done with fresh femurs harvested from the LSUHSC (Louisiana State University Health Sciences Center) Anatomy Laboratory. The femurs were stored in a freezer in the BioMechanics Laboratory at LSUHSC when they were not being prepared or tested.

Setup

The setup phase of this study involved assembling a testing apparatus and debugging the apparatus. The testing apparatus used in the experimental testing phase of this study consisted of an INSTRON machine, an angled base, two Linear Variable Differential Transformers (LVDT's), and LabView. The INSTRON applied the force to the femur and measured vertical displacement of the femoral head. The angled base held the femur at a predetermined angle. The two LVDT's measured displacements at specific points on the femur. Finally, the LabView program recorded all of the data.

Testing Apparatus. The fixture used in this study was designed to permit the bones to be rigidly held at a specific angle and linear variable displacement transducers (LVDT's) to be positioned at particular locations. The fixture was constructed in such a way that deflections would occur in the femur well before any deflection occurred in the fixture holding the femur. Additional cross bracing was used to secure the LVDT's to insure that they remained as motionless as possible and therefore only recorded the displacement of the femur.

One problem with the LVDT's remaining stable is that although the LVDT's did not move, the bone did. The problem comes from the fact that the bone will have two distinctly different deflections, before and after fixation. The intact bone, particularly the femoral head, will deflect differently after fixation. The LVDT's were placed in positions that would account for this femoral head movement, although it did create some slightly inaccurate data in the intact testing. The LVDT placement will be discussed thoroughly in a following section.

INSTRON. The main component of the testing apparatus was the INSTRON (Corporate Headquarters; 100 Royall Street; Canton, Massachusetts 02021-1089) servohydraulic testing machine used to apply forces. The INSTRON machine was an INSTRON model 4202. The INSTRON was equipped with a load cell for measuring the applied force, and measurements up to 10,000 N with an accuracy of 4.88 N are possible. Both the applied force and vertical displacement experienced by the cross head of the INSTRON were recorded during the testing. Since this INSTRON is capable of only

applying force in a vertical direction, an angled base was fabricated to hold the femur in a more anatomically correct position in relation to the applied force.

Angled Base. It was necessary to hold the femur at a 20-degree angle from the vertical to simulate anatomical loading conditions. The femur was held at this angle by an adjustable angled base which was constructed as part of this work. The base was constructed from two six-inch square, 5/8^{ths} inch thick steel plates and a 4-inch diameter round steel tubing. A diagram of the angled base is shown in **Figure 3.1**. The top plate of the base is set at a 15-degree angle. Two jackscrews were used to raise the angle of the top plate to the required 20-degrees. The jackscrews operate by raising or lowering one side of the base as they are threaded into or out of the baseplate of the fixture. By using the jackscrews, the angle of the femur can be set to exactly a 20-degree angle.

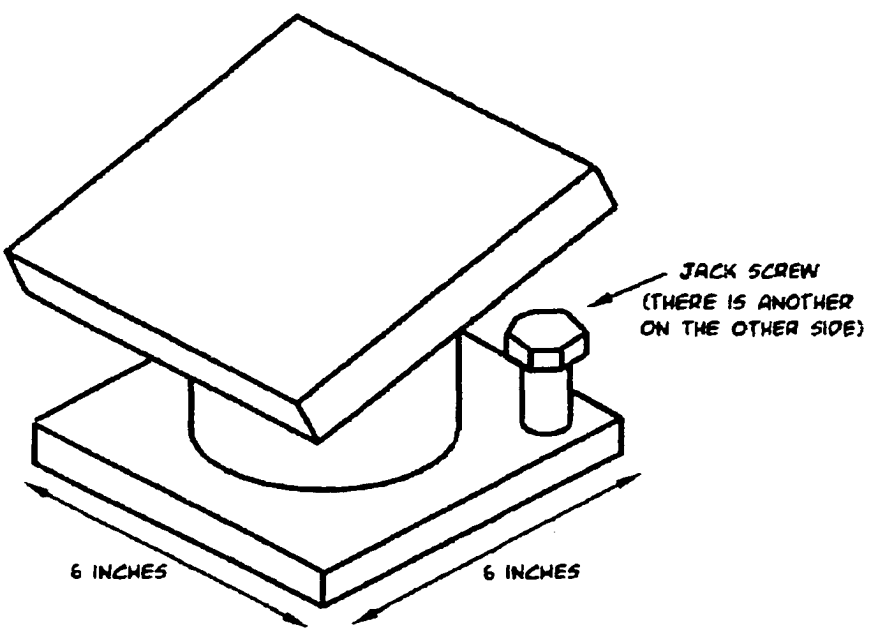

Figure 3.1 - Diagram of the angled base plate used to hold the femur during the experimental testing.

A V-block was attached to the top plate of the angled base and used to hold the shaft of the femur. A V-block is essentially a block with a V-shaped groove in one side. **Figure 3.2** is a diagram of the V-block. The shaft of the femur sits in the V-shaped groove and is held in place by two clamps. The V-block is two inches tall and four inches wide. The V-block was attached to the angled base by using a tie down that was bolted to the top of the angled base. A diagram of the complete assembly: angled base, jackscrews, V-block, and V-block tie down can be seen in **Figure 3.3**.

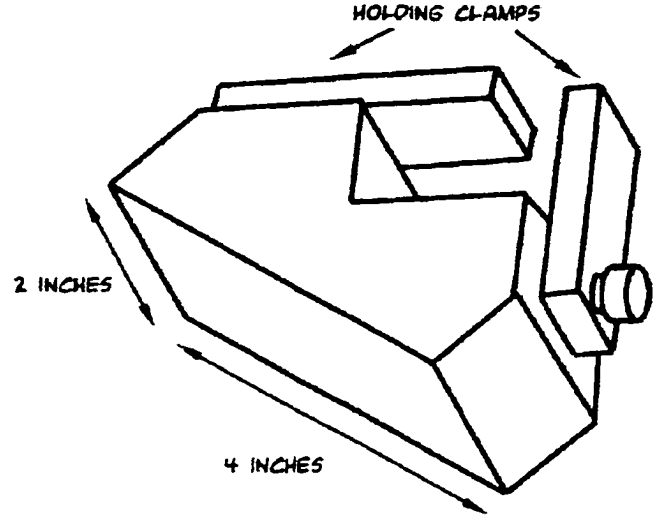

Figure 3.2 - Diagram of the V-Block used to hold the femur during experimental testing.

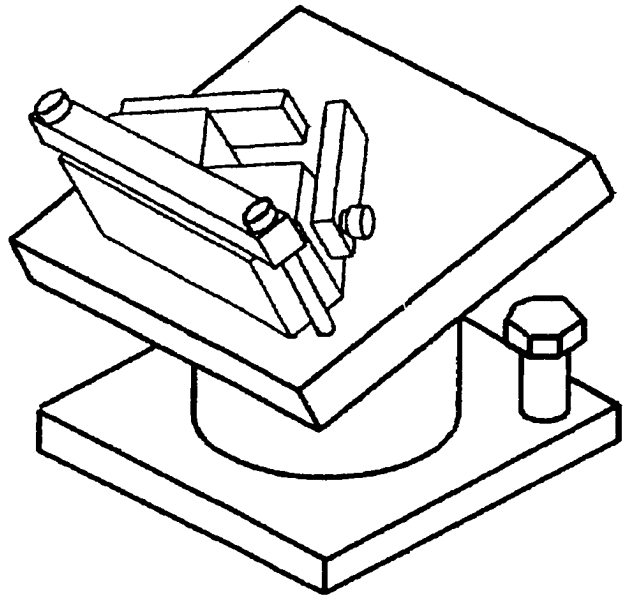

Figure 3.3 - Diagram of the assembled fixture, including the angled base, jackscrews, V-block, and V-block tie downs.

Linear Variable Differential Transformers. The displacements of the femurs were measured using LVDT's. Two of these LVDT's were used in conjunction with the displacement information from the INSTRON. An LVDT is a displacement transducer that operates on the principle of mutual inductance. A LVDT consists of a primary winding, two secondary windings and a movable inner core. An AC voltage is introduced into the primary winding induces a corresponding AC voltage in the secondary windings, in proportion to the position of the movable core. As the core moves, the voltages in the two secondary windings change. The two voltages from the secondary cores are recorded and used to determine the displacement of the core. **Figure 3.4** shows a diagram of an LVDT along with a schematic representation of an LVDT.

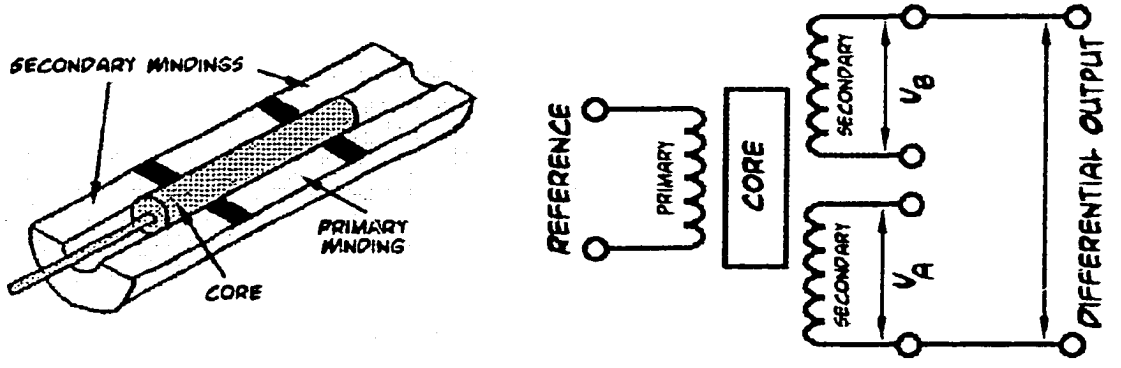

Figure 3.4 - Diagram of a cut-away view of an LVDT along with the corresponding electrical representation.

As stated earlier, two LVDT's were used in this study. The LVDT's were model number GCD-121-125 manufactured by LUCAS Control Systems (Schaevitz Sensors; 1000 Lucas Way; Hampton, Virginia 23666.) Both LVDT's have a useable stroke length of +/- 3.17mm. The output of an LVDT is dependent on the voltage supplied to its primary winding. The LVDT's in this test were supplied with +/- 15 volts DC. These LVDT's have sensitivity of 3.15 volts per mm.

One of the LVDT's was placed in contact with the greater trochanter while the other LVDT was placed under the femoral head. The LVDT contacting the greater trochanter was held at a 45-degree angle from the vertical. The LVDT under the femoral head was held parallel to the shaft of the femur. The LVDT on the greater trochanter was labeled as LVDT II and recorded the bending experienced by the shaft of the femur. The LVDT located under the femoral head was labeled LVDT I and was used to record the translation of the femoral head and the bending of the femoral neck. **Figure 3.5** shows the relative placements of the two LVDT's and the INSTRON.

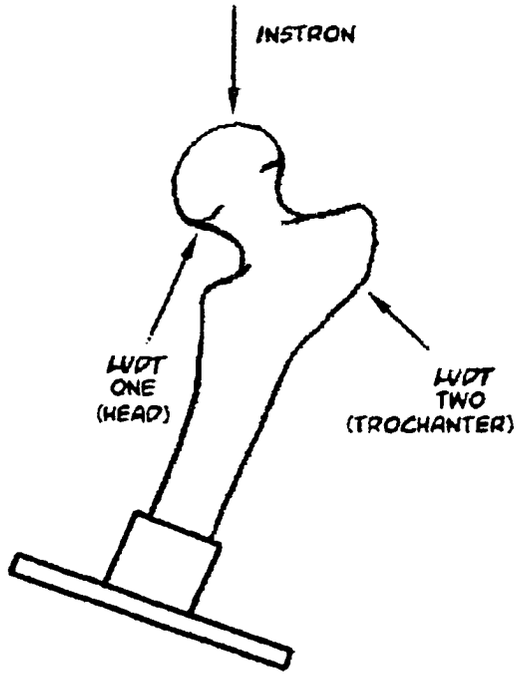

Figure 3.5 - Diagram of the general locations of the two LVDT's.

The LVDT's were held in place by tubular steel rods and specially fabricated mounting hoops. Two main uprights were secured to a large steel plate resting on the base of the INSTRON. Braces were used to stabilize the LVDT's. The braces were also tubular steel rods. The braces were attached to one another and to the main uprights by variable angle clamps. These clamps allowed two pieces of tubular mounting rods to be attached to each other at any angle. A picture of the experimental setup can be seen in **Figure 3.6**.

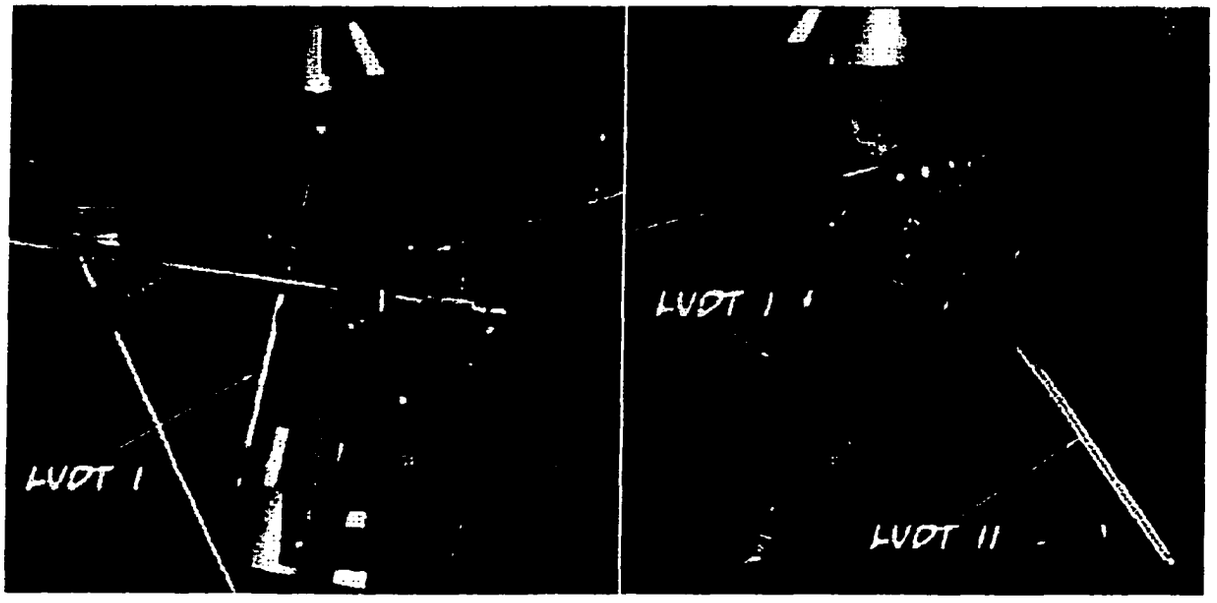

Figure 3.6 - The LVDT's and mounting fixture used to hold the LVDT's in the experimental phase of tests.

The LVDT's were connected to an analog to digital (A/D) converter, which in turn was connected to a Pentium PC. This PC was running Labview, which was used to record the data from the experiment. The INSTRON was also connected to this A/D converter and PC via the same A/D converter.

LabView. A computer running LabView (National Instruments Corporate Headquarters; National Instruments Corporation; 11500 N Mopac Expwy; Austin, TX 78759-3504; (512) 794-0100) version 5.1 recorded the data from the INSTRON and the two LVDT's. The data was passed through an A/D board (National Instruments Corporation; 11500 N Mopac Expwy; Austin, TX 78759-3504) model AT-MIO-16E. The purpose of an A/D board is to convert the analog signals produced by the instruments into digital signals that can be read by a computer. Four channels of information were recorded simultaneously at a sampling rate of 10 samples second. These four channels

were: INSTRON displacement, applied force, LVDT I, and LVDT II. Mr. Al Ogden and Mr. Clifton Frilot authored the LabView user interface that was used in these experimental tests.

The LabView program used for these experimental tests automatically converted the voltages from the LVDT's into displacement measurements. The program also converted the INSTRON data into Newtons of force and millimeters of displacement. Several test runs were completed before the actual testing to debug any problems in the fixture or data recording system.

Debugging the Fixture

It was necessary to make several test runs to insure that there were no problems with any of the experimental setup. Femur 1934L was prepared in the same manner as the femurs that would be used in the study. This femur was then used to test the setup. The initial testing showed that the angled base plate was tilting slightly as force was applied. This problem was solved by adding toe clamps to the raised edge of the base to hold it down. These clamps were bolted to the large steel plate that the angled base was resting on.

Two different LVDT placements were considered for LVDT I. This LVDT was responsible for measuring the movement of the femoral head. One placement had the LVDT contacting the head in a horizontal direction (position one), while the other placement had the LVDT underneath the head and parallel to the femoral shaft (position two.) **Figure 3.7** shows these two LVDT placements.

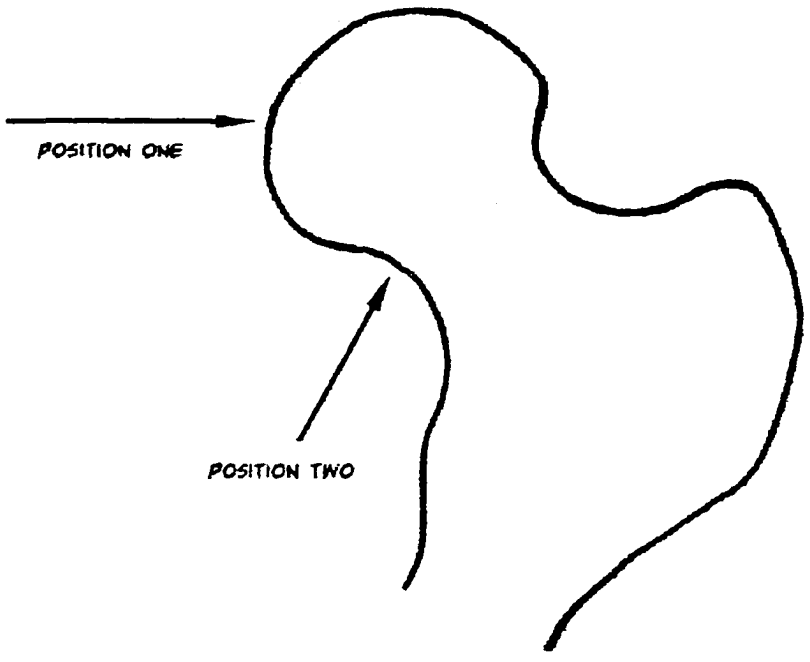

Figure 3.7 - Two possible positions for LVDT I to measure movement of the femoral head.

Position one was able to record a larger range of displacement; however, this position would not be able to sufficiently describe the movement of the femoral head after fixation. Position two did not show as large of a range in displacement in the preliminary intact testing, but seemed to be in a better location for recording displacement after fixation. However, there is one problem with the data recorded by the LVDT in placement two.

The problem with the measurements made by LVDT I in position two is a result of the inability of the LVDT to move with the deflecting femur. As the load was applied to the femur, the femoral shaft would bend. This bending of the shaft caused the intact femoral head to move roughly in an arc with its center located at the base of the femoral shaft. As the femoral head moved, the point of contact between the LVDT and the femoral head changed. This is not a large problem; however, it makes the data appear to

show the femoral head moving more than it actually did. **Figure 3.8** shows a diagram of the cause of the inaccurate data. Notice how the LVDT does not maintain contact with the same point on the femur throughout the deflection of the femur.

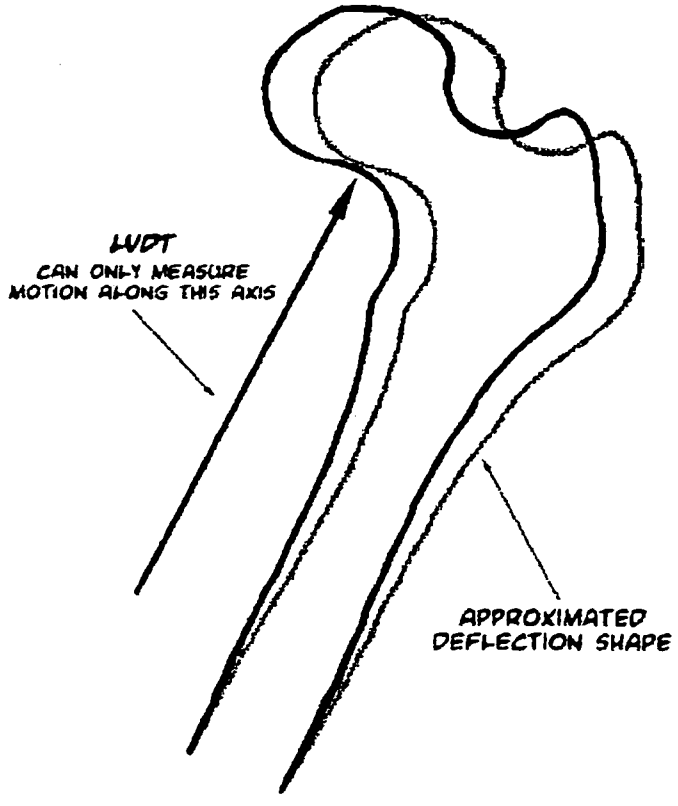

Figure 3.8 - Source of inaccuracy in measurements from LVDT II.

This problem could have been lessened by using a larger contact area between the LVDT and the bone, in a sense integrating the displacements over a larger surface area. However, in order to use a large LVDT probe tip, it would have been necessary to place the LVDT tip underneath the rounded portion of the femoral head. Putting the LVDT tip in this location would have meant that the LVDT was farther away from the fracture site. It was decided to use a small round LVDT probe tip and place it closer to the fracture site.

Procedure

After debugging the fixture and data recording devices, the experimental testing began. The experimental testing was done in the BioMechanics Laboratory in Louisiana State University Medical Center (LSUHSC) in Shreveport Louisiana. Cadaver bones were harvested from the LSUHSC Anatomy Laboratory. Before testing, the bones were cleaned and x-rayed. Two of the femurs, 1880L and 1880R, were scanned with a CT scanner. The CT scans were later used to create the finite element model geometry. While the femurs were not being tested, they were stored in a freezer in the lab.

Bone Preparation. Initially, two femurs, 1880L and 1880R, were harvested from the LSUHSC Anatomy aboratory. Later an additional two femurs, 1934L and 1934R, were also harvested. The bones were first cleaned of any excess tissue. The bones were manually cleaned by cutting and scraping the tissue from the bone. Bones 1880L and 1880R were scanned by a CT machine. These scans were used to generate anatomically accurate femur geometry for the finite element portion of this study. The CT machine used to scan the femurs was a General Electric High Speed System CT01 located in the LSUHSC Department of Radiology. The CT scans were taken at 1 mm increments and stored on a recordable CD.

Next, the femurs were cut to a length of 23 cm measured from the proximal tip of the greater trochanter. After installing the sideplate, there were some problems with holding the femur in the v-block. These problems were overcome, but a longer femur length would have been preferred. After cutting the femurs to length, the femurs were potted.

Potting the femurs consisted of aligning the shaft of the femurs in a vertical position and molding a Bondo™ cup around the base of the femur. The cup was 3.97 cm high and had a 4.13 cm inner diameter. The Bondo™ was mixed with an appropriate amount of cream hardener according to the manufacturers instructions. The mixture was placed in a steel tube. The femur was then placed in the tube thereby displacing some of the Bondo™. The shaft of the femur was held in a vertical position while the Bondo™ was allowed to harden. The excess Bondo™ was trimmed away as soon as the Bondo™ had reached a semi solid state. Upon completion of the hardening of the Bondo™, the steel ring was removed and a molded Bondo™ cup was left around the base of the femur. **Figure 3.9** shows a diagram depicting the potting process.

In **Figure 3.9**, step one shows the Bondo™ mixture placed in the steel cup. Step two shows the femur displacing some of the excess Bondo™ as it is positioned in the steel cup. Step three shows the trimmed Bondo™ with the cup still in place. The final step, step four, shows the potted femur with the steel cup removed and the Bondo™ completely hardened.

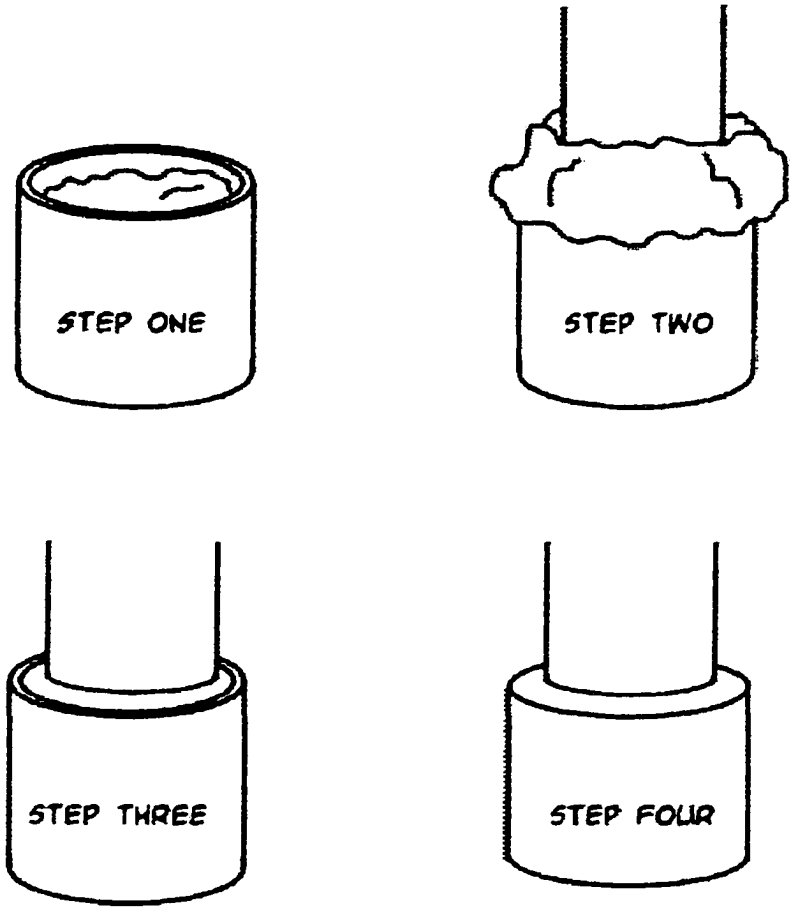

Figure 3.9 - The major steps in the potting process used in the experimental procedure.

Storage. When the femurs were not being used for any experimental testing, they were stored in freezer located in the BioMechanics lab at LSUHSC. The femurs were wrapped in damp cloth towels and placed in a sealed biological hazard storage bag. Before any testing was done of the femurs, they were removed from the freezer and allowed to thaw.

Installation of the Sliding Screw. The BioMet (Biomet, Inc.; P.O. Box 587; Airport Industrial Park; Warsaw, Indiana 46581-0587) variable angle sliding hip screw

model S 4 Hole 88 mm was used as the fixator in the experimental testing. This screw is made of medical grade stainless steel and has an adjustable screw angle. The angle for these screws can be adjusted from 90-degrees to 150-degrees. Two of these screws were used in this study. One screw with the sideplate set at a 135-degree angle, the other with the sideplate set to a 150-degree angle.

The first step in the fixation of the femur was to insert a guide pin at the appropriate angle. To do this, a guide pin was inserted in the chuck of an electric drill. The guide pin was then aligned so that it would penetrate the femoral shaft, travel through the femoral neck and land in the femoral head. A guide pin angle guide was used to keep the guide pin at the appropriate angle.

The angle guide was a metal block that rested against the shaft of the femur. The guide had several holes in it that corresponded to different screw angles. The guide pin was inserted into the correct hole in the guide block and drilled into the femur. For bone 1880L this angle was 135-degrees. The 150-degree screw was installed in bone 1880R initially; however, the bone did not survive the installation and the 150-degree screw was installed in bone 1934L.

After the guide pin was successfully installed, the osteotomy was performed. The bone was marked for a cut at a 70-degree angle measured from the horizontal tangent to the top of the femoral head. The cut was used to simulate a Garden III fracture. A hacksaw was used to perform the cut. The guide pin was left in the femur until it was necessary to remove it in order to complete the simulated fracture. After the femur was cut through, the guide pin was reinserted to stabilize the newly severed femur.

Next, the pilot hole for the screw and barrel of the sideplate were cut into the femur. The drill bit used to cut these holes was cannulated so that it could fit over the

previously installed guide pin. The purpose of the drill bit was to cut a pilot hole for the screw and also to cut a slightly larger hole for the barrel of the sideplate. The hole cut for the screw was approximately 8 mm in diameter while the hole for the barrel of the sideplate was approximately 12 mm in diameter. It was necessary to clamp and hold the femoral head in place as the bit cut a hole in it.

The screw was installed next. The screws had hexagonal rather than rounded shafts to prevent rotation of the screw once engaged in the similarly shaped barrel of the sideplate. A large T-handle was used to install the screw in the femur and the femoral head. As the screw passed into the femoral head, the head was again clamped and held to prevent rotation of the head during installation of the screw. When installing the screw in bone 1934L, for the 150-degree sideplate, it was necessary to hold the femoral head in a slightly varus position. Holding the head at this angle was necessary to achieve a better screw placement in the femoral head. Once the screw was installed, the sideplate could be attached.

The sideplate was installed next. The angle of the sideplate barrel was adjusted by turning a worm screw that raised or lowered the barrel angle with respect to the mounting surface of the sideplate. The sideplates were set at 135-degrees and 150-degrees and checked with an angle gage before installing. Installation of the sideplate consisted of fitting the barrel of the sideplate over the end of the screw. Once the screw was engaged in the barrel of the sideplate, a mallet was used to drive the sideplate flush against the femoral shaft.

It should be noted here that it was necessary to remove a portion of the Bondo™ cup from around the base of bone 1934L. This was done in order to be able to install the 150-degree sideplate flush against the bone. This type of removal was not necessary for

the 135-degree sideplate as it was not located as far down on the shaft of the bone and therefore did not come in contact with the Bondo™ cup. For this reason, the femurs should not have been cut to 23 cm lengths; they should have been longer. After the sideplate was driven flush with the bone, the pilot holes for the screws that would hold the sideplate to the bone were drilled.

The screws used to hold the sideplate in place were stainless steel non-cannulated cortical bone screws. An electric drill with the appropriately sized bit was used to cut pilot holes for the bone screws. A bit guide was used to keep the pilot holes somewhat straight. Shorter screws should have been used if this had been an actual surgery, as these protruded through the femoral shaft a centimeter or more in some cases. However, as this was only an experimental test, the longer screws did not pose any problems.

Figure 3.10 shows a step-by-step diagram of the procedure used to install the screws and sideplates used in this experiment. In **Figure 3.10**, the first frame shows the installation of the guide wire using the angle guide to properly align the wire. The second frame shows the pilot hole for the screw and barrel of the sideplate. In the third frame, the t-handle is used to install the screw. The final frame shows the installation of the sideplate. The installation of the sideplates was accomplished in a few hours and the experimental testing began immediately after installation.

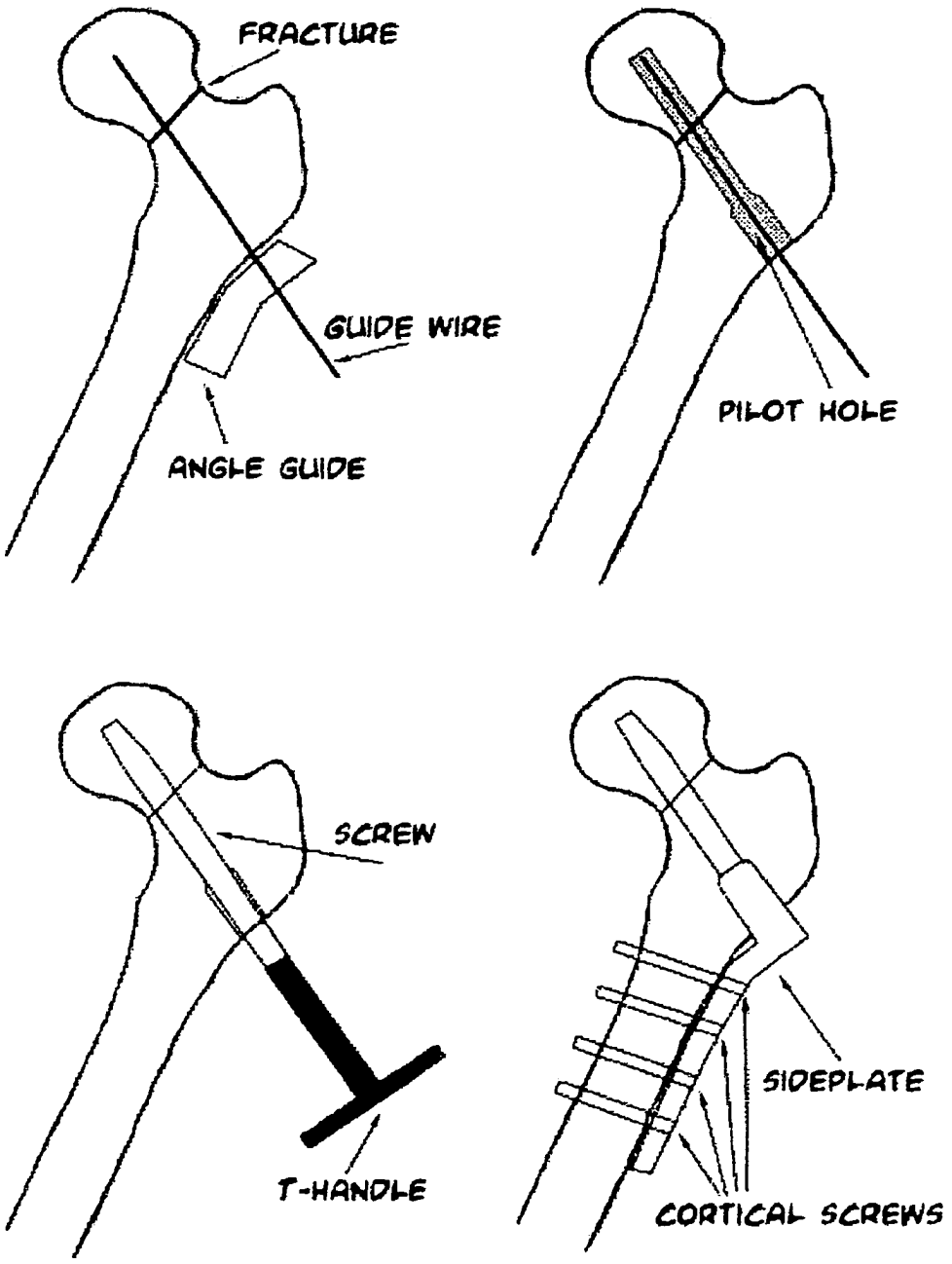

Figure 3.10 - Diagram of the major steps in the installation of the fixation device.

Experimental Testing Procedure

The experimental tests were divided into two sections. The first type of test was an intact test. The purpose of the intact tests was to establish a baseline from which to reference any change in the performance of the femurs after fixation by the different devices. The second type of testing was with the screw and sideplate installed. One femur was tested with a screw installed at a 135-degree angle and the other femur was tested with a screw installed at a 150-degree angle.

Intact Testing. Intact testing refers to testing the femur in an intact state with no fixation device or osteotomy. Intact testing serves as a baseline for the other tests. The first step in the intact testing procedure was to grip the intact femur in the v-block. The potted base of the femur was set in the v-block and the two bar clamps on the v-block were tightened to hold it in place. The angle of the femoral shaft was checked to ensure that the femur was angled 20-degrees from vertical. Next, the power supply for the LVDT's was turned on to allow its output to stabilize while the rest of the setup procedure continued.

As the power supply was warming up, the LVDT's were put in place. LVDT I was placed parallel to the femoral shaft, at approximately a 20-degree angle from vertical. LVDT II was placed in contact with the greater trochanter at an angle of 45-degrees from vertical. The positions of the LVDT's were checked with an angle gage several times throughout the setup process. After the positions of the LVDT's were satisfactory, they were zeroed.

The LVDT's were zeroed so that they would be at or near the center of their useful range. Zeroing the LVDT's consisted of moving them along their axis until their output was near zero volts. At this point, the LVDT is able to measure both positive and negative deflections. Also, the LVDT probe may bottom out or become fully extended in which case it could not possibly measure any more deflection. Therefore, if the LVDT's were not zeroed, their output may contain errors. Near the limits of the LVDT's measurement range, the output becomes nonlinear.

Once the LVDT's were placed and zeroed, the cross head of the INSTRON was fitted with a large flat aluminum block. This block was used to apply the force to the femoral head. The block was coated with petroleum jelly to allow the femoral head to slide underneath the surface of the block. The cross head of the INSTRON was now moved into a position just above the femoral head. When the distance between the block and femoral head approximately equaled the thickness of the sheet of paper, the testing was ready to begin.

The intact testing consisted of four rounds with three runs per round. The INSTRON was set to move the cross head down at a rate of 12.5 mm per minute until the predetermined maximum load was reached. During the first round of testing the femur was loaded from 0 N to 500 N. The second round increased the maximum load to 750 N, the third round to 1,000 N and the fourth and final round to 1,350 N. There was one exception to this procedure. Bone 1880R seemed too fragile to continue all the way to the 1,350 N round and testing was stopped at the 1,000 N round. Later this bone was removed from the study when it was destroyed during the installation of the 150-degree device. This bone was replaced by bone 1934L. Data from each round was stored upon completion of that round.

Fixation Device Testing. The fixation device testing was done immediately following the installation of each device. When mounting the fractured and fixed femurs in the v-block, it was necessary to rotate the v-block slightly to accommodate the sideplate. If the v-block had not been repositioned, the sideplate would have contacted the v-block. This would have created a new fulcrum point that did not exist in the intact testing. Again, this is another reason that a longer femur would have been preferred.

The same procedure for positioning and zeroing the LVDT's for the intact testing was followed for the device testing. The LVDT's were placed in the same locations as they were in the intact testing. The same order and number of runs were performed on the fixed femurs. The testing started with three runs with a 500 N maximum load and worked up to three runs with a 1,350 N load. Data from each run was stored upon completion of the run.

The data recorded during the experimental testing was transferred from LabView to a text file containing the force and displacement from the INSTRON along with the displacement measured by the two LVDT's. The text file was opened in Microsoft Excel for further analysis. The data consisted of the INSTRON cross head displacement, the measured load, the displacement measured by LVDT I, and the displacement measured by LVDT II. All of the data was exported to Excel in units of Newtons and millimeters.

Once in Excel, the data was zeroed. This was done because the output from the LVDT's did not reset to zero voltage after each run. Instead of rezeroing the LVDT's after each run, the amount of initial offset was simply removed from the data set for each LVDT in Excel so that all the LVDT readings started at zero. Charts and tables were prepared to visualize and further study the data.

Definition of Experimental Results Terms

The experimental data from this study was used to calculate stiffness values for the femurs. Stiffness was defined as the amount of load per deflection. The units for stiffness were N/mm. The nonlinearity of bone presented some challenges to calculating a stiffness value since stiffness is a function of the applied load. To produce an average stiffness value, a linear regression analysis was performed on each data set. The stiffness for the femur was defined as the slope of the linear trend line associated with each data set. Three distinct stiffnesses were calculated from the experimental results. Referring back to **Figure 3.5**, one can see the placements and locations of each of the measuring devices.

Stiffness at the Point of Load Application (Overall Stiffness). An overall axial stiffness was calculated from the displacement data recorded by the INSTRON. This stiffness value will be referred to as the overall stiffness since it was calculated from data that represents the overall displacement of the femur. It was calculated by dividing the force measured by the INSTRON during the tests by the overall displacement of the femur as measured by the cross-head of the INSTRON.

Stiffness at Point One (Neck Stiffness). The neck stiffness was measured by LVDT I. This data was recorded with the LVDT placed underneath the femoral neck at an angle of 20-degrees (parallel to the femoral shaft.) The previous study by Lynn did not include this type of displacement measurement.

The neck stiffness is essentially a measurement of the effect of screw angle on the bending of the screw. The intact measurements for neck stiffness contain misleading data. This misleading data was discussed previously in the section "Debugging the Fixture." With this misleading data, it is difficult to use the intact experimental results as a baseline for comparison. However, these results do give useful information on the overall deflection history of the femur during loading.

Stiffness at Point Two (Shaft Bending Stiffness). The shaft bending stiffness was recorded by LVDT II. This LVDT measured the deflection of the greater trochanter of the femur. LVDT II was placed at a 45-degree angle from the vertical. Most of the deflection measured by LVDT II is the result of the deflection of the femoral shaft.

CHAPTER 4

FINITE ELEMENT MODELING METHODS

In addition to experimental and analytical models, finite element (FE) models were also constructed to test the performance of the two different screw angles. Several different FE models were built. Both three-dimensional and two-dimensional models were constructed from an actual femur geometry.

The two-dimensional models consisted of an intact version, a version containing a 135-degree screw and one containing a 150-degree screw. The two-dimensional models were constructed from x-rays that were taken of the femurs both before and after the screws were installed.

The three dimensional models were constructed from CT scans of the femurs. Only intact versions of the three-dimensional model were constructed. Time and available processor power did not allow for three-dimensional models with a screw installed.

The finite element models were designed with ANSYS (ANSYS, Inc.; Southpointe; 275 Technology Drive; Canonsburg, PA 15317) versions 5.4 and 5.6. The initial models were developed under ANSYS 5.4. Later, an update to version 5.6 was purchased, and all the final simulations were run with ANSYS 5.6. The computers used to run the simulations were IBM compatible PCs running Windows NT. The computers

used to develop the initial geometry and some of the meshes were 200 MHz machines containing only 35 MB of RAM. However, it soon became necessary to switch to computers that were more powerful to continue the work. The computers used for the remainder of the FE formulation and solutions were Dell Pentium III 866 MHz machines with 256 MB of RAM and 20.4 GB hard drives.

Two-Dimensional Finite Element Models

Building the Intact Femoral Geometry from the CT Scout Image

The first step in building the FE models was to transfer the actual geometry of the femur into a digital format. The intact two-dimensional models were constructed from the CT scout images taken of the femurs during the CT scanning process. The scout images were taken before the installation of the fixation device. The scout images were digital images, and a software program was used to locate keypoint coordinates along the contour of the femur. The software program used for the keypoint coordinate location step was Image Tool version 2.00 for Windows (The University of Texas Health Science Center; San Antonio, Texas.) ANSYS 5.4 and 5.6 were used to convert the keypoints coordinates into a FE model.

Generating Keypoint Data for Model Creation. Using Image Tool, keypoints were manually selected from the CT images and stored in a database. This database was simply a text file containing the x and y coordinates of the keypoints. The

keypoints chosen for the model were points lying along both the inner and outer perimeters of the cortical bone of the femur. By choosing these keypoints, an outline of the cortical and cancellous areas of the femur was defined. The database of keypoints was copied to the Windows clipboard and imported into Notepad where it was saved as a text file. Notepad is the Windows text editor found under the startup menu in the Accessories folder. **Figure 4.1** shows a sample of the selected keypoints, and **Table 4.1** lists the corresponding database generated by Image Tool.

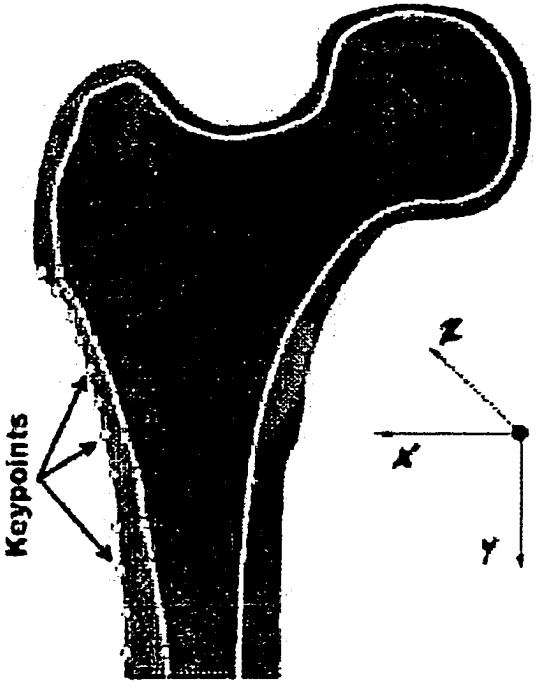

Figure 4.1 - Example of the keypoints used to define the geometry of the two-dimensional FE models (the image has been edited to remove the dark background for clarity.)

Table 4.1 - Database generated by ImageTool for the keypoint coordinates highlighted in **Figure 4.1**.

Keypoint Number	X	Y	Keypoint Number	X	Y
1	179	219	13	177	172
2	187	220	14	174	172
3	185	212	15	175	166
4	178	211	16	173	166
5	178	204	17	173	160
6	184	203	18	171	160
7	183	195	19	171	155
8	177	194	20	169	155
9	181	185	21	169	152
10	176	185	22	167	151
11	179	179	23	168	148
12	176	178	24	165	148

Notice in **Figure 4.1** the level of pixelation, or graininess of the image, that occurs when enlarging the image to a useable size. Although the external geometry is still recognizable, the internal geometry is very difficult to define. In the final two-dimensional models, the internal geometry was determined based on manual measurements of cortical thickness at several locations. Average values of six measurements per side per cross section were used to determine the cortical thickness in the XY plane.

Model Creation Using the ANSYS Preprocessor. The text file of keypoint data was opened in Notepad and ANSYS was started. Once opened, the ANSYS preprocessor was used to create the geometry of the femur. The command to enter keypoints by their X, Y, and Z coordinates was selected and the keypoints were entered

into the ANSYS environment. The Z coordinate for all of the two-dimensional models was left at zero.

The next step was to connect the keypoints with lines. The ANSYS command to create straight lines was selected and lines were made between the keypoints. Creating the lines was a simple matter of selecting the keypoints that represented the endpoints of a line segment. After creating the outline of the geometry, the distance from the tip of the greater trochanter to the bottom of the femur was measured and scaled to match the dimensions of the actual femur if necessary.

From the newly created lines, areas were defined. These areas represented the different bone densities of the bone. Each area was given material properties based on the area of bone that it was representing. The cortical bone received a modulus of elasticity (E) of 17,000 MPa, and the cancellous bone was given a modulus of elasticity of 300 MPa. All areas representing bone were assigned a Poisson's ratio of 0.33. Also, in a later step, each area was assigned an element thickness to help simulate three-dimensional properties in the two-dimensional models. **Figure 4.2** shows the general steps involved in creating one of the two-dimensional intact finite element models.

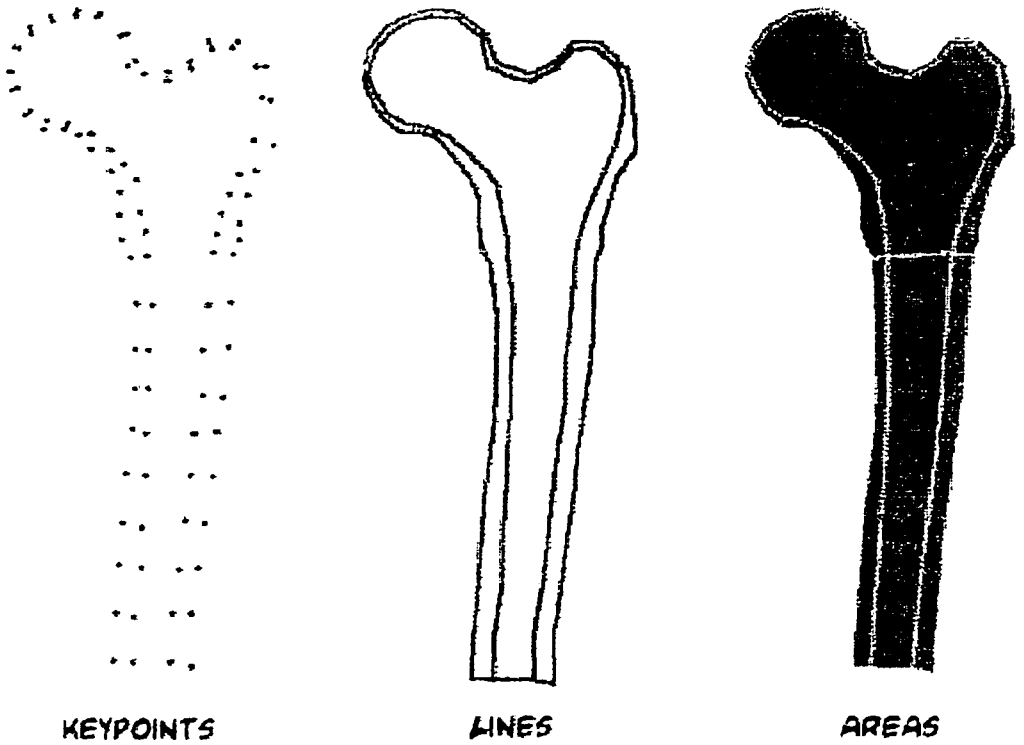

Figure 4.2 - Diagram of the three major steps in creating the two-dimensional FE geometry, from the definiton of the keypoints to the creation of lines between the keypoints to the creation of areas based on the boundary lines.

Building the Fixated Geometry

The 135- and 150-degree fixated geometries were created from the intact geometry. First, a fractured base model was built. This base model was essentially the intact model with a fractured femoral neck. The fracture was simulated by creating a line across the femoral neck at a 20-degree angle from the y-axis and using it to divide the areas of the femoral neck. It is important that the femoral head fragment is completely separate from the rest of the femur. No keypoints may be shared between the fragment and the femur. Also, no gap was left between the fragment and the femur. The base

geometry is shown in **Figure 4.3**. There is no visual difference in the picture in **Figure 4.3** and the intact geometry. Note that the colors in **Figure 4.3** correspond to regions of the femur where the thickness of the 2D model was changed, as discussed later. The difference between the intact and fixated geometry lines in the separation of the femoral head from the rest of the femur, even though no actual separation can be seen.

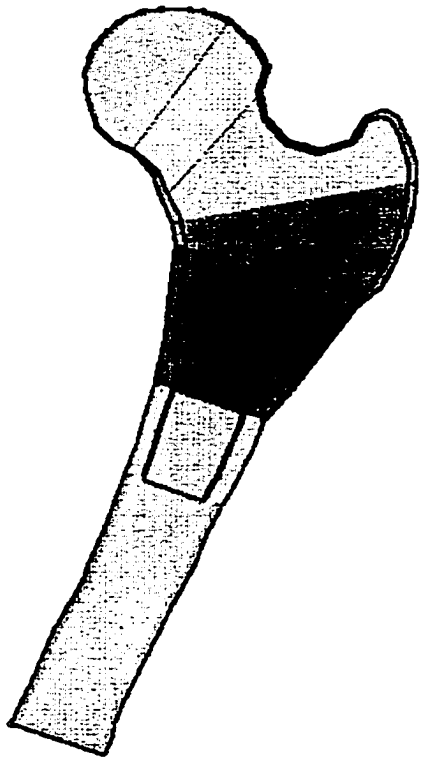

Figure 4.3 - The base geometry created for the FE fracture models, also very similar in appearance to the intact geometry.

Next, the screw and sideplate barrel were added to the base geometry. To create the screw, the working plane was rotated to correspond to the angle of the screw. A rectangular area was created at the new angle. The area representing the screw was 7.22 mm by 85 mm for the 135-degree fixation and 105 mm for the 150-degree fixation. A

second rectangular area was created to represent the barrel of the sideplate. The barrel area was 12.6 mm wide by 37.3 mm long.

The area representing the barrel was subtracted from the base geometry. Subtracting the barrel from the base geometry simulates the cutting the hole that is drilled for the barrel. Next, the area representing the screw was subtracted from the base geometry and the barrel simulating the hole cut for the screw.

Upon cutting the areas for the screw and barrel hole, the area of the greater trochanter is no longer connected to the rest of the model. It is no longer connected to the femoral head because of the fracture and the screw has separated it from the rest of the femur. This is a consequence of using the two-dimensional model. **Figure 4.4** shows the region that is disconnected from the rest of the model.

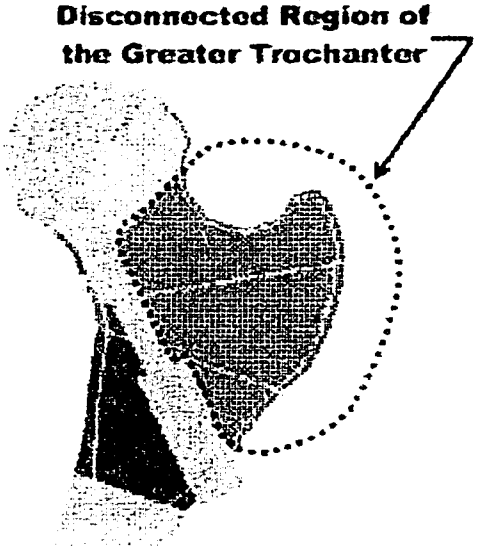

Figure 4.4 - Illustration of the disconnected greater trochanter region.

The greater trochanter region was connected by using a common boundary between the screw / sideplate and the cancellous bone of the greater trochanter region. The screw and sideplate were also attached to the bone below it in a similar manner. This

solution restricted the screw from sliding past the cancellous bone of the intertrochanteric region. Although the sliding of the screw against the cancellous bone would have been perferred, the much softer material properties of the cancellous bone to which the screw was bonded allowed for some relative motion. Fortunately, since the fracture gap was set to zero, only a limited amount of sliding would be expected. The screw was not bonded to the barrel of the sideplate and the fracture surfaces remained separate from each other by using contact elements, as described later.

Manual Measurements of Cortical Bone Thickness

Due to difficulties in detecting the interface between the cortical bone and the cancellous bone from the CT scout images, physical measurements of cortical thickness were taken. The first step in performing the measurements was to section one of the femurs and take measurements of the cortical thickness for each section. **Figure 4.5** shows the locations of the cross sectional cuts where measurements were recorded. These cross sections were scraped clean of any cancellous bone and other material, leaving only the harder cortical bone.

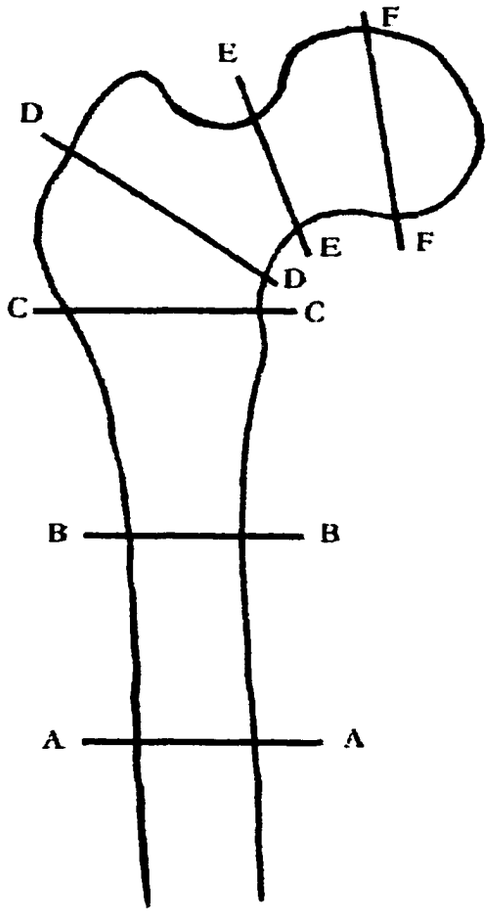

Figure 4.5 - Location of the cross-sectional cuts made for determining cortical and cancellous thickness.

Ten thickness measurements were made per cross-section. The ten measurements were equally spaced around the perimeter of the cross-section and normal to the cortical surface. Also, the diameters corresponding to the x and z axes were measured. **Figure 4.6** shows the locations of the ten measurements for cross-section D-D shown earlier in **Figure 4.5**. All of the measurements along with sketches of the six cross sections can be seen in **Appendix A**.

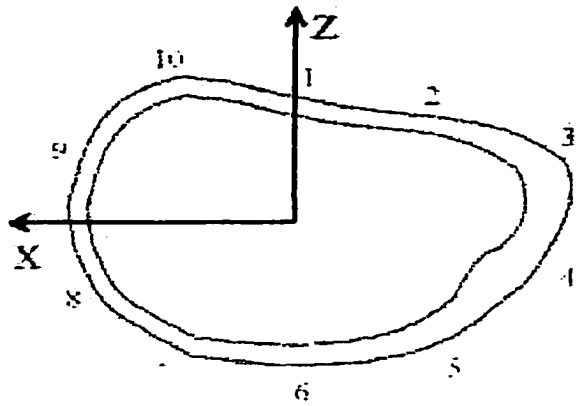

Figure 4.6 - Locations of the ten measurements for the cross section D-D.

To determine the thickness of the cortical shell in the two-dimensional finite element model, the measurements from one half of the cross-section (measurements 1 through 6) were averaged to define an average cortical thickness for that side of the two-dimensional model. The other measurements (6 through 10 and the measurement at location 1) were used to determine the average cortical thickness on the opposite side of the cross section. **Table 4.2** lists the cortical thickness calculated at each cross section.

Table 4.2 - Cortical thickness calculated by averaging the measured thickness values.

Section	Right Thickness (mm)	Left Thickness (mm)
AA	6.15	6.15
BB	6.07	5.95
CC	3.49	2.54
DD	2.50	2.06
EE	2.38	1.43
FF	0.52	0.48

Embedding Measured Thicknesses into the Two-Dimensional Finite Element Models

Using the data from **Table 4.2**, the two-dimensional FE model was modified to better represent the cortical thickness. For instance, the average cortical thickness at section C-C is 3.49 mm on the right-hand side and 2.54 mm on the left-hand side. Using this information, keypoints were defined at section C-C that would set the cortical thickness of the FE model to 3.49 mm on the right-hand side and 2.54 mm on the left-hand side at section C-C. This process was repeated for each cross section, and a new cortical thickness was established based on these average cortical thicknesses. The cortical thickness keypoints between sections were linearly interpolated. **Figure 4.7** shows the results of the new manually measured cortical thickness data, on the left is the FE model created using the physical measurements of cortical thickness and on the right is the FE model created from the CT scout image. Although image processing techniques could be used to obtain a closer match between the CT based model and the model based on direct measurement of thicknesses, such techniques were not pursued as part of this work.

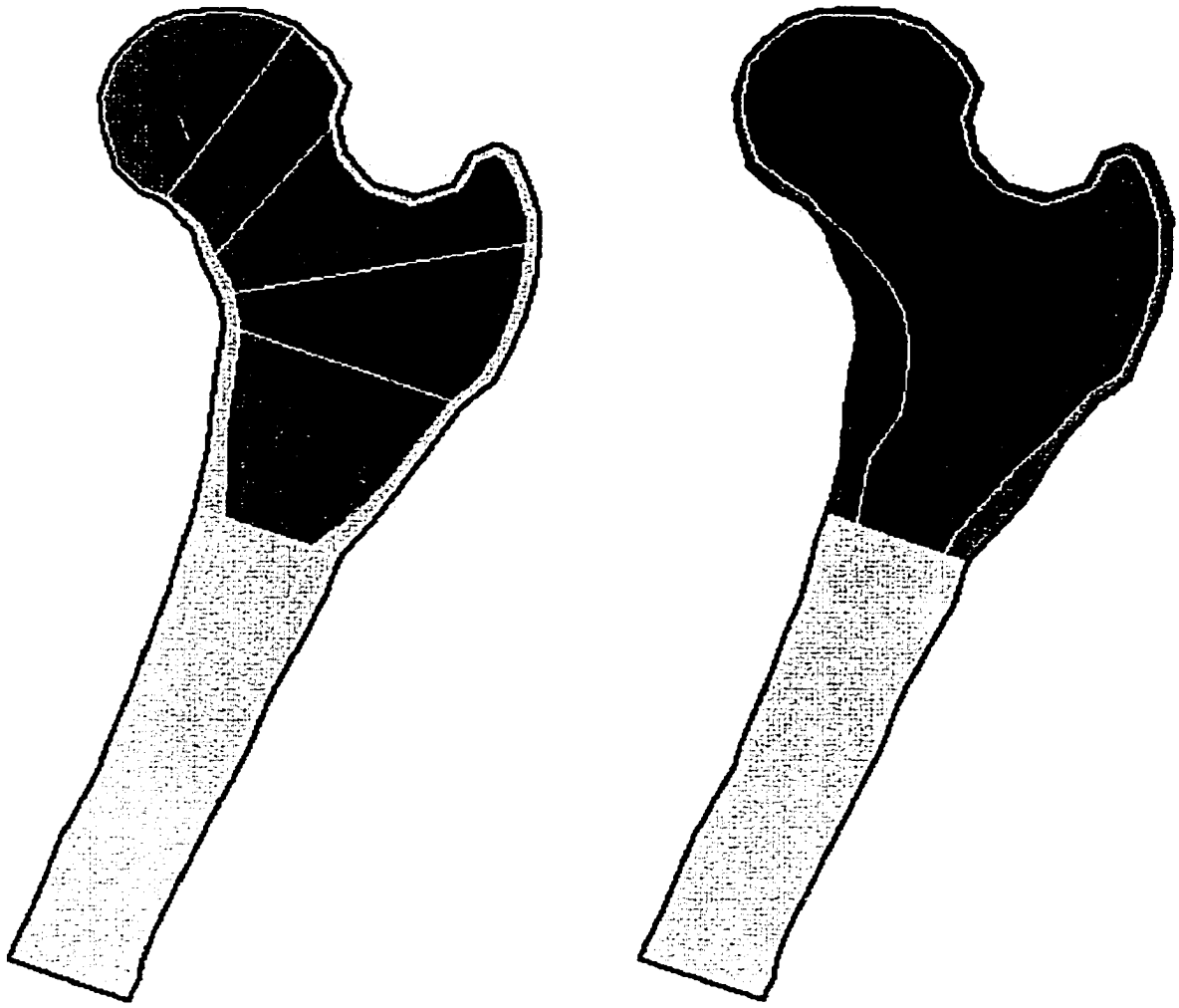

Figure 4.7 - Comparison of the two-dimensional models based on physical measurements of cortical bone thickness (left) and the CT scout image (right).

Determination of Element Thickness

Simulating the response of a femur using a two-dimensional FE model requires that thicknesses be chosen for each region of the femur based on the major and minor diameters of the femur in each of these regions. The first step in calculating the element thickness (the thickness in the z-direction) for each region was to compute the moment of inertia for the region assuming the cross-section had an elliptical shape. The elliptical cross sections were

based on the major and minor diameters measured for each cross section, as listed in **Table 4.3**. These z-direction thicknesses were computed by equating the moment of inertial of the assumed elliptical cross-section with a rectangular cross-section, where the thickness of the rectangular cross section corresponds to the thickness in the z-direction.

Table 4.3 - Major and minor diameters measured for each cross section.

Section	Major Diameter (mm)	Minor Diameter (mm)
AA	27	14.7
BB	26	14
CC	35	24.6
DD	57.2	34.5
EE	34.1	27.8
FF	42.1	41.1

An Example Element Thickness Calculation

Using Section D-D as an example, the first step in calculating the element thickness in the z-direction is to solve for the elliptical moment of inertia of the cross section. From **Table 4.3** the major and minor diameters for Section D-D are 57.2 mm and 34.5 mm respectively. From **Table 4.2** the cortical thicknesses for Section D-D are 2.5 mm and 2.06 mm for the right and left sides, respectively. A reference diagram for Section D-D can be seen in **Figure 4.8**.

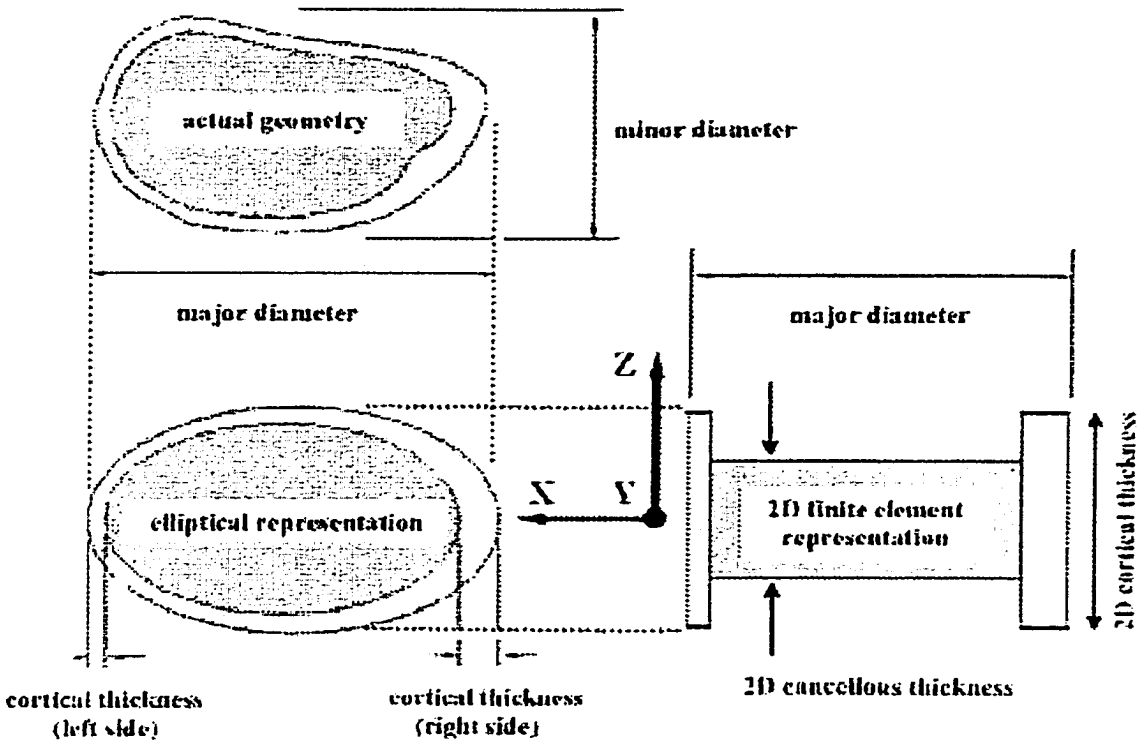

Figure 4.8 - Reference diagram of Section D-D for the example element thickness calculation.

Next, the moments of inertia for the elliptical cortical and cancellous bone areas are calculated. The equation for the moment of inertia about the centroid for an elliptical area is given as

$$Ielliptical = \pi \cdot a \cdot b^3 / 4 \qquad \textbf{4.1}$$

where a is the minor radius and b is the major radius of the ellipse defining the boundary of the cancellous bone.

Using **Equation 4.1** and the parallel axis theorem, the equation for the moment of inertia of the cancellous bone is determined to be

$$Icancellous = \pi \cdot a \cdot b^3 / 4 + A \cdot y^2 \qquad \textbf{4.2}$$

where A is the area of the cancellous bone and y is the distance between the centroid of the cancellous bone and the centroid of the entire cross section. The equation for the moment of inertia of the cortical bone is

$$Icortical = \pi \cdot a \cdot b^3/4 - Icancellous \qquad \textbf{4.3}$$

where a is the minor radius and b is the major radius of the ellipse defining the boundary of the coritical bone (note that a and b now relate to the cortical bone, not the cancellous bone as used in **Equations 4.1** and **4.2**). After calculating the elliptical moments of inertia, equations for the rectangular moments of inertia were derived. The unknown variable in the rectangular moments of inertia was the element thickness in the Z-direction. The equation for the moment of inertia about the centroid for a rectangular area is given as

$$Irect = b \cdot h^3/12 \qquad \textbf{4.4}$$

where b is the base of the area (element thickness) and h is the height of the area. Based on **Equation 4.4**, the moment of inertia for the cancellous bone is

$$Icancellous(rect) = b \cdot h^3/12 + A \cdot y^2 \qquad \textbf{4.5}$$

where A is the area of the cancellous region and y is the distance between the centroid of the cancellous area and the centroid of the entire cross section. Similarly, the moment of inertia for the cortical bone is

$$Icortical(rect) = b \cdot h_l^3/12 + A_l \cdot y_l^2 + b \cdot h_r^3/12 + A_r \cdot y_r^2 \qquad \textbf{4.6}$$

where h_l and h_r are the average cortical thickness of the left and right sides of the cross section, respectively as calculated from the measured cortical thickness; A_l and A_r are the

areas of the left and right cortical regions of the rectangular equivalent cross section; and y_l and y_r are the distances between the centroid of the left rectangular equivalent cortical area and the centroid of the rectangular equivalent cross section

The final step in calculating the element thicknesses was to set the rectangular moments of inertia equal to their elliptical counterparts and solve for the unknown variable representing the element thickness. All of these calculations were performed in MathCad and the equations for each section can be seen in **Appendix B**.

Averaging the Element Thicknesses

Since the newly calculated element thicknesses were to be assigned to entire areas instead of point locations from which they were calculated, the final element thickness for an area was based on the average of the element thicknesses from the two bounding cross sections. An exception was made for the area representing the tip of the femoral head. This area only had one cross section associated with it, therefore, the element thickness for this area was averaged between the thickness calculated at section FF and zero. Zero was used because the element thickness at the tip of the femoral head would indeed be zero.

Another exception worth mentioning is the femoral shaft. The two-dimensional model uses a solid femoral shaft, instead of a hollow shaft. In the two-dimensional model, the shaft is one area it is not broken into smaller areas like the more complex geometry of the proximal femur. Therefore, it is assigned a single element thickness. **Figure 4.9** shows the areas representing the different element thicknesses and **Table 4.4** lists the corresponding thicknesses assigned to those areas.

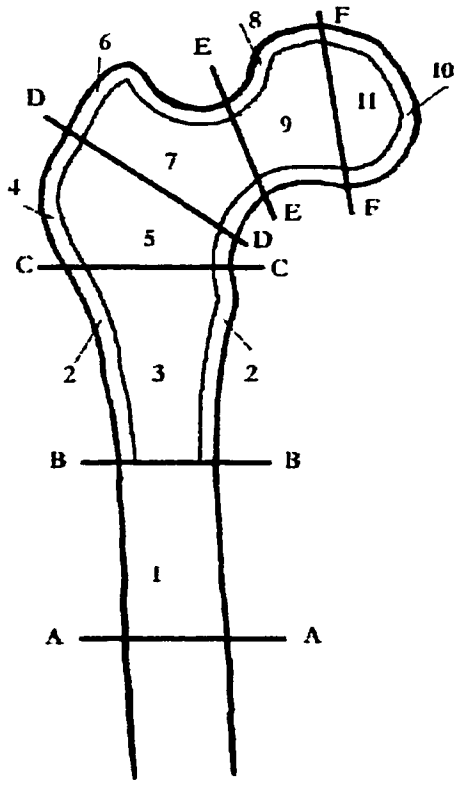

Figure 4.9 - Areas of the two-dimensional finite element model, each area represents an area with a different element thickness. Each of the even numbered areas occurs on both sides of the model as shown for area 2.

Table 4.4 - Element thicknesses assigned to each of the areas of the finite element model, the area numbers correspond to the numbered areas in **Figure 4.9**.

Area	Thickness (mm)
1	14.5
2	17.0
3	13.0
4	23.0
5	15.5
6	25.0
7	16.5
8	27.0
9	19.5
10	16.5
11	12.0
Screw	4.1

Defining Material Properties

Three different material properties were defined for use in the finite element models. These three materials were cortical bone, cancellous bone, and stainless steel. The properties defined for each material were Young's Modulus and Poisson's Ratio, as listed in **Table 4.5**.

Table 4.5 - Materials used in the finite element models and their corresponding properties.

Material	Material Number	Young's Modulus (GPa)	Poisson's Ratio
Cortical Bone	1	17	0.33
Cancellous Bone	2	0.3	0.33
Stainless Steel	3	190	0.3

Meshing the Geometry

The elements used to mesh the two-dimensional models were six-noded triangular elements (known as ANSYS's plane2 elements). These elements have nodes at each vertex and at the midpoint of each side. The area representing the interior of the femoral head and neck was meshed first in each of the two-dimensional models.

Intact Mesh. The meshing method used in the final models was a combination of automatic mesh generation and manual element size control. ANSYS allows the user to control the element size based on either the average element side length or a certain

number of elements per boundary line. Initially the global element size was set to 3 mm and the interior proximal areas of the model were meshed. The cortical shell of the proximal femur was meshed with the element size set to 2 mm. Finally, the shaft of the femur was meshed with an average element side length of 5 mm.

Fixated Mesh. For the models containing hip screws, the screw and sideplate barrel were meshed first with the element side length set to 3 mm. Then the interior of the proximal femur was meshed with 3 mm elements followed by the proximal cortical shell being meshed with 2 mm elements. Finally, the femoral shaft was meshed with 5 mm elements.

Mesh Refinements. To improve the accuracy of these models, the elements surrounding the fracture site were further refined. This process was repeated for the intact models as well even though there was no fracture present. The elements were refined by selecting them and using the ANSYS MeshTool to refine the elements by one level. This mesh refinement was an automatic process, except for the selection of the elements to be refined.

Contact Elements. For the models containing screws, it was necessary to add contact elements along certain surfaces. Without contact elements ANSYS does not recognize that certain regions should make contact with each other, instead the regions would simply pass through one another without resistance. Contact elements were used to

allow sliding between the screw and the barrel of the sideplate. Also, contact elements were applied to the fracture surface.

The contact elements were created using the ANSYS contact wizard which allows the lines where contact could occur to be selected and a frictional coefficient to be assigned. The frictional coefficient used to model the interaction of the screw and barrel of the sideplate was 0.2. This value was based on research of sliding hip screws conducted by Kyle and colleagues (Kyle, et. al., 1980.) The friction coefficient for the fracture surface was set to 0.5. In an actual fracture, the interlocking of bone surfaces would allow high frictional forces to be transmitted. The red areas shown in **Figure 4.10** indicate the locations of the contact surfaces.

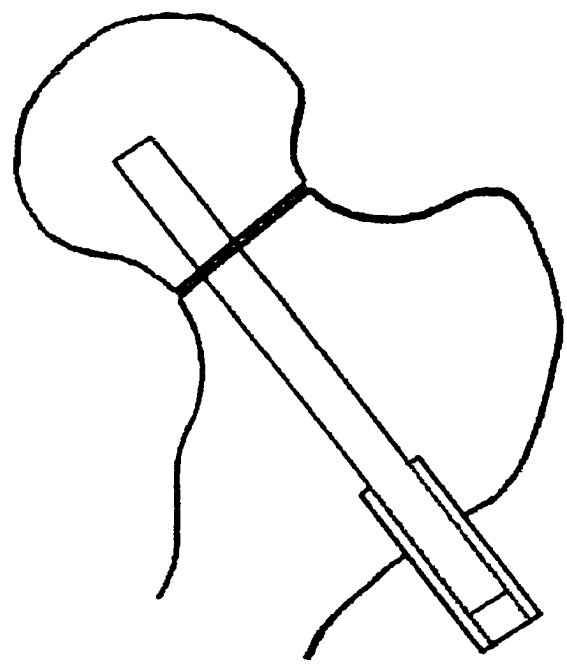

Figure 4.10 - FE fracture model showing the location of contact elements (red).

Loading and Boundary Conditions

To simulate the loading conditions applied experimentally, the bottom of the femur was completely restrained. This constraint was simulated by applying a fixed displacement of 0 cm in the X and Y directions to the nodes along the bottom of the femur. The model femur was loaded with a force of 1,350 N applied to the femoral head at an angle of 20-degrees from the vertical.

Convergence Testing

Once the initial meshes were satisfactorily completed, it was necessary to run convergence tests. The convergence tests were used to determine the minimum number of elements required for an accurate solution. Convergence tests are necessary for FE modeling because as the number of elements increases, the stresses and displacements predicted by the model should become more accurate, or at least should converge on a solution. However, by increasing the number of elements in the mesh, the solution time is also increased. The point of convergence tests is to determine the point of diminishing returns, the point at which an increase in the number of elements in the model provides only a minor increase in accuracy.

The convergence study involved constructing four meshes with different numbers of elements for the 135-degree screw geometry. Displacements were compared for each of the four meshes, and the percent difference was computed with respect to the results for the most refined mesh, as shown in **Table 4.6**. Although all of the meshes gave reliable displacement results, meshes containing around 3,000 provided smoother stress contour plots.

Table 4.6 - Results of convergence testing.

Number of Elements	Percent Difference in Displacement from Highest Level Mesh
924	2.79
1,791	4.35
3,122	2.36

These convergence tests do not show the model directly converging to a particular stiffness. In **Table 4.6**, the second mesh, with 1,791 elements, predicts stiffness values with a percent difference higher than that of the 924 element mesh. It should be noted that none of the models predicted stiffness values that were greater than 5% from the highest element mesh. Additional convergence tests should be run to confirm that the meshes converge on a solution.

Final Two-Dimensional Finite Element Meshes

Using the guidelines set forth in this chapter, the three two-dimensional finite element models were created. The final intact mesh contained 2,742 elements, the 135-degree fixated mesh contained 3,179 elements, and the 150-degree fixated model contained 3,307 elements. The intact mesh required much fewer elements because the screw did not have to be modeled. The three final two-dimensional meshes can be seen in **Figure 4.11**.

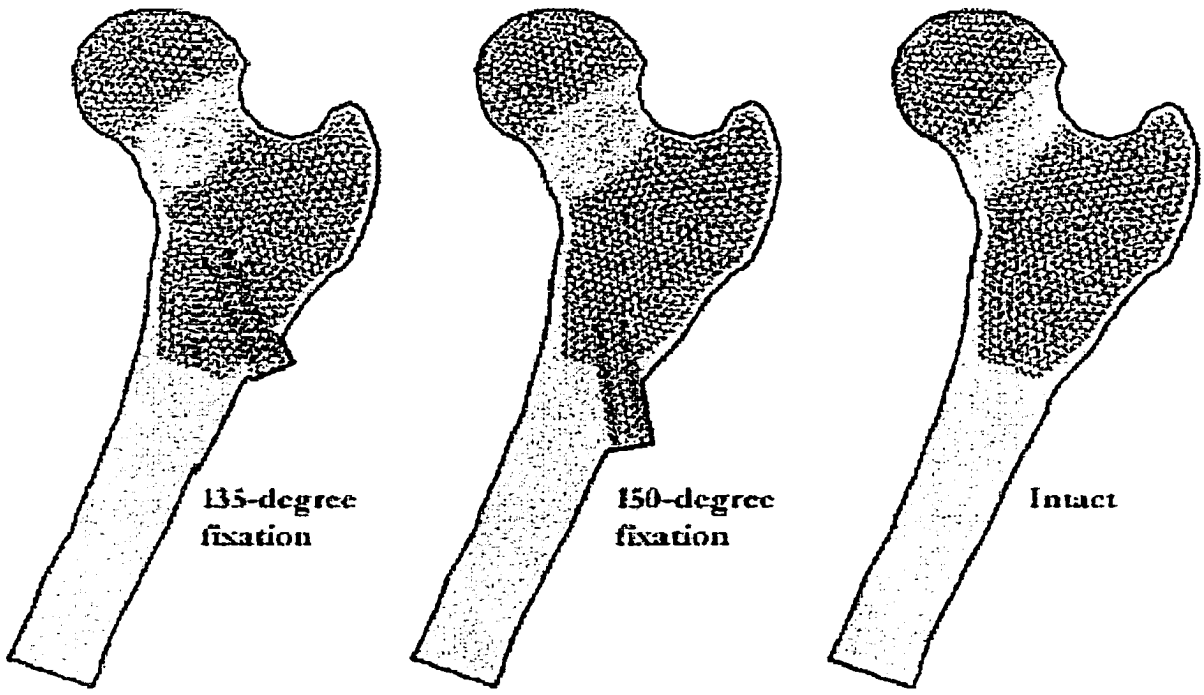

Figure 4.11 - The final two-dimensional meshes created for the study.

Three-Dimensional Models

The three-dimensional models were constructed in a similar manner to the two-dimensional models. The first step in construction of the three-dimensional models was to take a CT scan of the femurs. The CT scan for femur 1880L was to create the three-dimensional model geometry. The FE model was built up, one layer at a time, from the data in the CT scans.

Building the Intact Femoral Geometry from the CT Slices (ANSYS)

A CT, or Computed Tomography, scan is an x-ray based procedure that uses many parallel x-ray images to produce cross-sectional views of the object being scanned.

The cross-sectional views can be stacked one on top of another to create a three-dimensional representation of the scanned object. Each individual slice in a set of CT scans is an x-ray representation of the cross-section of the object in one plane. All of the planes containing the cross sections of the object are parallel. The spacing between the slices is the axial resolution of the scan.

For the CT scan in this study, the axial resolution was 1 mm in the proximal portion of the femur. This 1 mm resolution was increased to 10 mm at a distance of 9 cm from the tip of the greater trochanter. It was deemed unnecessary to include every slice in the FE model. The model would become too complex if all of the slices were used to create the geometry. Therefore, only every fifth slice was used in the proximal portion of the femur to create the three-dimensional geometry. This procedure left the proximal portion of the femur to be constructed of slices that were 5 mm apart and the distal portion to the constructed of slices that were 10 mm apart. **Figure 4.12** shows the lines representing the CT slices that make up the geometry of the FE femur. **Figure 4.13** is an isometric view of the same lines as shown in **Figure 4.12**. These two figures show that the geometry is very recognizable as a femur, even without using every slice from the CT scan set.

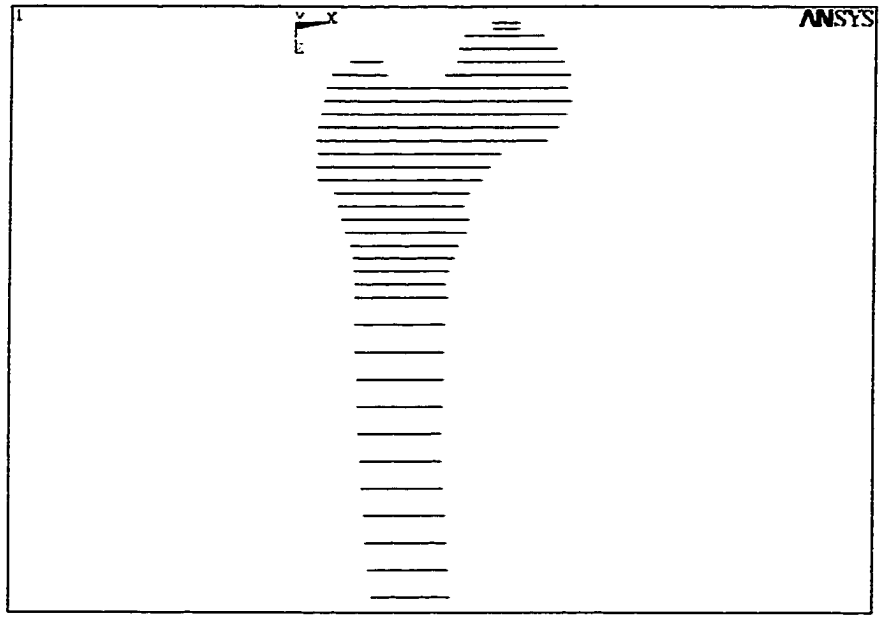

Figure 4.12 - Plot of the lines used to create the three-dimensional model.

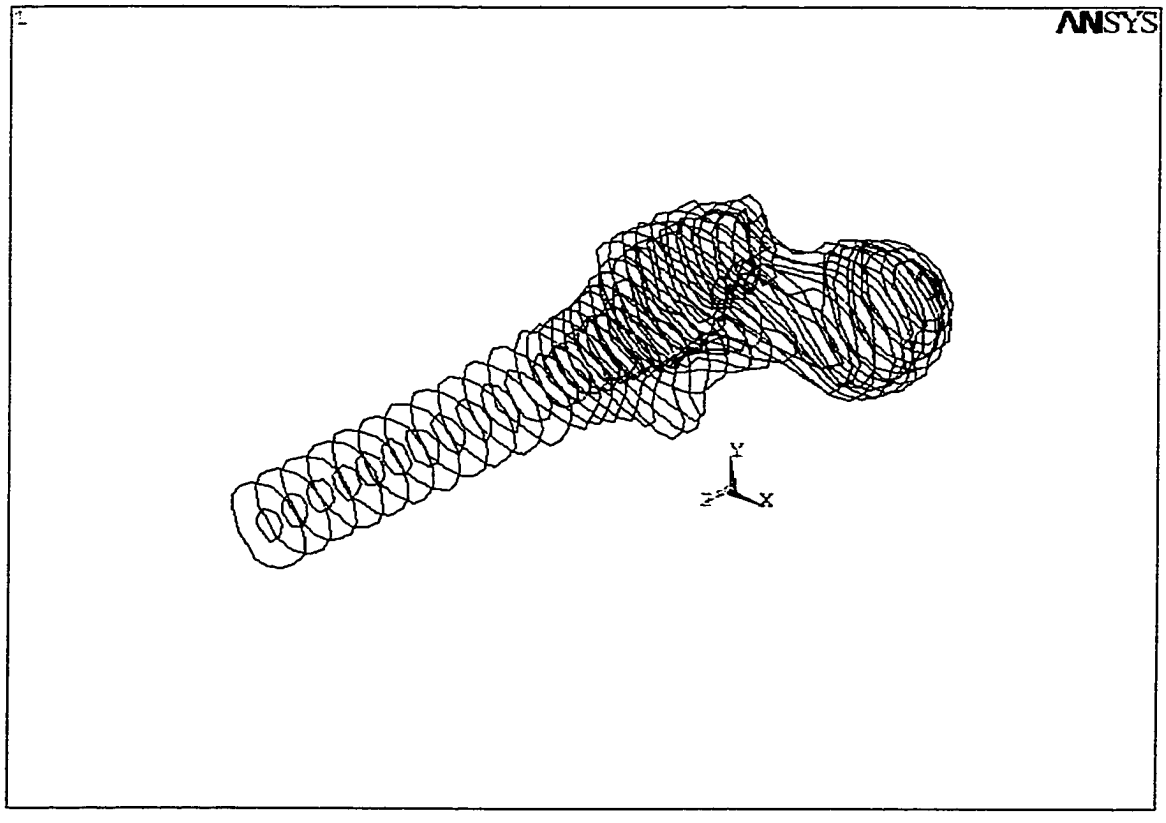

Figure 4.13 - Isometric view of the same lines shown in **Figure 4.12**.

To create each of the contours shown in **Figure 4.13**, keypoints were extracted from each CT slice using Image Tool. This process was very similar to the process used for the two-dimensional model, except that there were many more cross-sections from which to extract keypoint data. A typical cross section with keypoints marked for selection can be seen in **Figure 4.14**. The slice in **Figure 4.14** is taken from the shaft of the femur.

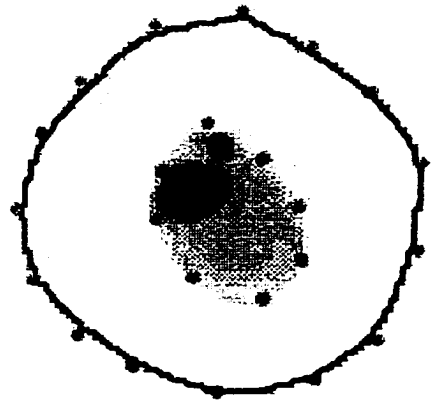

Figure 4.14 - CT scan showing the selection of the keypoints used to create the three-dimensional model. The keypoints are shown as dots on the CT slice.

The keypoint data information was saved in text files using the Windows Notepad program just as in the creation process of the two-dimensional models. The data from each file was used to create keypoints in the ANSYS program. The only difference between the creation of the two-dimensional models and the three-dimensional models was the assignment of the z-coordinates to the separate the slices (the z-coordinate is vertical for the three-dimensional models). The keypoints from the first slice were input into ANSYS with a value of zero for the z coordinate. Keypoints from the next CT slice were given a z coordinate of 13.25.

The z-coordinate value did not represent 13.25 millimeters, but was calculated based on the resolution of the CT images. The ratio between a known measurement and the corresponding measurement in pixels of the CT slice was used to calculate the z dimension of the model. It was known that the aperture off the CT was 19.4 cm; this distance was easily seen on the CT slices. The corresponding distance on the slices was 511 units (pixels.) That gave a ratio of 26.3 units (pixels) per centimeter. Since the slices in the proximal femur were to be 5 mm apart, there should be a distance of 13.25 units between consecutive slices. The entire model was scaled upon completion to reflect units of meters.

As the keypoints from each CT slice were created in ANSYS, lines were drawn between them to create the outline of the slice. After all of the slices were in ANSYS and the keypoints from each slice were connected with lines, the lines from each section represented two contours for each CT slice. One of the contours represented the outer perimeter of the cortical bone. The second contour represented the inner perimeter of the cortical bone. These contours were used to define the boundaries of volumes.

To create the volumes, areas were created by "skinning" the contours. The skinning process is an ANSYS option for creating areas. In the skinning process, the contours that are to define the area are selected and ANSYS creates the area based on the shape of the selected lines. From these areas, the volumes were created.

A volume was created by selecting the surfaces that would define its boundaries and using the ANSYS command to create volumes from surfaces. The only condition for creating volumes or surfaces this way is that the selected lines create a closed loop. As each volume was created, the properties for that volume were defined. These properties

included the material number and element type. The three-dimensional femur created by this process is shown in **Figure 4.15.**

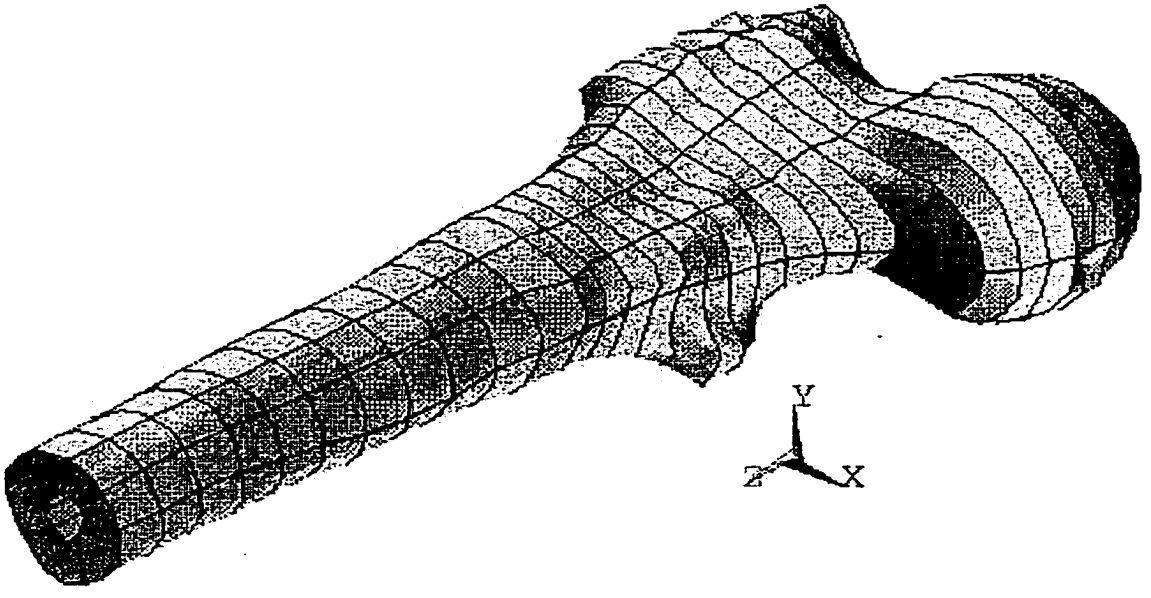

Figure 4.15 - Three-dimensional model created from the CT slices.

Defining Material Properties

The same set of materials and material properties used in the two-dimensional model were used for the three-dimensional model. The materials are listed in **Table 4.5** in the section titled Finite Element Modeling Methods: Two-Dimensional Finite Element Models: Defining Material Properties.

Meshing the Three-Dimensional Model

Once all the volumes that made up the geometry were created, the meshing process could begin. Problems that may occur with elements often involve the aspect ratio of the elements. Elements with sharp angles or high aspect ratios are not desired. Fortunately, ANSYS is capable of searching through the meshed model for elements that may cause errors in the solution. This is fortunate, as it would be nearly impossible to manually check through each of the models 20,000+ elements. Several manual adjustments to the models automatic meshing method were necessary to produce a working mesh. Usually these adjustments were accomplished by manually defining the number of elements that would occur along a line segment.

When meshing the model, the first attempt was to set the global element size to a certain value, 5 mm to begin with, and let the automatic meshing utility do as much of the work as it can. The automatic meshing utility will go through the model and divide the lines of the model to create elements with sides as close to the global element size value as possible. Occasionally, the meshing utility will be unable to mesh a volume because of extremely irregular geometry. In these cases, the program issues a warning stating which volume or line it can not mesh. It is then a simple matter of manually selecting that particular volume or line and giving it a smaller local element size or increasing the number of element divisions on the irregular side.

The next step in meshing the model is to plot all of the borderline elements. ANSYS has a feature that can plot all of the bad or warning elements which was used here. The bad elements are plotted in red and the warning elements are plotted in yellow. The elements that ANSYS considers acceptable are not plotted. The volumes containing

bad or warning elements were remeshed with smaller elements to eliminate any potential elemental problems.

Boundary and Loading Conditions

Once the model was meshed, the boundary conditions were applied to the model. A 1,350 N load was applied at an angle of 20-degrees from the Z-axis. Note that in the three-dimensional models, the Z-axis runs parallel to the femoral shaft. The load was applied directly to the nodes of the elements that would have been in contact with the INSTRON in the experimental setup. Five nodes surrounding the force application point were coupled together. This coupling spread the force over a larger area. The base of the model was constrained by applying a boundary condition to the nodes of the base. This boundary condition allowed the nodes no degree of freedom in the x, y or z directions.

Three-Dimensional Intact Finite Element Model

The final meshed three-dimensional model is shown in **Figure 4.16**. This model bases the interior boundary of the cortical bone on the CT scan, which results in larger thicknesses than was physically measured by sectioning. Therefore, predictions by this model are significantly stiffer than predictions by the two-dimensional model and measurements from the experimental tests.

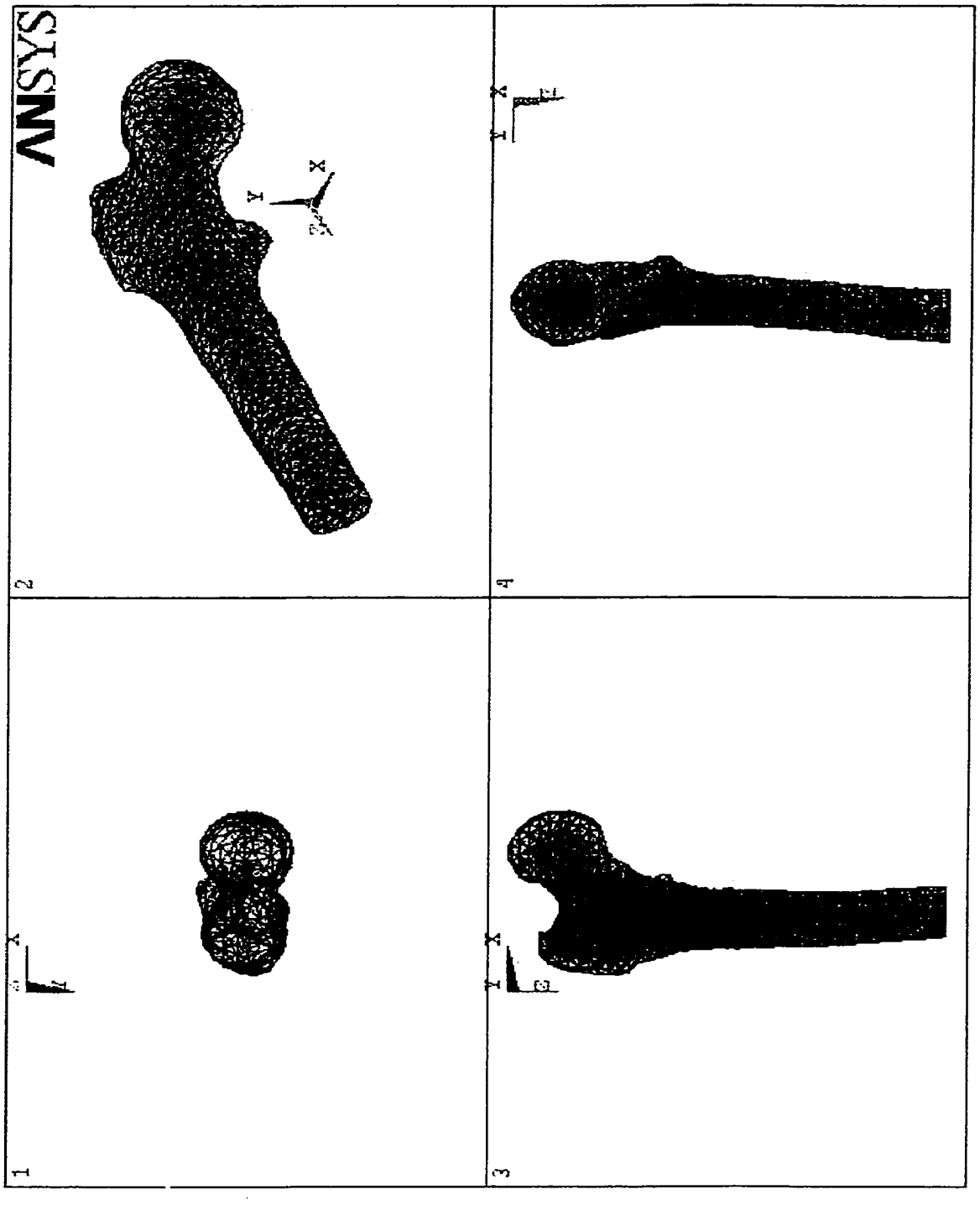

Figure 4.16 - Three-dimensional model meshed entirely with tetrahedral elements, this model contains approximately 22,000 elements.

Building the Intact Femoral Geometry from the CT Slices (I-DEAS)

The ANSYS three-dimensional finite element model created predicted stiffness values that were significantly high. The intact stiffness calculated from the three-dimensional model was over 7,000 N/mm whereas the experimental and two-dimensional model intact stiffness values were much lower. Therefore, another three-dimensional model was created using different methods.

Due to the difficulty in performing Boolean operations in ANSYS on very complex models, the I-DEAS software was used to create a second three-dimensional FE model. Portions of the new model were created using another three-dimensional modeling package, Rhinoceros. The new model is much smoother and has a thinner cortical thickness than the old model. Also, I-DEAS is able to perform the necessary Boolean operations on the geometry. The cortical thickness of the new model is based on manually measured cortical thickness values used in determining cortical and element thickness for the two-dimensional model.

Creating the new three-dimensional model began by exporting the original CT based contours from ANSYS to Rhinoceros in an IGES format. IGES is a uniform translation of three-dimensional geometry used by many three-dimensional modeling packages. Once the outer contours were imported into Rhinoceros, they were lofted from the bottom of the femoral shaft up to the beginning of the bifurcation of the proximal femur into the greater trochanter and the femoral head. The remaining contours were lofted to form the top of the greater trochanter and the top of the femoral head. It was necessary to loft the contours separately like this because when lofting, the number of contours per construction plane must be equal for each construction plane in the loft. The

contours were lofted using the loose fit option. The loose fit option was chosen to smooth out the resulting surface.

New contours were made next. The new contours were made by creating cutting planes and using the cutting planes to slice the lofted surfaces of the femur. The cutting planes were not all parallel; they fanned out, following the shape of the femur. Next, keypoints were placed along the edges of the sliced surfaces. These keypoints were connected with three-dimensional splines to create the new lofting contours. The new contours can be seen in **Figure 4.17**. Note that these contours are angled, whereas the contours in **Figure 4.12** are all horizontal.

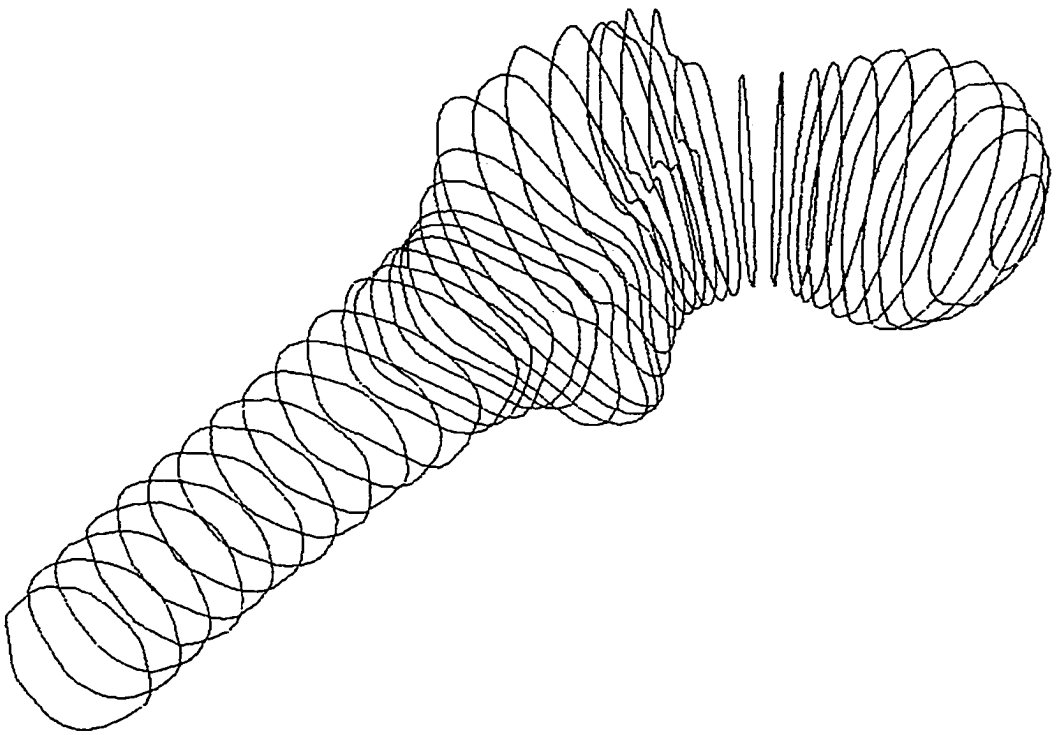

Figure 4.17 - New fanned contours for the three-dimensional model.

These outer contours were exported to I-DEAS via the IGES file format. The contours were still too rough for lofting. Lofts were attempted and the resulting surfaces

were not smooth enough for meshing. There were also several large creases in the intertrochanteric region. These creases were results of the large transition from the tip of the greater trochanter to the femoral neck. To correct this problem, the contours were smoothed by creating points along the contours at 10 mm increments. These points were connected with three-dimensional splines. The contours made in this manner were much smoother than the original contours and maintained the basic geometry only without the small bumps. However, the creases were still a problem in the area of the greater trochanter.

To smooth the creases around the greater trochanter and femoral neck, the contours defining the greater trochanter were modified. The modifications to the contours essentially chopped off the tip of the greater trochanter and smoothed the top to provide an easier transition between greater trochanter and femoral neck. These modifications did change the geometry of the greater trochanter some; however, the changes will have little effect on the results of the finite element model under the assumed loading conditions since this portion of the femur is away from the stress path.

.The inner geometry was created by offsetting the outer contours by a certain amount. The amount of offset for each contour was based on the cortical thickness measurements made earlier in the study. One exception to the cortical thickness was in the femoral head area. The measured cortical thickness for the femoral head was approximately 0.5 mm. This thickness value was too small for meshing and had to be increased to 1.5 mm.

After lofting the inner and outer contours, it became apparent that there were too many contours in the loft series. The surfaces from the lofts were still bumpy and irregular. Several contours were removed from the loft series to produce a much smoother geometry. The final contours used to create the femoral geometry can be seen in **Figure 4.18**.

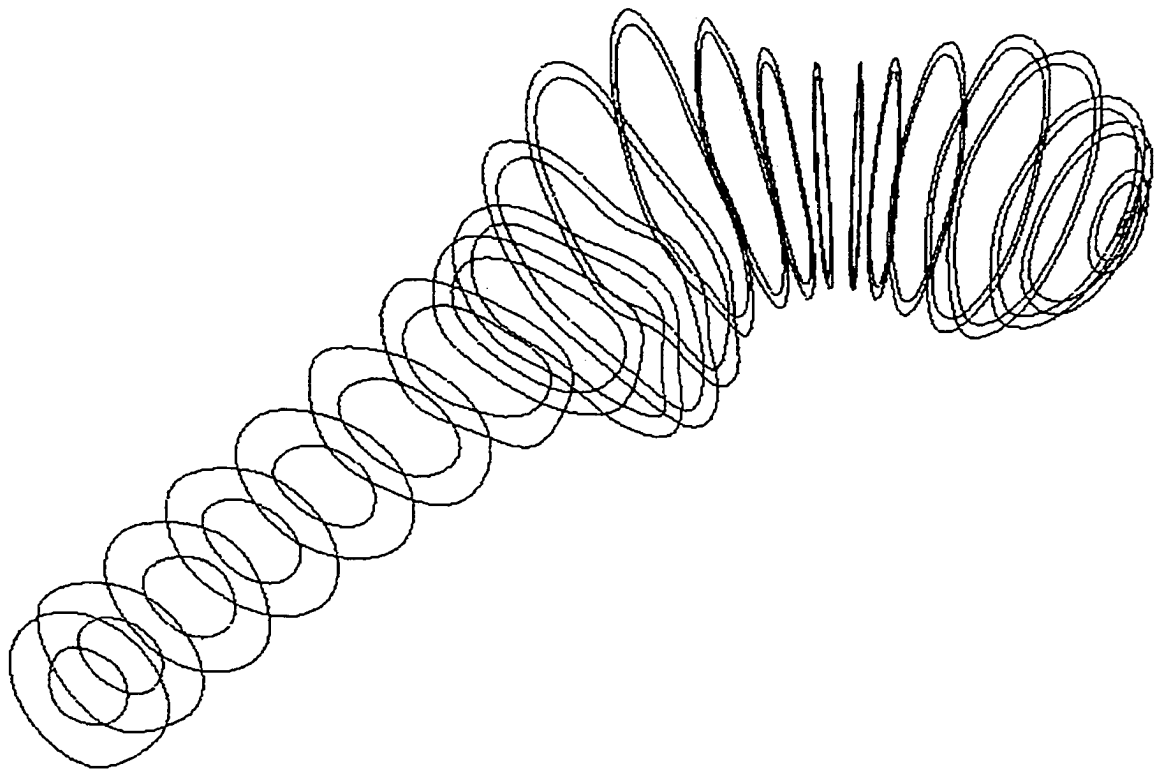

Figure 4.18 - Contours used to create the new three-dimensional geometry.

The next step in creating the femoral geometry was to create the surfaces defining the inner and outer bone boundaries. These surfaces were created by lofting the contours representing each surface. It was necessary to manually modify the seams of the lofted surfaces so that the seams lined up with the axis of the femoral shaft and followed the

contours up along the bottom of the femoral neck and head. Without modifying the locations of the seams, the lofted surfaces were distorted in some locations around the greater trochanter. By specifying that endcaps be added to the lofted surfaces, volumes were created.

Following the creation of the inner and outer bone volumes, the cortical bone area was created by subtracting the inner volume from the outer volume. The volume created by subtracting the volumes represented the area of cortical bone. The area of cancellous bone in the femoral head was created by partitioning the cortical bone volume across the shaft where the cancellous bone ends. The surface representing the bottom of the cancellous bone volume was created from the partitioned edge of the cortical bone. The volume model of the femur can be seen in **Figure 4.19**.

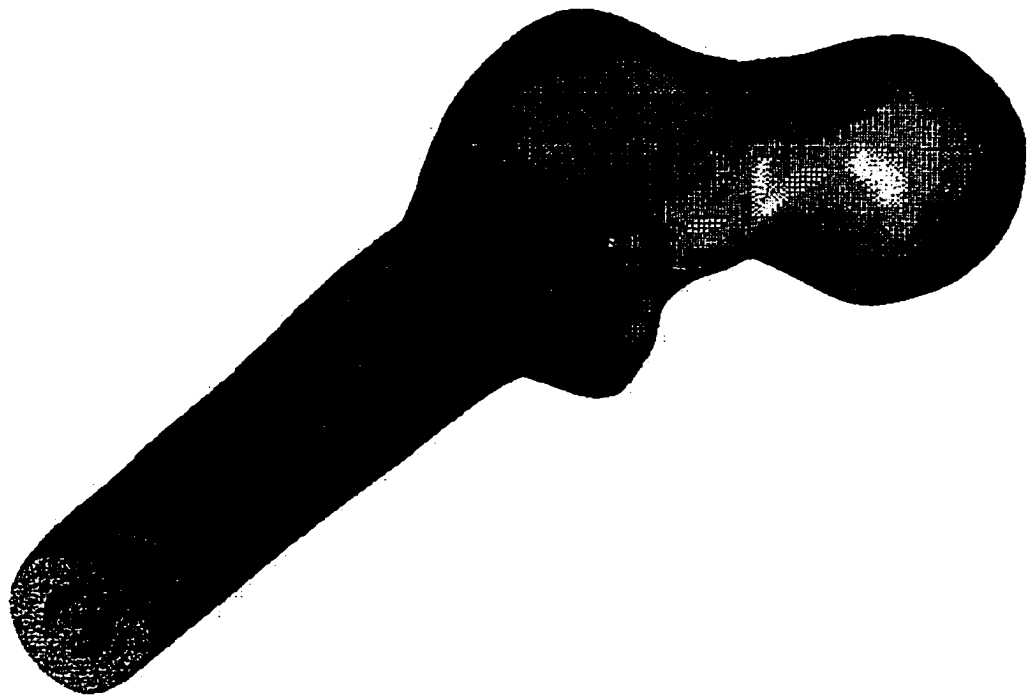

Figure 4.19 - Solid model created in I-DEAS.

Lastly, the three-dimensional volume was meshed. Due to the cortical thickness in the femoral head, parabolic elements could not be used. There was an element facet collapse when trying to use the parabolic elements. Instead, the model was meshed with linear tetrahedral elements. The element edge length was set to 1 mm, and the cancellous bone area was meshed. Next, the proximal cortical bone was meshed using an element edge length of 1 mm. The femoral shaft was meshed last with an element edge length of 3 mm. The meshed three-dimensional model can be seen in **Figure 4.20**. Results from these models are presented in Chapter 7.

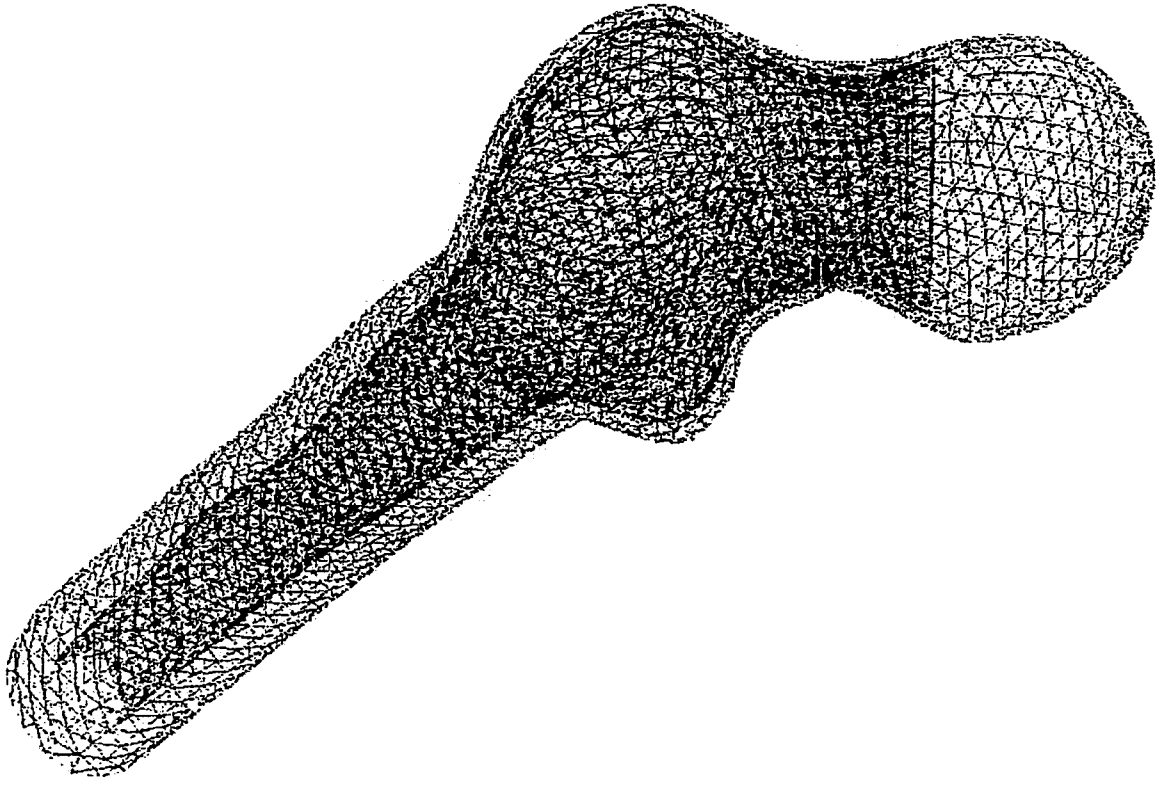

Figure 4.20 - Meshed three-dimensional model created in I-DEAS.

Sensitivity Study

The sensitivity of the model to various parameters such as element thickness, material properties, and cortical thickness needs to be explored. It was noted that the stiffness of the model is very dependent on the cortical thickness. This dependence on cortical thickness was evident in both the two- and three-dimensional models. As the cortical thickness increased, the stiffness of the model increased. It was necessary to make manual measurements of the cortical thickness to correct the stiffness of the model. A more detailed sensitivity study should be performed to determine numerical values for the sensitivity of the model to these parameters.

CHAPTER 5

ANALYTICAL MODELING METHODS

The analytical models presented in this chapter compute the forces and moments acting at the fracture plane using elementary statics coupled with the kinematics of the fixation. Additional analytical models of the stresses in the screw are given based on the solution for a beam on an elastic foundation. These models provide new information into the mechanics of hip joint fixation and give explanations for the stresses and displacements predicted by the finite element models and experimental results.

Free Body Diagrams

To understand the forces and reactions in the intact and fixated femurs, it is necessary to construct free body diagrams of the systems. These diagrams will include the applied force and the reactions to the applied force. The applied force will be labeled P and will be at an angle of 20-degree from the femoral shaft. The femoral shaft will be rotated 20-degrees from the vertical as it was in the experimental setup. This rotation will cause the force P to be vertically oriented. The force P will be applied at the point where a horizontal tangent meets the femoral head. **Figure 5.1** is a diagram of the application of the force P in relation to the femur. The weight of the femur will not be considered in any of these calculations.

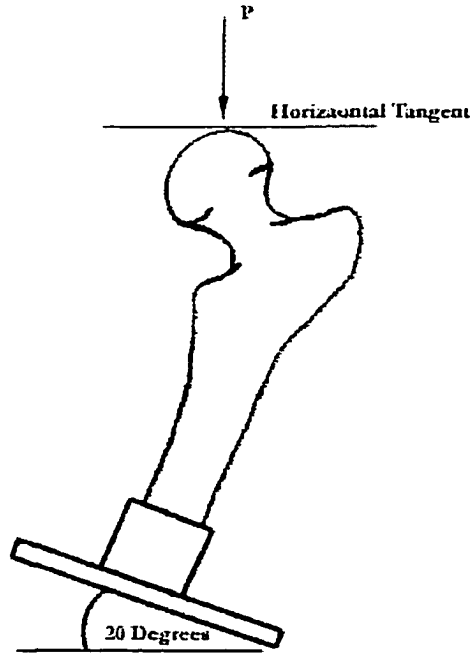

Figure 5.1 -The setup showing the relation of the applied force P to the femur.

Using **Figure 5.1**, a basic free body diagram of an intact femur can be constructed. The external forces applied to the free body are the force P and the reaction forces that occur where the femur is held, as shown in **Figure 5.2**. The reaction forces on the femur are divided into a reaction moment, M_r, and a reaction force, P_r.

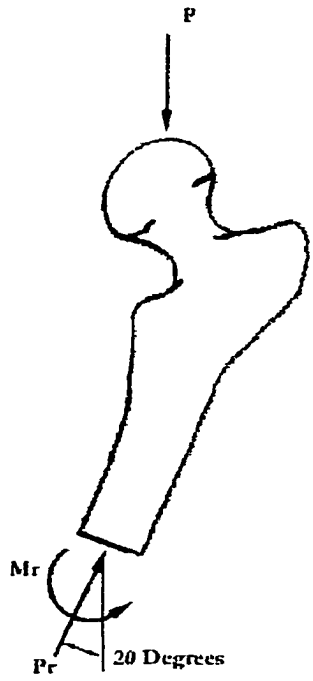

Figure 5.2 - Free body diagram used for the analytical calculations, where P is the applied force, M_r is the reaction moment and P_r is the reaction force.

Assumptions for the Analytical Model

The complexity of the stresses and displacements of fixated femurs requires that assumptions be made in order to develop meaningful analytical models. The first assumption deals with the sliding action of the screw within the bone and sideplate barrel. The screw / sideplate fixation mechanism is designed to allow sliding of the screw within the barrel. The analysis presented here assumes that no friction is associated with the sliding of the screw as it moves relative to the cancellous bone or through the barrel. This assumption means that the screw can take no axial load, which requires that the fracture surface take all of the component of the external force, F, that acts along the screw axis, as shown in **Figure 5.3**.

The axial force, F, will be transferred across the fracture surface as a compressive contact force (or contact pressure) and as a shear force (or shearing stress.) The shear force that develops is assumed to be equal to the component of F that acts in the plane of the fracture. This shearing force, which is a function of the screw angle, is assumed to be smaller than the static coefficient of friction multiplied by the contact force.

The kinematics of the screw and bone are such that when the load, P, is applied to the femoral head, the screw acts as a hinge. The hinge action of the screw creates a triangular distributed load profile between the axis of the screw and the outer edge of the cortical bone below the screw. This triangular profile has its maximum value at the outer edge of the cortical bone and approaches zero at the axis of the screw. This distributed load has resultant magnitude of F located at the centroid of the triangular loading. In other words, the total contact force, F, transmitted across the fracture surface acts parallel to the axis of the screw at 2/3 of the distance from the axis of the screw to the outer fiber of the cortical bone below the screw. The resultant of the triangular load profile is assumed to act through point C as can be seen in **Figure 5.3**.

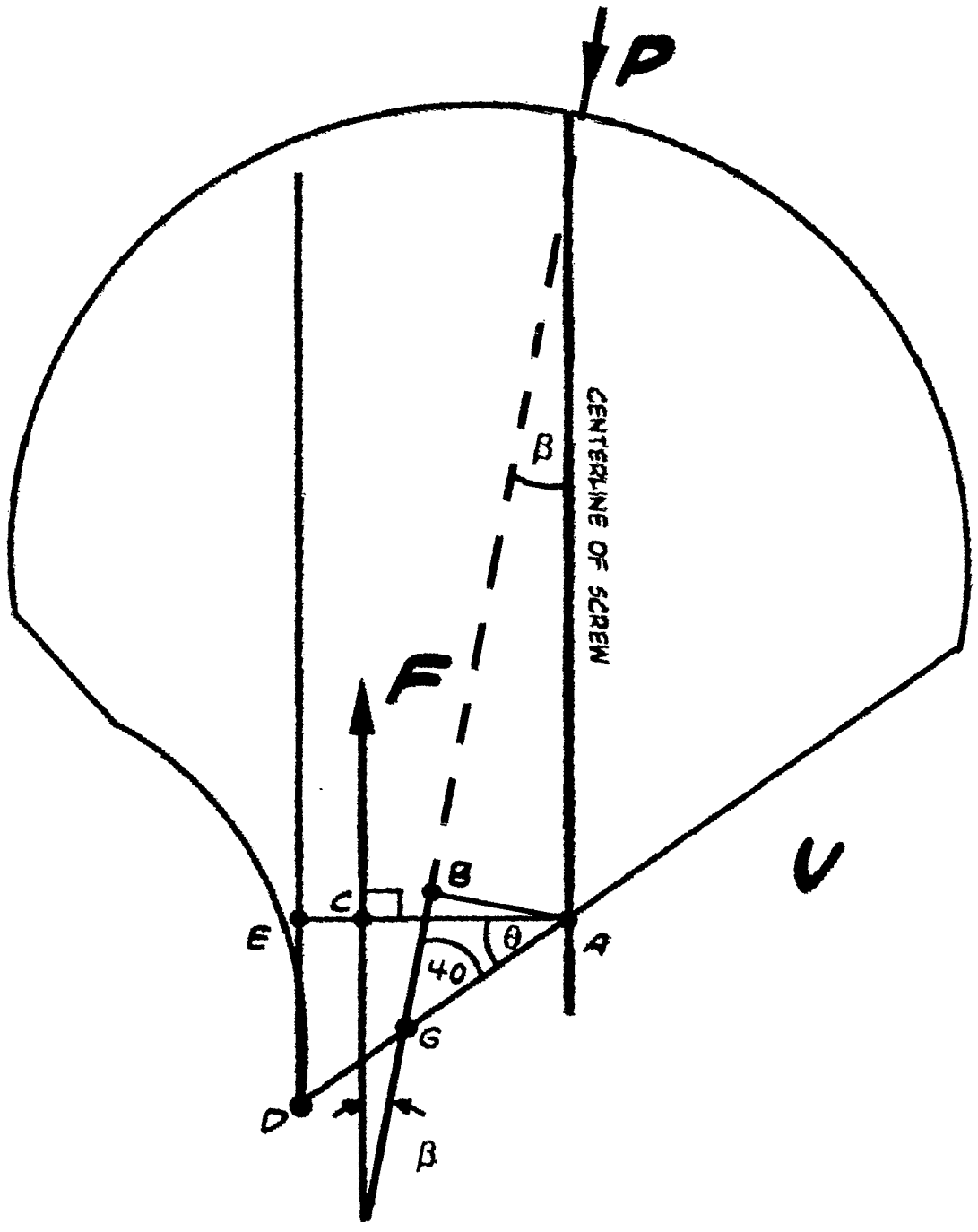

Figure 5.3 - Location of moment arms, AC and AB, and the lumped force, F.

Component Forces of Applied Force, P

The first step in the analytical analysis of the fixated femur is to break the applied force into component forces acting on the screw. In order to break the applied force, P, into the axial force, F; the shear force, V, and the moment, Mo, the angular relationship between the screw and the direction of the applied force must be determined. These angular relations can be seen in **Figure 5.4**. The angle labeled α represents the installation angle of the screw, either 135-degrees or 150-degrees.

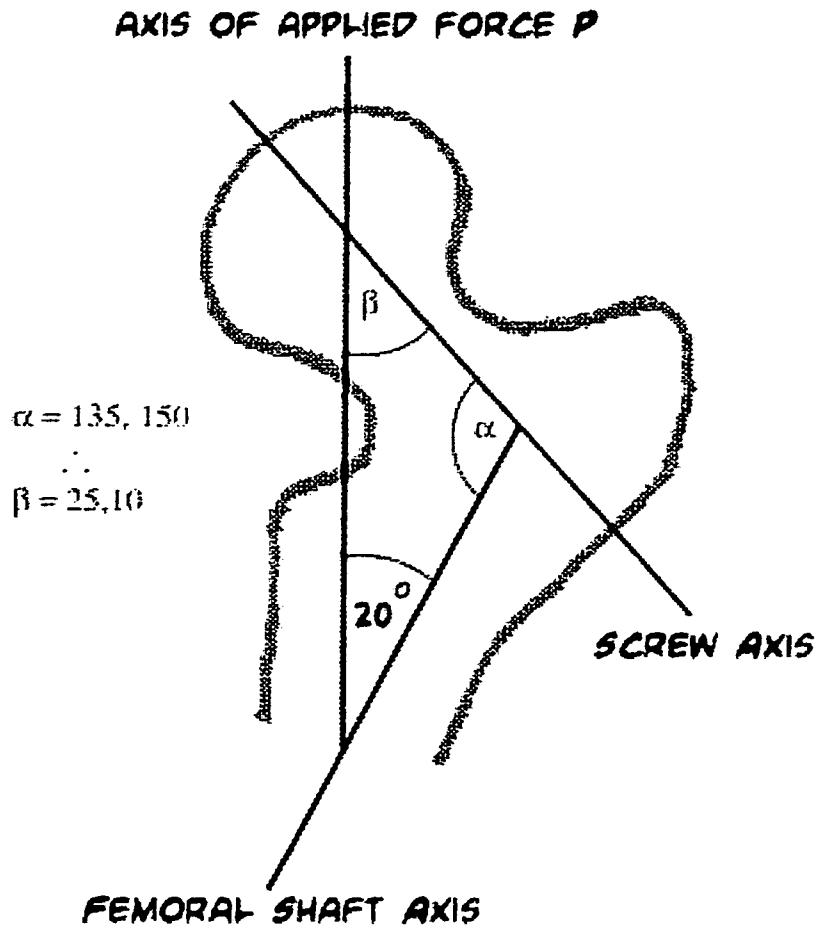

Figure 5.4 - Angular relationships between the screw axis, applied force and femoral shaft.

The free body diagrams of the femoral head for the 135- and 150-degree fixations are shown in **Figures 5.5** and **5.6**, respectively. Also seen in those figures are force triangles showing the relationships between the component forces. Line segment AC represents the moment arm of the axial force, F, acting on the axis of the screw. In addition, line segment AB represents the moment arm of the applied force, P, about the point A along the axis of the screw. The lengths of line segments AB and AC were calculated based on the position of the screw in the fracture plane. The length of AC is given as

$$\overline{AC} = \frac{2}{3} \cdot x \cdot \cos(\theta) \qquad \textbf{5.1}$$

where AC is the length of the moment arm for the applied force, P, and x is the position of the screw in the fracture plane measured from the bottom edge of the fracture and the angle, θ, can be determined from **Figures 5.3** and **5.4** as θ = 50-degrees - β. Consequently, θ is 25-degrees for the 135-degree fixation, and is 40-degrees for the 150-degree fixation.. The length of AB is given as

$$\overline{AB} = (x - \overline{DG}) \cdot \cos(50^{\circ}) \qquad \textbf{5.2}$$

where AB is the length of the moment arm for the axial force, F, and DG is found to be 4.5 mm from physical measurement.

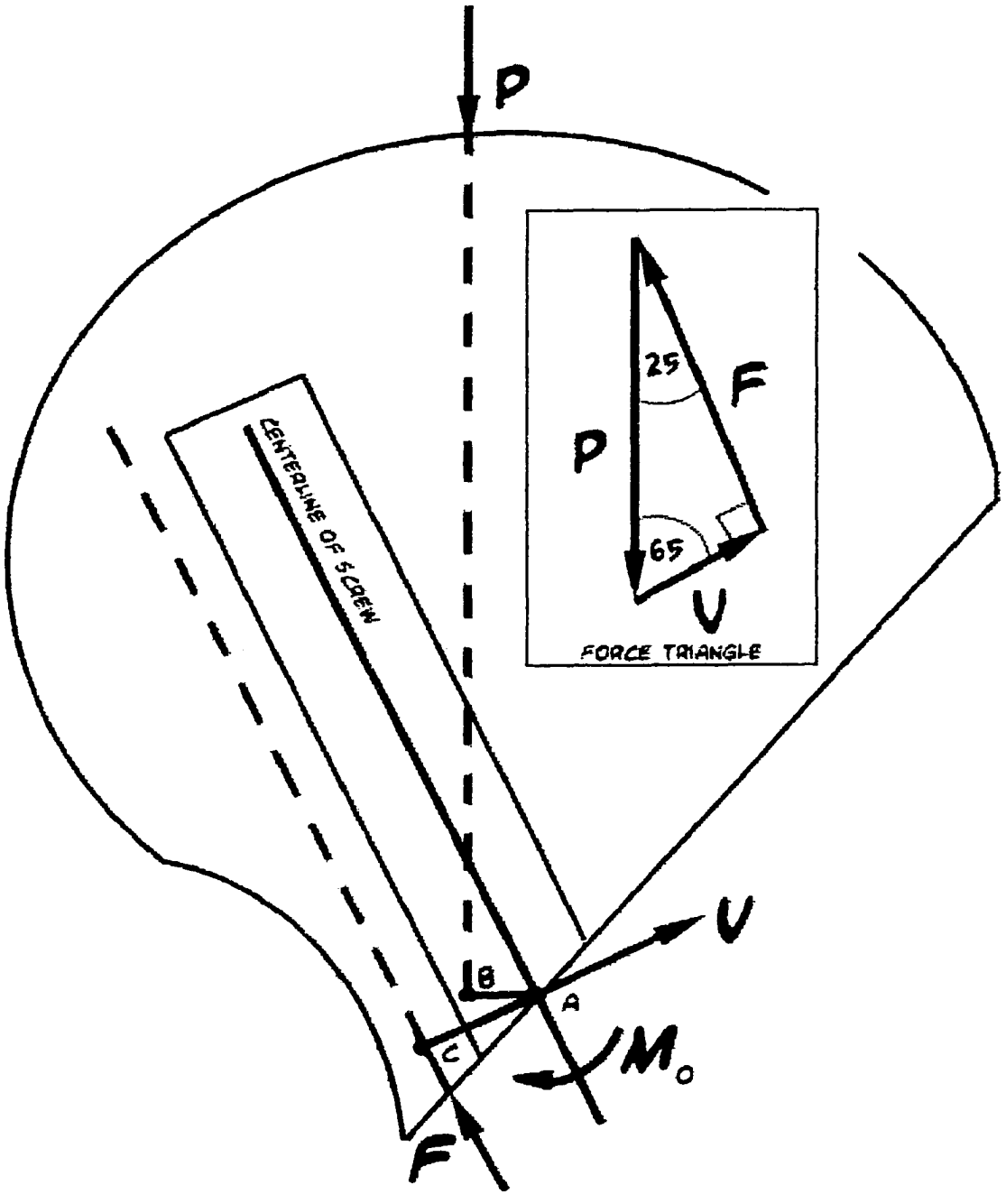

Figure 5.5 - Free body diagram and force triangle for the femoral head with the 135-degree fixation.

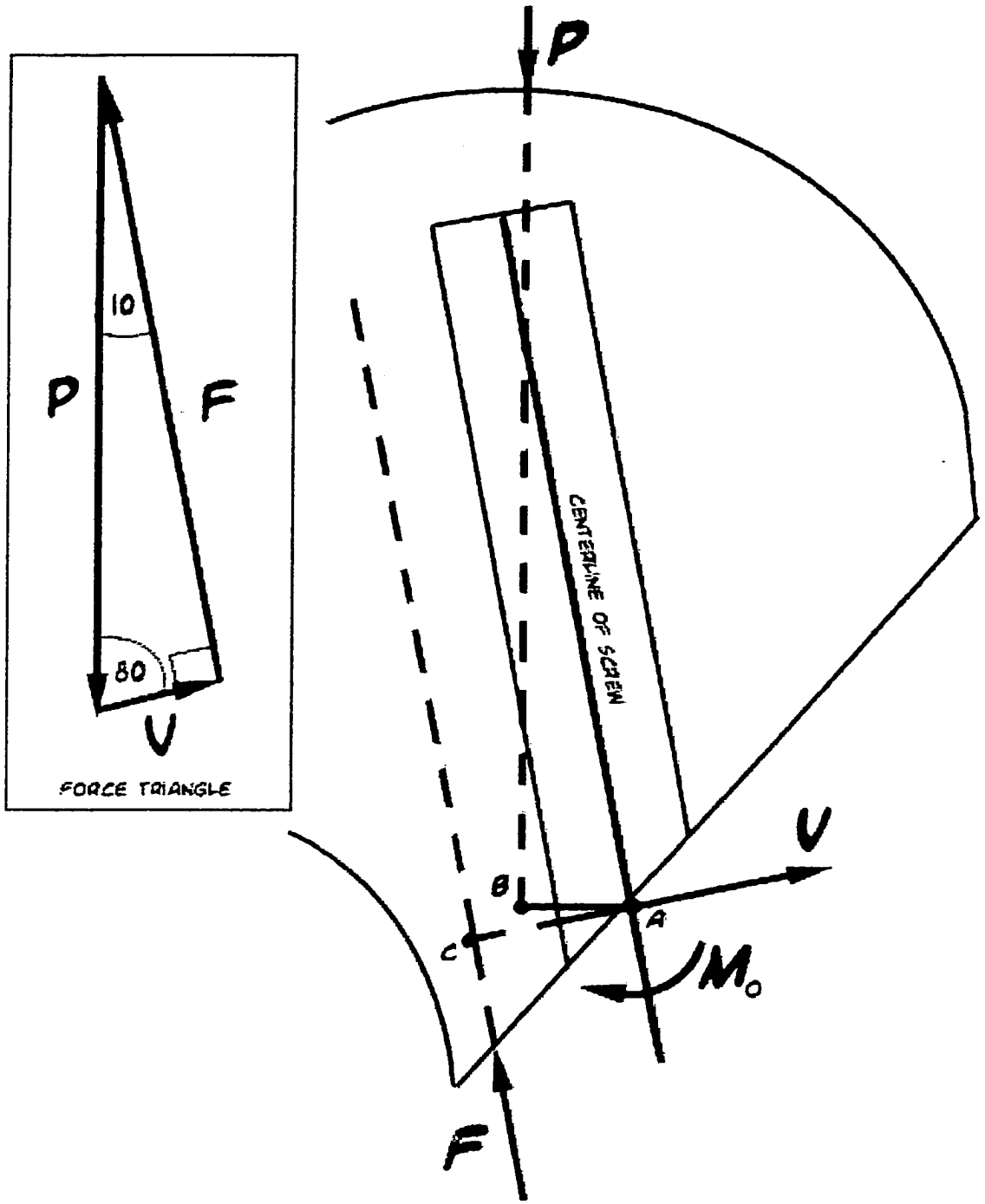

Figure 5.6 - Free body diagram and force triangle for the femoral head with the 150-degree fixation.

Using the free body diagrams in **Figures 5.5** and **5.6**, the component forces of the applied load can be calculated. The axial force, F, is found as

$$F = P \cdot \cos(\beta) \qquad \textbf{5.3}$$

where β is 10-degrees for 150-degree fixation and is 25-degrees for 135-degree fixation. The shearing force, V, which acts normal to the axis of the screw, is computed as

$$V = P \cdot \sin(\beta) \qquad \textbf{5.4}$$

The moment, Mo, is found by summing moments around point A as

$$Mo = F \cdot \overline{AC} - P \cdot \overline{AB} \qquad \textbf{5.5}$$

where AC is the moment arm of the axial force, F, and AB is the moment arm of the applied load, P. These forces and moment can now be used to estimate the stresses that are encountered in the screws.

Analogy to a Beam on an Elastic Foundation

An analytical analogy can also be drawn between a beam on an elastic foundation and a fixation screw on a bone foundation. Solutions already exist for beams on elastic foundations (Boresi, Schmidt, and Sidebottom, 1993; Young, 1989.) These solutions are based on semi infinite beams loaded at one end resting on infinite foundations.

Before the beam solutions can be used, a constant, ko, must be determined. This constant, ko, represents the spring constant of the foundation. The value of ko was determined from a finite element simulation of a beam resting on a foundation of cancellous bone. To determine ko, a known load was applied to the end of the beam in the finite element model, and the deflection of the cancellous bone underneath the beam was measured. This deflection, along with the geometry and loading of the problem, was used to back-out the constant, λ, as

$$\lambda = \sqrt[3]{\frac{W}{2 \cdot E \cdot I \cdot disp}} \qquad \textbf{5.6}$$

where W is the load applied to the end of the beam, E is the modulus of elasticity of the foundation material, I is the moment of inertia of the cross section of the beam, and *disp* is the displacement of the beam at the loaded end. Knowing λ, the constant ko was then determined as

$$ko = \frac{\lambda^4 \cdot 4 \cdot E \cdot I}{bo} \qquad \textbf{5.7}$$

where bo is the width of the beam. The material constant, ko, is then used to study the interaction of the bone with the screw.

Two equations for a beam on an elastic foundation are analogous to a screw resting on bone. The first set of these equations is based on a concentrated load, V, placed at the free end of the beam acting in a direction normal to the top surface of the beam. The second set of the beam equations is based on a concentrated moment, Mo, acting on the free end of the beam. These two equations will be superimposed to simulate the system of forces acting on the screw.

The variable λ must be solved for again, this time based on the fixation screw and cancellous bone. The equation for λ is

$$\lambda = \sqrt[4]{\frac{do \cdot ko}{4 \cdot E \cdot I}} \qquad \textbf{5.8}$$

The moment created in the beam by the concentrated load, V, applied at the end of the beam is given as

$$M_v = \frac{V}{\lambda} \cdot e^{-\lambda \cdot y} \cdot \sin(\lambda \cdot y) \qquad \textbf{5.9}$$

where M_v is the moment applied to the beam as a result of the normal force, V, and y is the distance in the screw measured from the fracture surface where the moment, M_v, is calculated. The moment created in the beam by the concentrated moment, Mo, is given by as

$$M_{Mo} = -Mo \cdot e^{-\lambda \cdot y} \cdot [\cos(\lambda \cdot y) + \sin(\lambda \cdot y)] \qquad \textbf{5.10}$$

where M_{Mo} is the moment applied to the beam by the concentrated moment, Mo, acting on the end of the beam. When superimposed, the equations **5.9** and **5.10** predict the magnitude of the moment applied to the beam at any distance, y, measured from the fracture surface. In the equations above, a positive shear force, V, will cause tensile flexural stresses in the upper fiber of the screw, while a positive bending moment, Mo, will cause compressive flexural stresses in the upper fiber of the screw.

Three different, yet related, analytical approaches were presented in this chapter. Each approach is capable of standing alone in their predictions about the behavior of the fixated femur; however, when coupled together they support one another to form a unified analytical analysis of the system. Together, the kinematics based evaluation, analysis of the forces and reaction forces on the screw and fracture plane, and analogy to a beam on an elastic foundation provide an analytical insight into the behavior of a fractured femur fixated with a sliding hip screw.

CHAPTER 6

EXPERIMENTAL RESULTS

The results of both of the experimental intact and fixated experiments will be reported here. Additional experimental results from previous studies were given earlier in Chapter 2.

Intact Experimental Results

The intact experimental data set serves as a baseline for the fixated experiments. To make the data easier to work with, the results at 500, 750, 1,000, and 1,350 N were extracted from the data set. Since the testing equipment recorded data at a given time increment and not at a given load increment, linear interpolation was performed to obtain the results at the desired load levels. Only the summarized data is reported in this chapter, more complete data sets can be found in **Appendix C**.

Intact Stiffness Calculated at the Point of Application (INSTRON)

The stiffness calculated at the point of load application is referred to as the overall stiffness. The experimental results from the INSTRON indicate that the force-displacement relationship is approximately linear, as shown in **Figure 6.1**. The overall stiffness is 1297

+/- 55 N/mm for the bones that were to receive the 135-degree fixation. The bones that were to receive the 150-degree fixation had an overall stiffness of 1290 +/- 145 N/mm. These values of stiffness are very close, which illustrates the high level of repeatability of the experiments. The plus or minus ranges cited with the above stiffness results correspond to 95% confidence levels, which are based on the standard deviation and size of the sample.

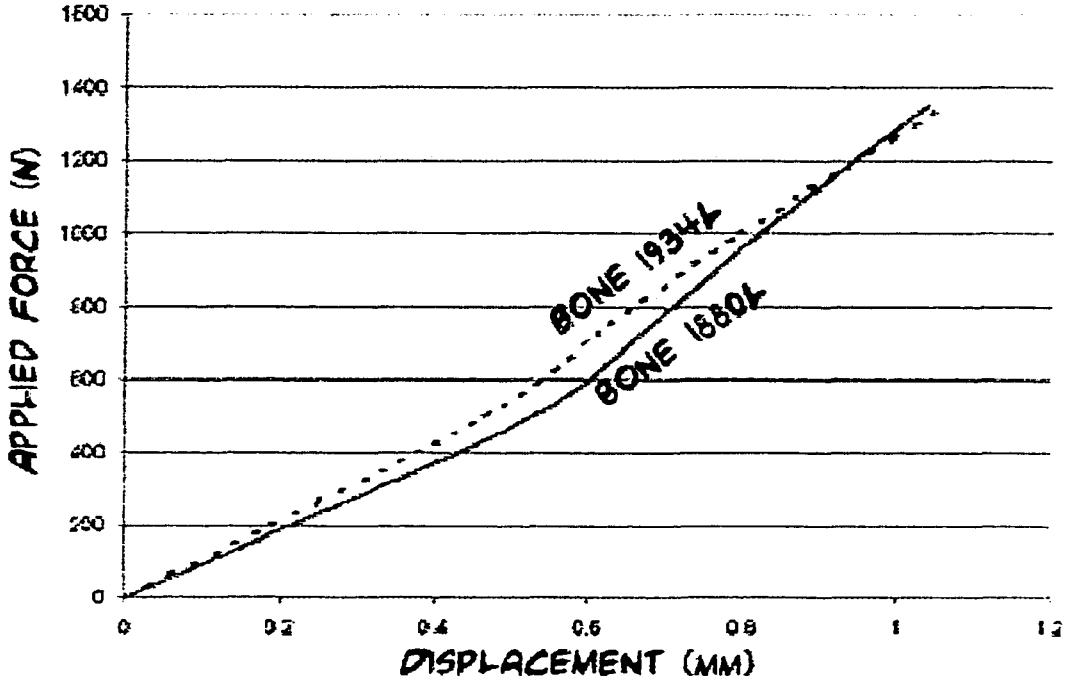

Figure 6.1 - Intact force versus displacement data recorded by the INSTRON.

Intact Stiffness Calculated at Point One (LVDT I)

Point one coincides with the placement of LVDT I (placed underneath the femoral neck and parallel to the femoral shaft.) **Figure 6.2** shows a plot of the data recorded by LVDT I. The intact femoral stiffness calculated from the displacement measured by LVDT I is –3274 +/- 18 N/mm for the 135-degree bones and –3031 +/- 424 N/mm for the

bones that would receive the 150-degree fixation. Notice that these stiffnesses are significantly higher than those measured by the INSTRON. This increased stiffness is partially the result of measuring the deflection of the head only, and not the whole femur as was the case for the INSTRON. Also, negative displacements are measured, since LVDT I follows a point that translates in an arc as the femoral shaft deflects.

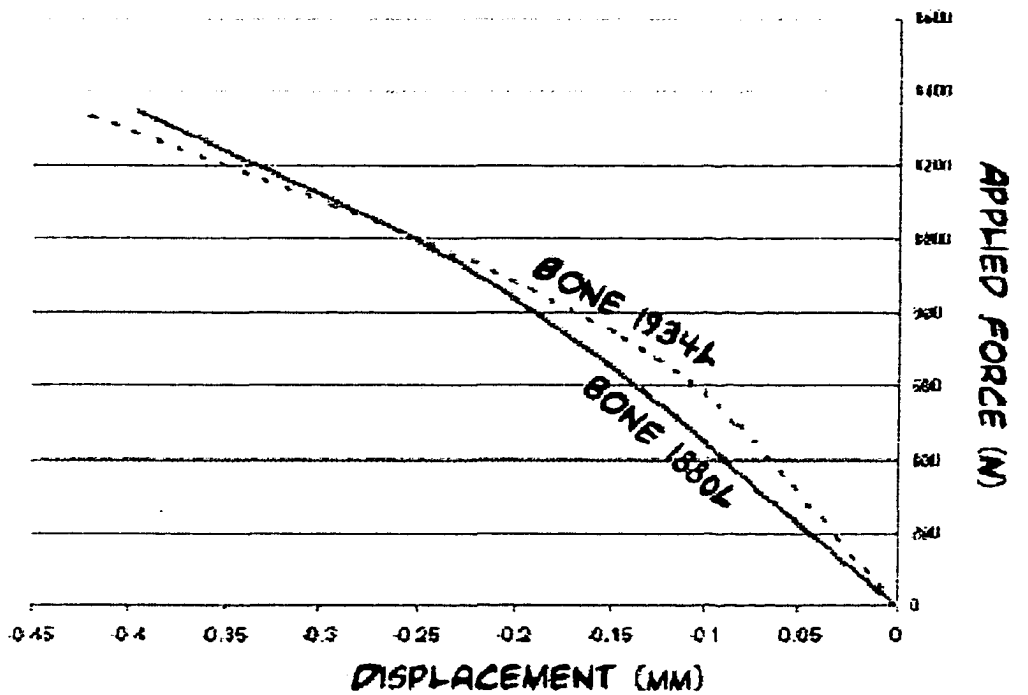

Figure 6.2 - Intact force versus displacement data recorded by LVDT I during the experimental testing.

Intact Stiffness Calculated at Point Two (LVDT II)

Point two coincides with the placement of LVDT II (placed on the greater trochanter at an angle of 45-degrees to the vertical.) **Figure 6.3** is a plot of the data recorded by LVDT II during the intact experimental testing. The results show a bending

stiffness of 1062 +/- 5 N/mm and 842 +/- 148 N/mm for the bones that were to receive the 135- and 150-degree fixations, respectively.

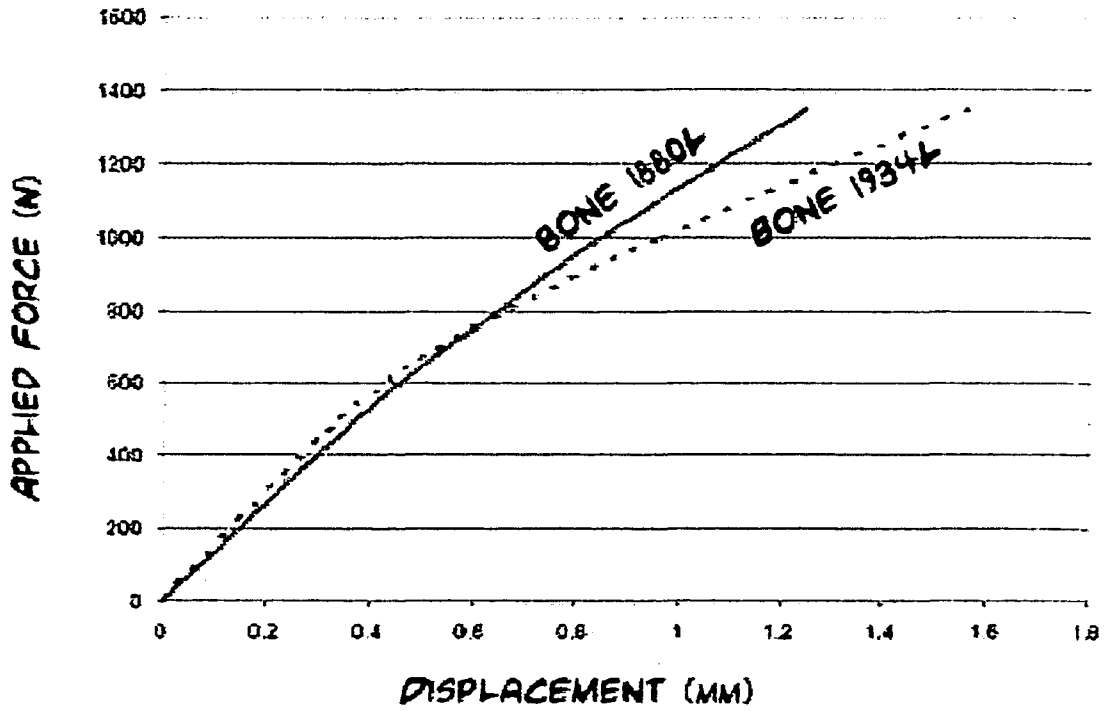

Figure 6.3 - Intact force versus displacement data recorded by LVDT II during the experimental testing.

Fixated Experimental Results

Bone 1880L was fitted with the 135-degree screw and sideplate combination, and bone 1934L was fitted with the 150-degree screw and sideplate combination. Data points were interpolated for load levels of 500, 750, 1,000, and 1,350 N from the data recorded for the these fixations, as in the case of the intact results.

Fixated Stiffness Calculated at the Point of Application (INSTRON)

This data set was recorded by the INSTRON at the point of force application. **Figure 6.4** is a plot of the experimental results as measured by the INSTRON during the testing of the 135- and 150-degree screws. The overall fixation stiffness values from the current study are 791 +/- 6 N/mm and 639 +/- 75 N/mm for the 135- and 150-degree fixations, respectively. The lower initial stiffness experienced by the 150-degree fixation is the result of impaction of the femoral head onto the femoral neck. After contact, the stiffness rises considerably and actually exceeds that of the 135-degree femur.

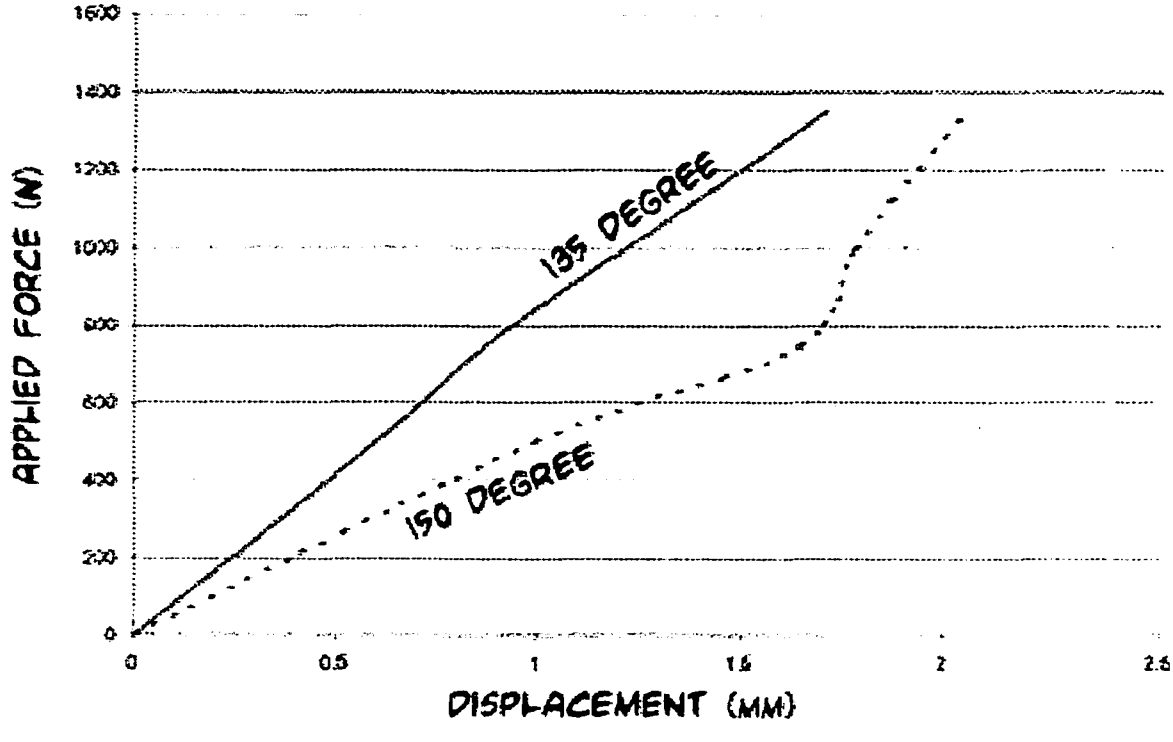

Figure 6.4 - Fixated force versus displacement data recorded by the INSTRON during the experimental testing.

Fixated Stiffness Calculated at Point One (LVDT I)

The experimental data recorded from LVDT I during the testing of the 135-and 150-degree screws is shown in **Figure 6.5**. The fixated neck stiffness values calculated from the data recorded by LVDT I during the experimental testing are 2170 +/- 21 N/mm for the 135-degree fixations and 1185 +/- 228 N/mm 150-degree fixations. Notice that this plot also shows a dramatic increase in stiffness after impaction.

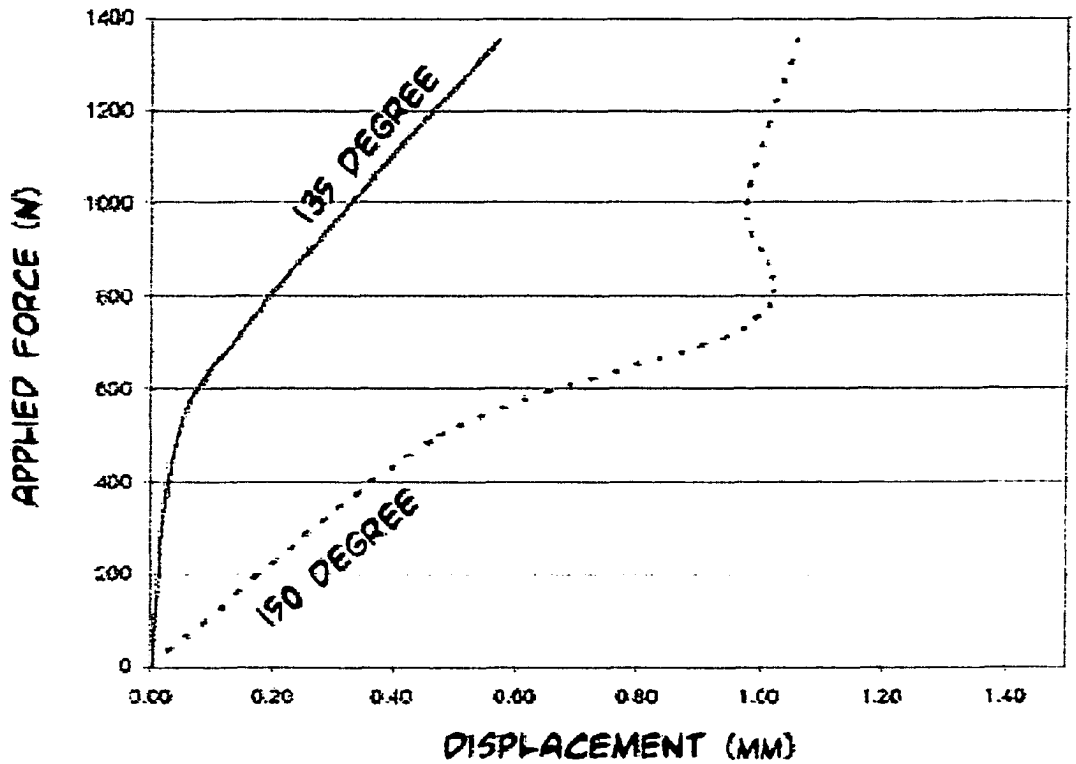

Figure 6.5 - Fixated force versus displacement data recorded by LVDT I during the experimental testing.

Fixated Stiffness Calculated at Point Two (LVDT II)

The experimental data recorded from LVDT II during the testing of the 135-degree screw is shown in **Figure 6.6**. The stiffness values calculated from the data

recorded by LVDT II during the device testing are 817 +/- 29 N/mm for the 135-degree fixation and 774 +/- 68 N/mm for the 150-degree screws. Unlike the stiffnesses plotted for the INSTRON and for LVDT I, there is little change in the stiffness in the 150-degree fixation at impaction. This is due to the fact that LVDT II primarily measures the deflection of the femoral shaft.

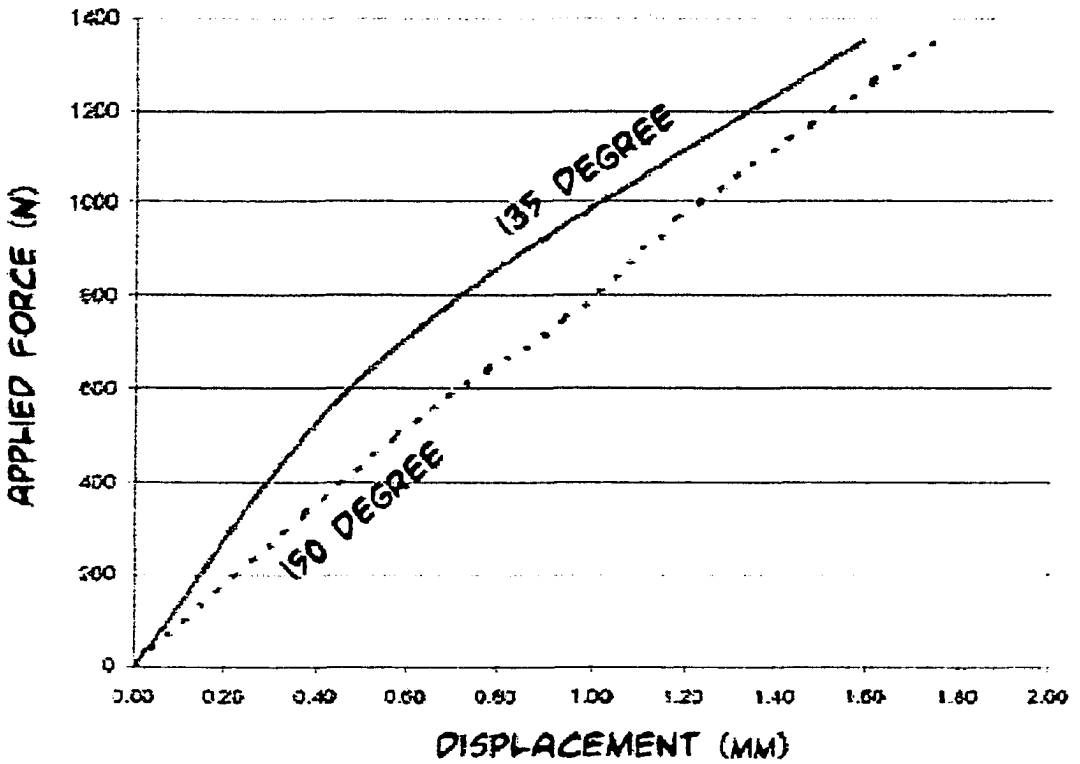

Figure 6.6 - Fixated force versus displacement data recorded by LVDT II during the experimental testing.

The results from these experimental tests will be discussed along side the analytical and finite element results in Chapter 9.

CHAPTER 7

FINITE ELEMENT MODELING RESULTS

This chapter summarizes results of the two-dimensional models created using ANSYS and the three-dimensional model created using I-DEAS. The mechanical behavior of the fixations is explored by studying the stiffnesses, stresses, and contact pressures associated with each of these models.

Intact Stiffness Calculated at the Point of Application (INSTRON)

The finite element results predict a linear load versus deflection response from the intact femur. This is expected since the material is assumed to be linear elastic and the deformations involved are small. The overall stiffness is computed by dividing the peak load by the peak deflection at the point of load application. For the two-dimensional intact model developed in ANSYS, the stiffness is 1,781 N/mm. The three-dimensional model developed in I-DEAS has a value of 1,517 N/mm. These stiffness values compare favorably with each other and with the experimental results for the intact femur, thus helping to validate the FE results.

Fixated Stiffness Calculated at the Point of Application (INSTRON)

The overall stiffness was also calculated for the 135- and 150-degree fixated FE models. The stiffness from the 135-degree fixation was calculated to be 2,259 N/mm, and the 150-degree overall stiffness was calculated to be 2,665 N/mm. Notice that the fixated stiffnesses are higher than the stiffnesses computed for the intact femur. This is not surprising when considering that a tightly fitting metal screw has been added to a much softer bone. However, any slack in the system, as often occurs experimentally, would act to reverse this trend, sometimes making the stiffness of the intact bones higher than those of fixated bones.

Stresses Predicted by the Two-Dimensional Finite Element Models

The ANSYS two-dimensional FE models were also used to predict stress profiles in the bone and screw. A contour plot of the Von Mises effective stress for the 135-degree fixation can be seen in **Figure 7.1**. The Von Mises stress is a measure of the distortion energy in the material. The maximum stress predicted by the 135-degree fixation model was 284 MPa. This maximum stress occurs at a point between the fracture surface and the barrel of the sideplate. This is counter intuitive, since it would seem that the peak stress should occur at the fracture. Reasons for this unexpected location are given in Chapter 8.

A similar contour plot for the 150-degree fixation is given in **Figure 7.2**. The maximum stress predicted by the 150-degree fixation model was 175 MPa, which is lower than the maximum stress predicted for the 135-degree fixation. Maximum stresses in both models occur in the bottom fibers of the screws some distance distal to the fracture surface.

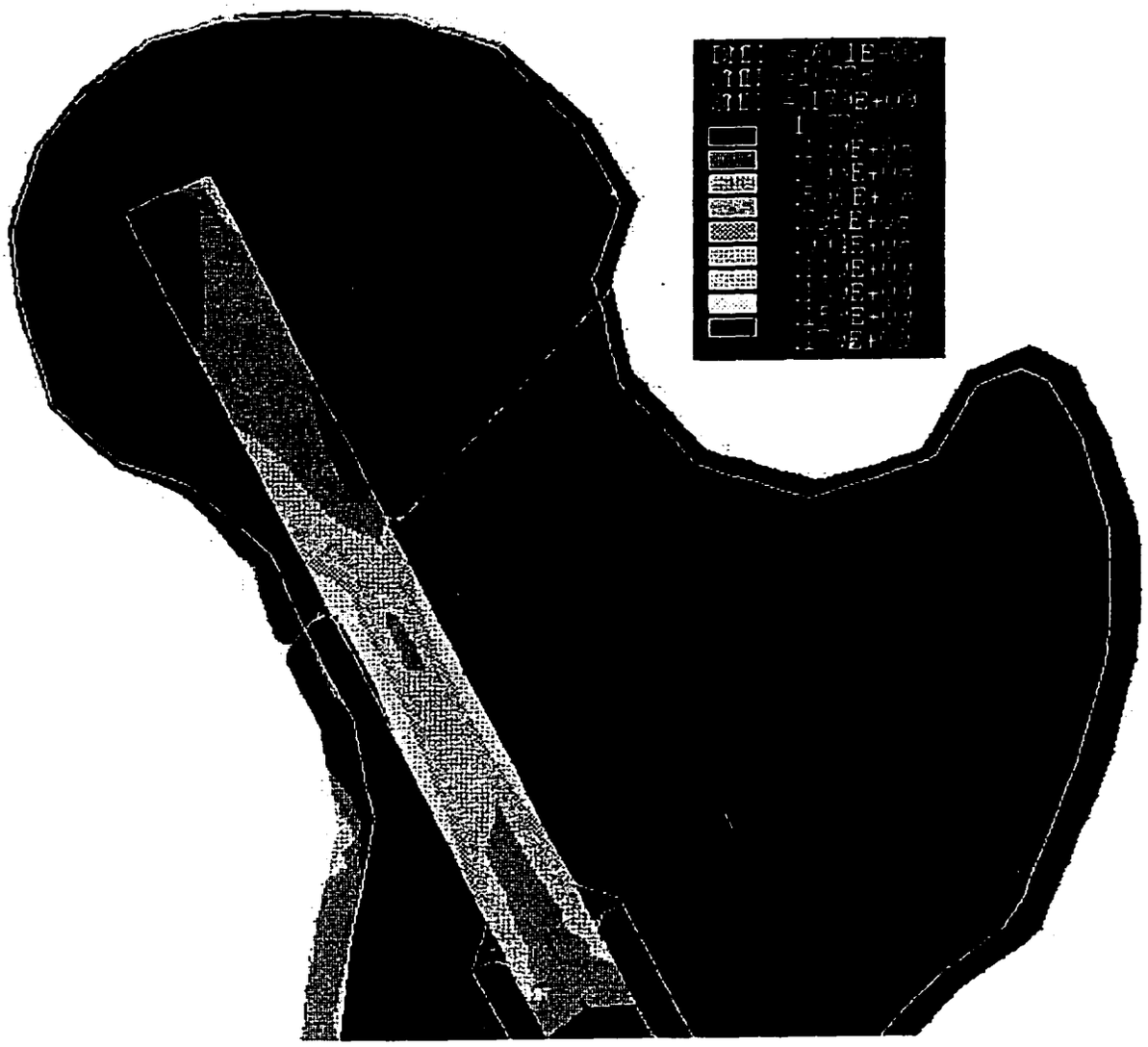

Figure 7.1 - Von Mises stresses in the 135-degree fixation.

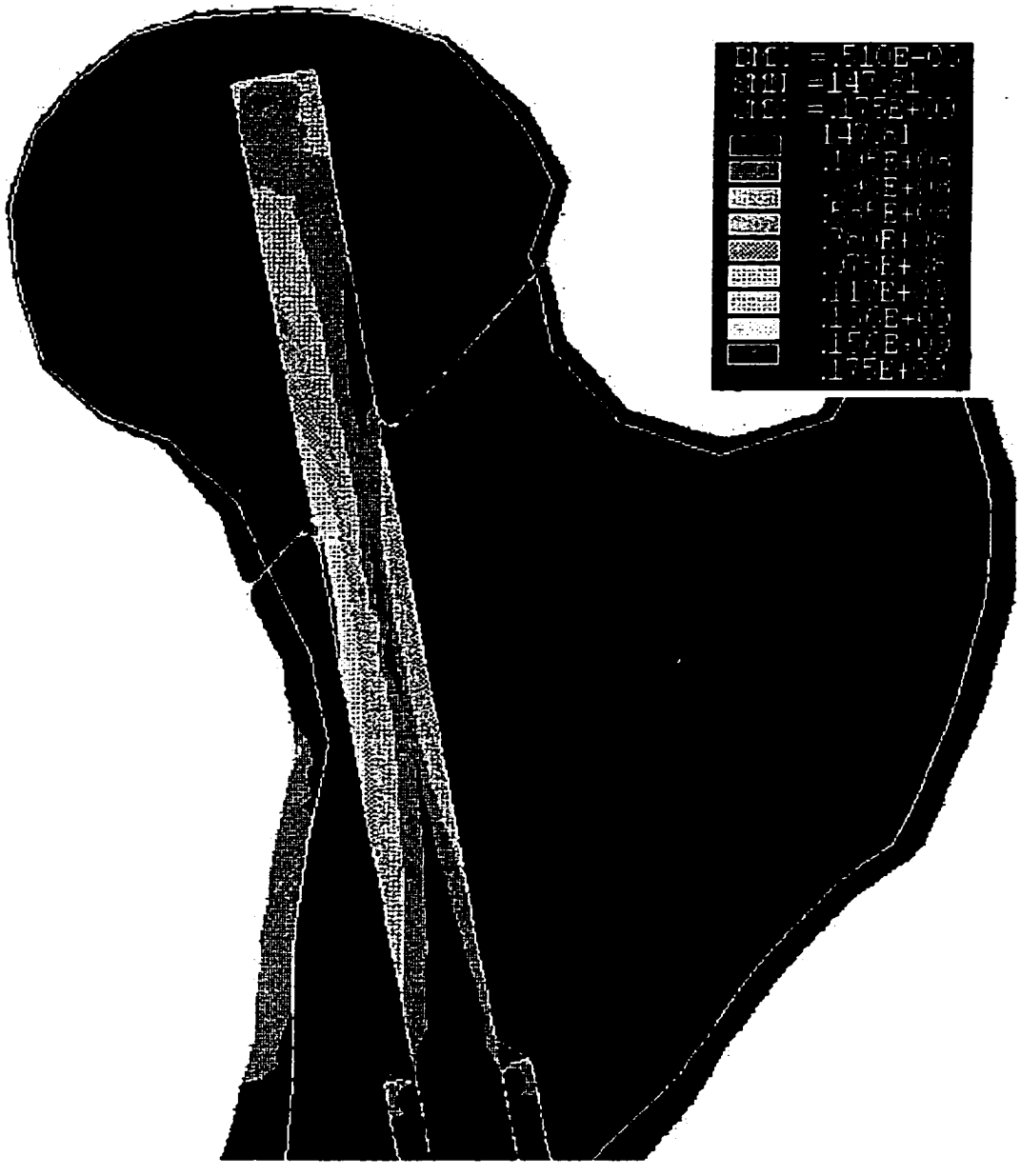

Figure 7.2 - Von Mises stresses in the 150-degree fixation.

Location of Contact Forces in the Two-Dimensional Models

The contact elements at the fracture plane simulate the interaction of the femoral fragment with the femur. The two-dimensional finite element models predict that the

contact pressures on the fracture surface are located below the screw are largest near the outer edge where the stiffer cortical bone is located. A diagram of the contact pressures predicted by the 135-degree finite element model can be seen in **Figure 7.3**. A similar profile of contact pressure was observed for the 150-degree model.

This concentration of the contact force on the stiffer material is expected when a soft and a stiff material act together. For the case of the two-dimensional model, the contact pressure is highly concentrated around the intersection of the inner side of the cortical bone and the cancellous bone. In the real three-dimensional case, however, a smooth gradient of contact force would be expected to extend to the neutral axis of the bone / screw combination, since a ring of cortical bone exists around the outer perimeter of the bone (it does not just exist at the outer fiber as in the two-dimensional case.) This information helps to validate the assumption of a linear gradient in contact force at the fracture face that was presented in chapter 5.

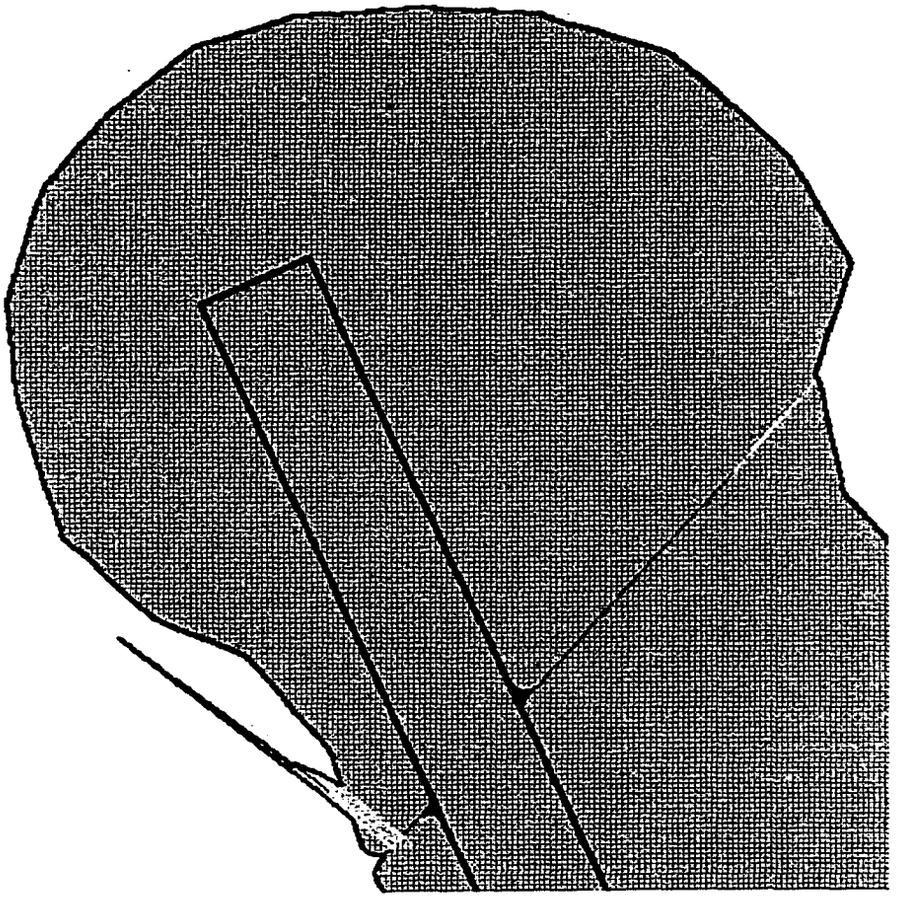

Figure 7.3 – Diagram of the location of the contact pressure predicted by the finite element models.

Three-Dimensional Model Results for the Stresses in an Intact Femur

A contour plot of the Von Mises effective stress for the intact three-dimensional model is shown in **Figure 7.4**, where the units are in MPa. Although the peak stresses for the intact model occur directly under the point of load application (the load is concentrated over a small area as it was in the experiments), the peak stresses away from the loading point occur in the femoral neck and in the lesser trochanter. These stress values are on the order of 25 MPa. These stresses are lower than those in the lesser

trochanter shown for the fixated femurs in **Figures 7.1** and **7.2**. The source of much of this stress is the contact pressure exerted at the cortical bone below the screw and due to the fact that the screw transfers some of its load to the cancellous and cortical bone directly beneath its axis.

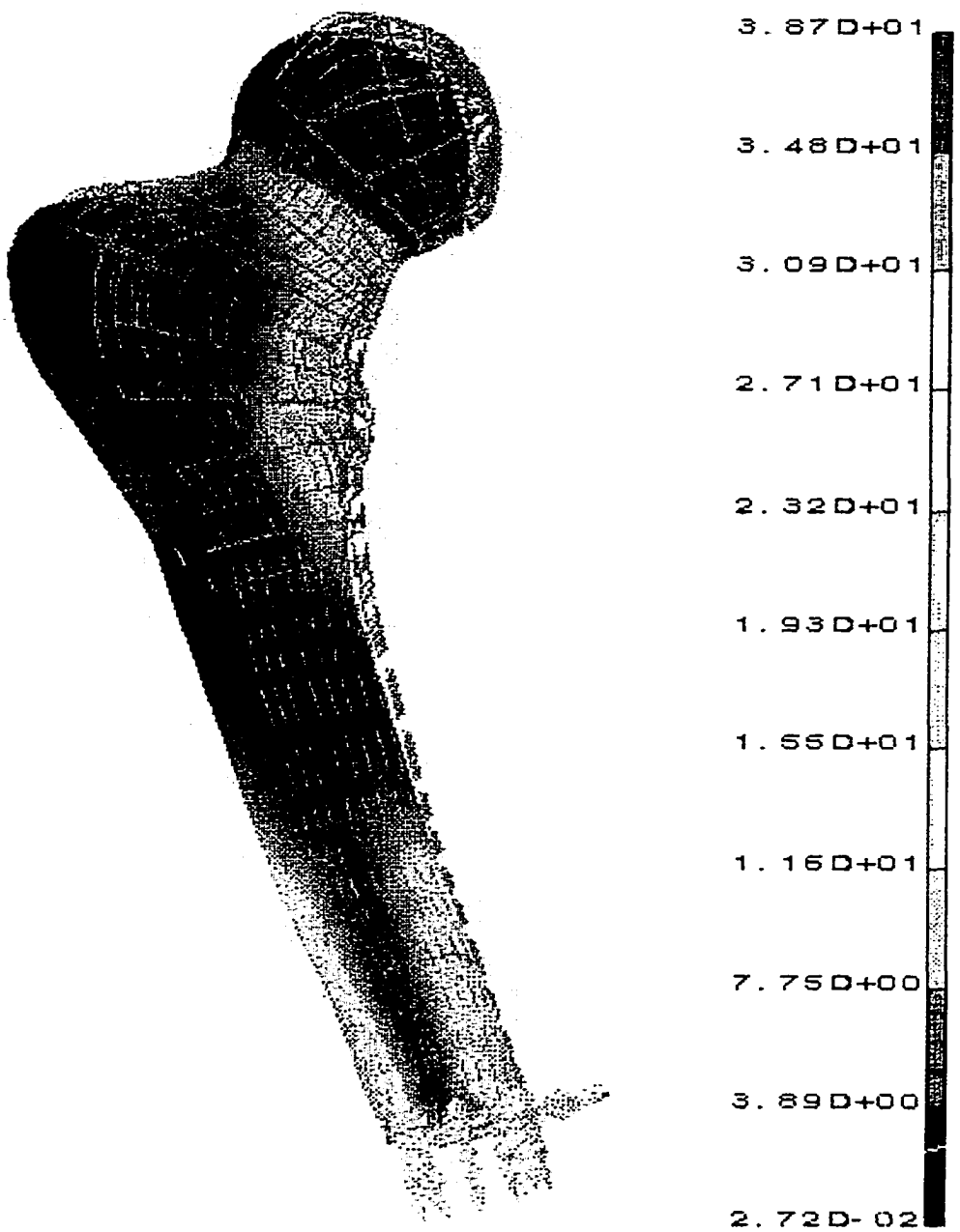

Figure 7.4 - Stress contours and deflection profile predicted by the three-dimensional model.

CHAPTER 8

ANALYTICAL MODELING RESULTS

The analytical models developed in Chapter 5 will be applied here to estimate the forces, moments and stresses in fixated femurs.

Stress Distribution at the Fracture Surface

The shearing force, V, and the concentrated moment, Mo, shown earlier **in Figures 5.5** and **5.6** induce flexural stresses in the screw. The analysis given in Chapter 5 showed that a positive shear force, V, from **Equation 5.4**, tends to cause tensile stresses in the upper outer fiber of the screw. Fortunately, the moment, Mo, from **Equation 5.5**, which is induced by the contact force, F, acting below the screw, produces compression in the upper fiber of the screw. In other words, the contact force, F, below the screw induces a moment, Mo, that opposes the stresses in the screw induced by the shear force V.

As stated in Chapter 5, the screw is assumed not carry any of the axial force, F. Assuming the distribution of the contact force varies from a maximum at the cortical bone below the screw to zero at the neutral axis of the screw leads to a triangular load profile across the contact surface, as shown in **Figure 8.1**. It is important to note that most of the contact force at the fracture surface will be carried by the ring of stiffer cortical bone, which is expected when a stiff material is coupled with a soft material.

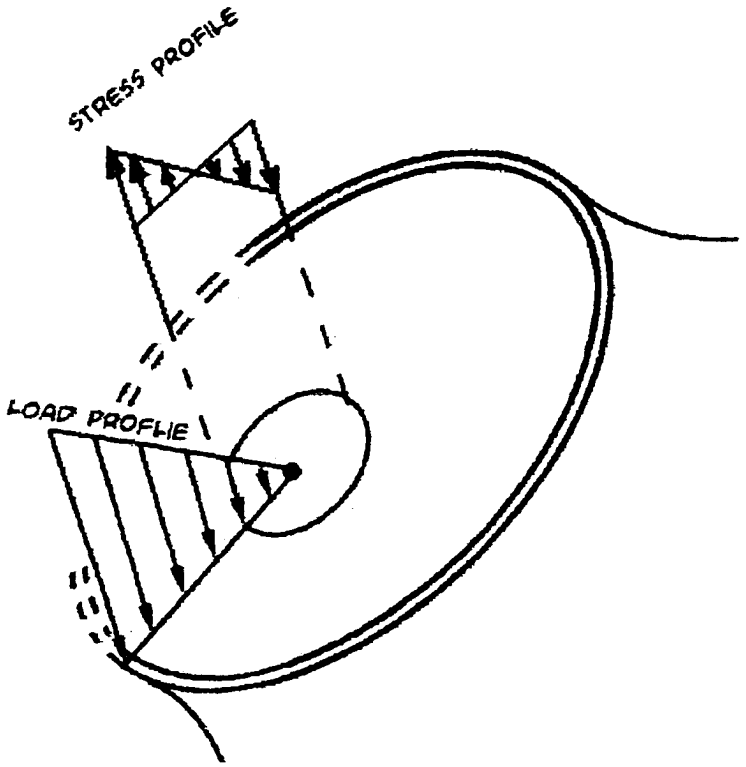

Figure 8.1. Kinematics based load profile on the fracture surface and stress profile in the screw.

Shear Forces on the Screw

The shear force, V, from **Equation 5.4** is computed here based on the angle of the screw. The calculations of shear force based on screw angle show that a lower angle screw (135-degrees) carries a higher shear force than a higher angle screw (150-degrees.) A plot of the shear force versus screw angle can be seen in **Figure 8.2**.

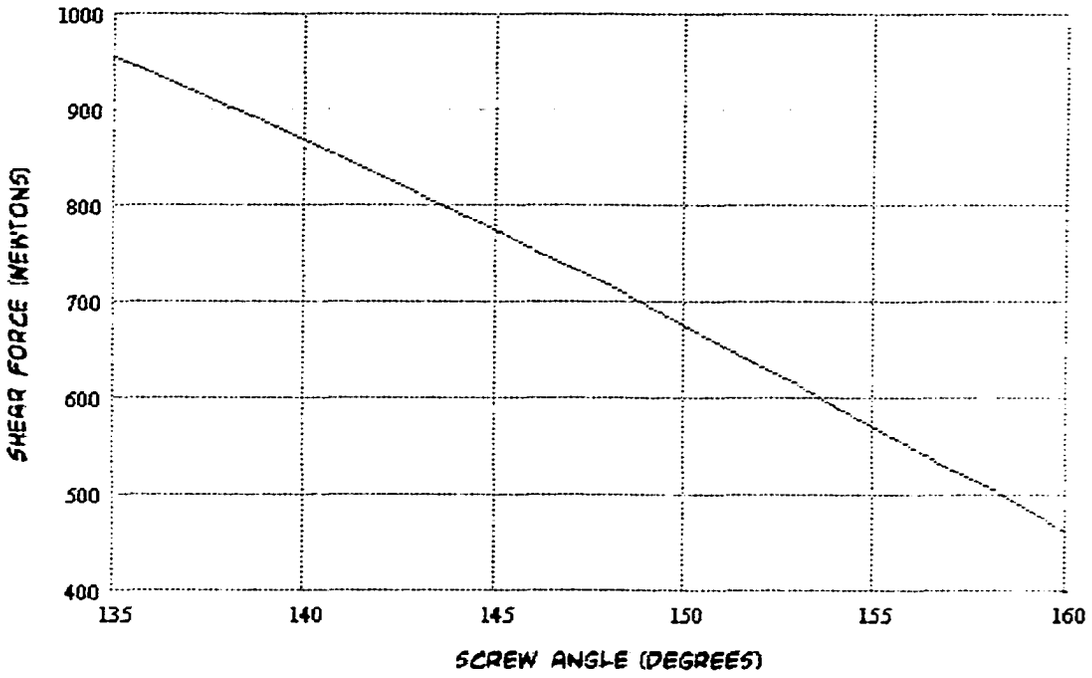

Figure 8.2 - Shear force applied to the screw as a function of screw angle.

Analogy to a Beam on an Elastic Foundation

Equations 5.9 and **5.10** for the moments in a beam on an elastic foundation show that the maximum bending moment applied to the screw as a result of the shear force, V, and the concentrated moment, Mo, does not occur at the fracture surface. Rather, the maximum bending moment (and the maximum stress) occurs some distance distal to the fracture surface. A plot of the maximum bending moment from in the 135-degree fixation and the 150-degree fixation can be seen in **Figure 8.3**. This figure corresponds to the same geometry analyzed in the experimental and finite element models. A positive bending moment in this plot indicates tension in the upper fiber of the screw and compression in the lower fiber of the screw. Notice that compression is predicted in the upper fiber of the

screw at the fracture interface. A different result is predicted by the two-dimensional FE model because of the bonding of the screw with the bone. Much of the component of the applied load that acts along the axis of the screw is absorbed by shear stresses which develop at the screw / cancellous bone interface. If the two-dimensional model could allow for sliding at this interface, most of the axial force would be carried as a contact pressure at the fracture surface, thus increasing the concentrated moment at the end of the screw and inducing compressive stress in the upper fiber of the screw at the fracture surface.

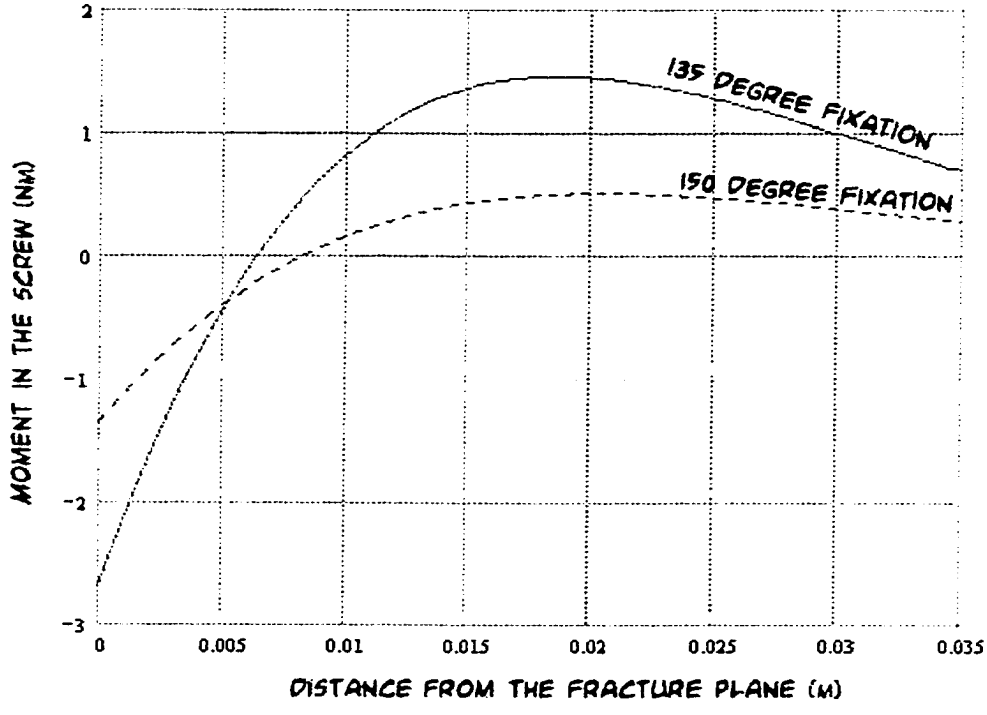

Figure 8.3 - Bending forces from the concentrated moment, Mo, and from the shear force, V, in the two fixations calculated from equations for beams on elastic foundations.

The effect of screw installation position on the stresses in the screw was also studied. **Figure 8.4** shows a diagram describing the screw installation position. The analytical equations were adapted to account for the distance, x, between the axis of the

screw and the bottom of the fracture surface, as shown in **Appendix D.** It was discovered that as the screw is positioned higher on the fracture surface, the maximum stress in the screw increases. **Figure 8.5** shows the magnitude of the maximum stress in the screw as a function of the screw installation position along the fracture surface.

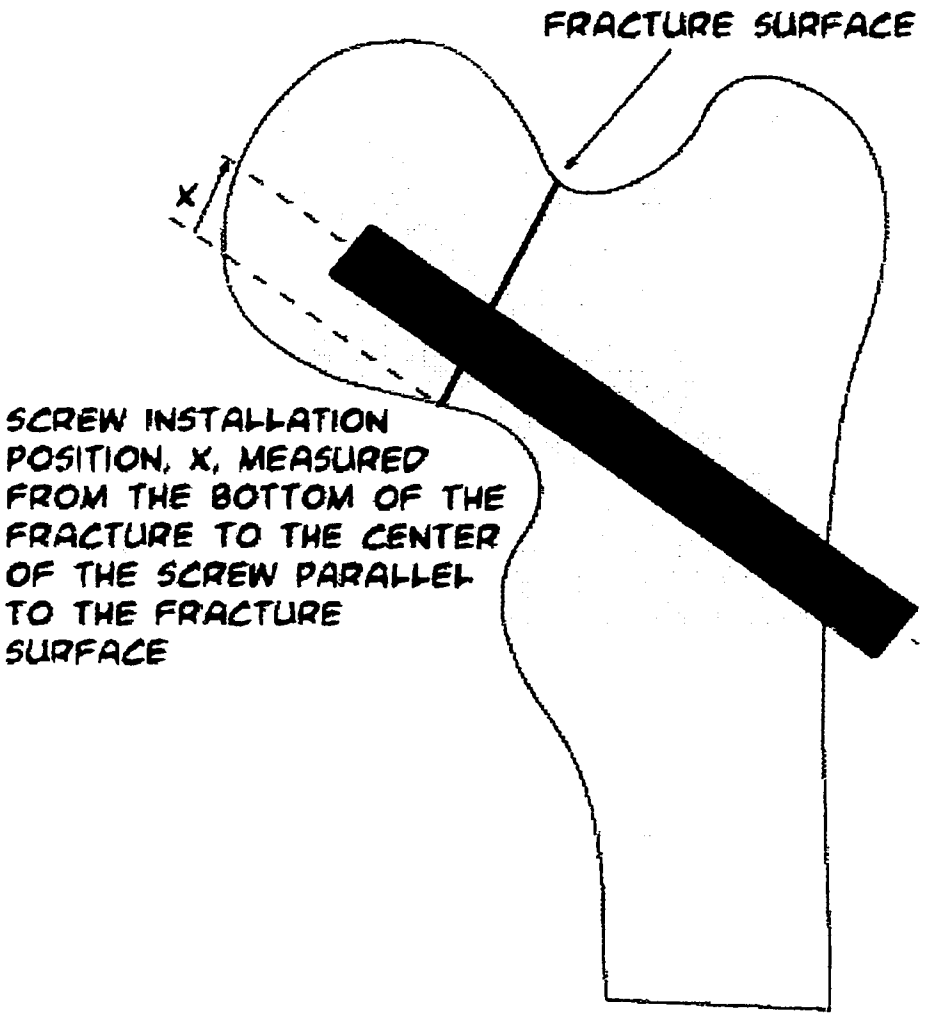

Figure 8.4 – Diagram of the screw installation position.

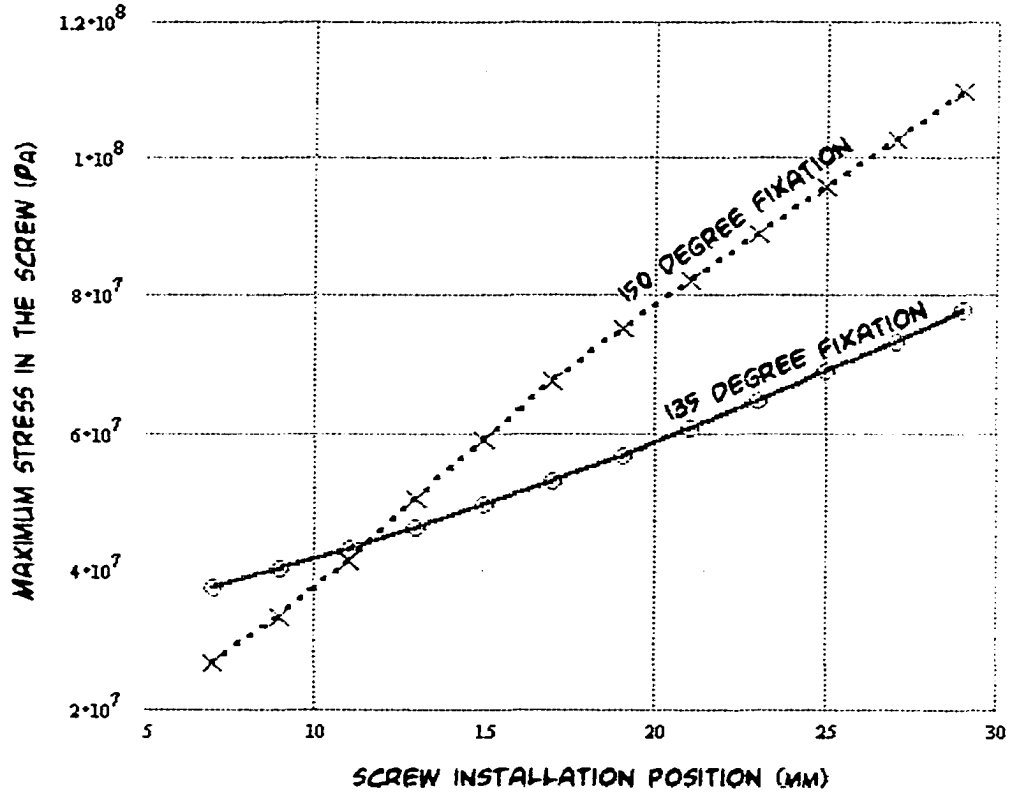

Figure 8.5 - Maximum stress in the screw for 135- and 150-degree fixations as a function of the position of the screw in the fracture surface.

Not only will the value of the maximum stress in the screw change based on the position of the screw on the fracture surface, but the location of that maximum stress will also change. The analytical equations show that as the screw is placed higher on the fracture surface, the location of the maximum stress in the screw moves closer to the fracture. Plots of the location of the maximum stress versus screw position for both the 135- and 150- degree fixations can be seen in **Figure 8.6**. The effect of the position of the screw on the location of the maximum stress is greater in the higher angle screw, as can be seen in **Figure 8.6**. The significance of the above analytical modeling of the forces, moments and stresses in fixated femurs will be discussed in Chapter 9.

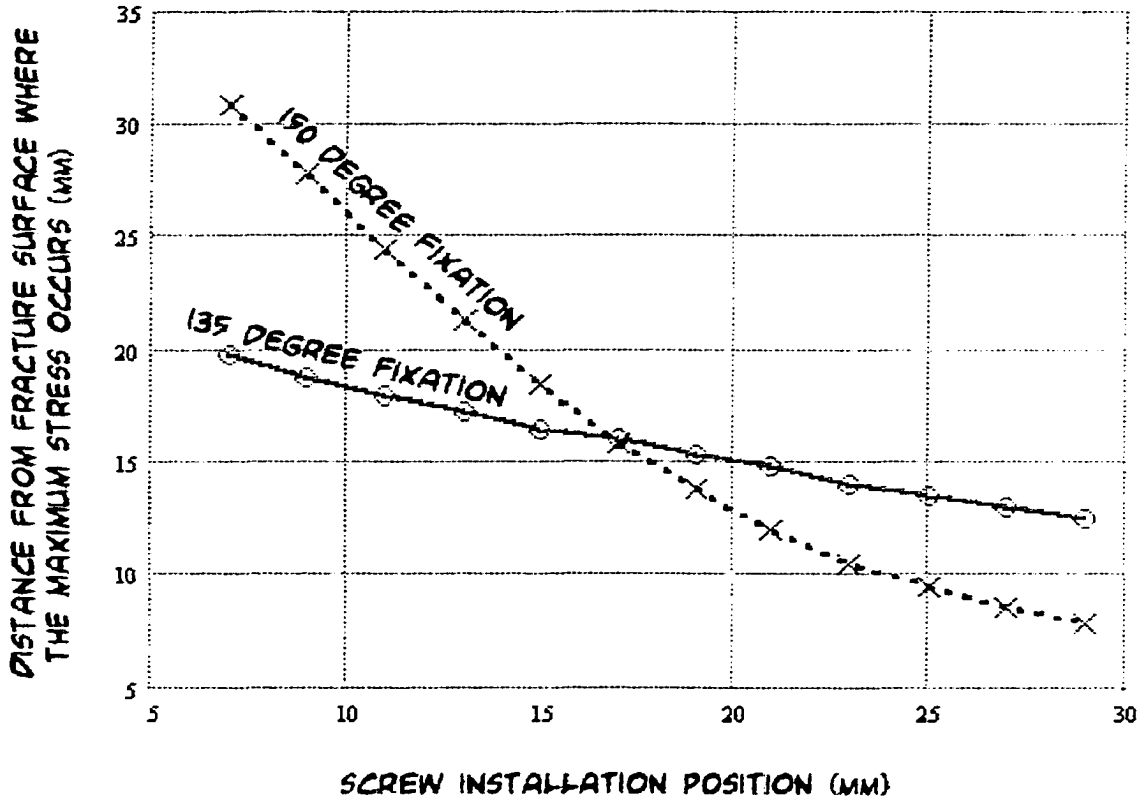

Figure 8.6 - Location of maximum stress in the screw as a function of screw position in the fracture surface.

CHAPTER 9

DISCUSSION

This section will discuss the significant findings of the experimental, finite element and analytical models. The discussion will involve the kinematics of the response of the fixation to loading, the stress and contact force distributions associated with the finite element and analytical solutions, and the relative stiffnesses of the 135- and 150-degree fixations.

Kinematics of the Fixation

Sliding hip screws are designed to slide in the barrel of the sideplate when weight is applied to the femoral head. This sliding action could only take place in the presence of limited frictional forces in the barrel of the sideplate and at the interface of the screw and the bone. The analytical solution developed in this work assumes that the component of the load applied at the femoral head that acts in the direction of the axis of the screw is completely carried by the contact forces at the fracture surface. Based on this argument, it is clear that higher angle fixations are associated with higher contact pressures at the fracture.

Study of the finite element solution for the contact force given in **Figure 7.3** shows that all of the contact force at the fracture interface occurs below the screw where the cortical bone meets the cancellous bone. Contact forces are near zero on all other locations

on the fracture surface. This indicates that a hinge action is taking place at the neutral axis of the screw. It is well known that a stiffer material will carry a higher portion of the total force when coupled to a softer material, particularly when the ratio of the elastic modulii is high. In this case, the ratio of the elastic modulus of the cortical bone to that of the cancellous bone is 56 (17 GPa / 0.3 GPa), suggesting that most of the load will be carried over the half-ring of cortical bone that lies below the neutral axis of the screw. Assuming a linear gradient of strains from the hinge-point to the outer fiber, the contact pressure distribution will be linear, varying from zero at the neutral axis of the screw to a maximum at the outer fiber below the screw.

Forces and Stresses in the Screw and Bone

The linear distribution of contact pressure below the screw will exert a force, F, on the femoral fragment, that acts in the direction of the axis of the screw. The portion of the screw in the femur, which constrains the fragment, will exert a shearing force, V, and a bending moment, Mo, on the fragment / screw combination, as shown in the free body diagrams of **Figures 5.5** and **5.6**. Using elementary statics, the forces and moment can be determined (see **Equations 5.3** through **5.5**). It is clear from the resulting forces that the moment induced by the external applied load, P, and the contact force, F, oppose one another. This is beneficial to the bearing stresses of the screw on the cancellous bone and for the flexural stresses in the screw itself.

Using the equations for a beam on an elastic foundation to approximate the behavior of the screw on the cancellous bone, it appears that the stresses in the screw are lower when the screw is installed at a location lower on the fracture surface. This

supports the current practice of installing the screw as close as possible to calcar region of the lesser trochanter. But, the reasoning for a low installation position is different from what is currently thought by the medical community. These equations also show that the maximum stresses in the screw will be lower in 150-degree fixations when the screw is installed in a low position (see **Figures 8.4** and **8.5**.) However, one possible drawback to screws installed in the lower portion of the fracture surface is that the contact pressures will be larger since the area over which the total force is distributed will be smaller.

The finite element results show that the peak stress in the screw does not occur at the fracture plane (**Figures 7.1** and **7.2**.) Instead, the peak stress occurs between the fracture and the barrel of the sideplate. A similar behavior was shown based on the analytical solution shown in **Figure 8.3**. This result shows that the analytical and finite element models are predicting similar stress profiles in the screw, indicating that modeling the screw as a beam on an elastic foundation can be a useful method for analytical modeling.

Another important factor to consider is that sliding may not necessarily occur for the 135-degree fixation. If the screw sometimes happens to lock in the barrel before sliding can occur, as reported by (Kyle, Wright, and Burstein, 1980), then the 150-degree screw becomes much more desirable since limited contact would occur at the fracture surfaces.

Stiffness Comparisons

Normalized Stiffness

The data from the Lynn's study that was reported in Chapter 2 is analyzed here along with the results obtained from the current study. The normalized overall stiffness calculated from data recorded in Lynn's experimental tests is shown in **Table 9.1** along with FE results and experimental results from the current study. The data was normalized by dividing the fixated stiffness by the intact stiffness for each femur. It is necessary to normalize the data to be able to compare the results between different femurs, particularly when embalmed femurs are compared to fresh frozen femurs. Lynn's study provides a much better statistical spread than the data of the current study as there were only two femurs in the current study and sixteen in Lynn's study.

Table 9.1 - Stiffness values computed from experimental data of Lynn's study and from the two-dimensional finite element models.

Overall Stiffness (N/mm)	135-Degree Fixation	150-Degree Fixation
Lynn Normalized	0.96 +/- 0.22	1.17 +/- 0.39
2D FE Normalized	1.27	1.50
Peak Chapter 6 Normalized	0.61	1.12

From Lynn's data in **Table 9.1**, it appears that the 135-degree fixation is slightly softer than the 150-degree fixation over the load range from 0 to 1,350 N. The data from

Lynn's study does not show a significant difference in the two averages because of the high standard deviation of the samples; however, the average values do show the 150-degree fixation being stiffer. The finite element models show that there is a considerable difference in the overall stiffness between the 135- and 150-degree fixations.

Figures 6.4 and **6.5** indicate a sudden shift in the stiffness after approximately 800 N of force is applied. These plots suggest that sliding occurred in the 150-degree fixation, as evidenced by the sudden increase in stiffness. This higher stiffness is believed to be appropriate and is given in **Table 9.1** for comparison with the Lynn's data and the FE results.

Absolute Stiffness Values

It is important to compare the actual stiffnesses resulting from experimental and numerical results. Lynn's study used embalmed femurs which can not be compared to the fresh frozen femurs of the current study due to large differences in material properties. Fortunately, Karastinos' study, which included sixteen femurs, used fresh frozen femurs. Unfortunately, however, Karastinos' study used whole femurs whereas the femurs and models in the current study were cut at mid shaft. Also, only intact tests were done in Karastinos' study.

To compare the intact results of the current study to the intact results of Karastinos' study, a correction for the length of the femur must be used. Clearly, a longer bone will experience larger deformations than a shorter bone under the same loading. Since Karastinos' bone were approximately twice as long as the bones in the current study, it was assumed that the stiffnesses of Karastinos' bones would double if they were half as long.

Table 9.2 shows the overall intact stiffness results of the current study, the finite element study and Karastinos' study (modified for femur length.) **Table 9.2** shows that the current experimental and finite element results compare favorably.

Table 9.2 - Absolute stiffness values from the intact tests compared with Karastinos' intact results after modifying them for femur length.

Study Name	Intact Overall Stiffness (N/mm)
Experimental Results (this Study)	1293 +/- 70
Two-Dimensional Finite Element Results	1781
Three-Dimensional Finite Element Results	1517
Karastinos' results (modified for length)	1476 +/- 211

CHAPTER 10

CONCLUSIONS

The following conclusions can be drawn from the research presented in this thesis.

- The fixation device is designed to allow impaction of the femoral fragment against the femur during loading. Frictionless sliding of the screw through the bone and sideplate barrel is assumed, causing the fracture surface to bear the component of the external force that acts in the direction of the screw axis.

- Based on finite element analysis, the contact pressure on the fracture surface is carried below the screw and is concentrated in the cortical bone.

- A kinematic analysis of the fixation revealed that a hinge develops at the neutral axis of the screw, causing the contact forces to be confined to the fracture face below the screw.

- Due to the large mismatch in elastic constants of the cortical and cancellous bone materials and an assumed linear strain distribution below the neutral axis of the screw, the contact pressure can be approximated as a triangular shaped distributed load.

- The resultant of the triangular distributed loading induces a moment about the neutral axis of the screw that opposes the moment and stress induced by the component of the external load that acts normal to axis of the screw.

- The component of the external load which acts normal to the screw causes a bending moment and a tensile bending stress in the upper fiber of the screw.

- The analytical model shows that a lower screw angle carries a higher shearing force (a higher force which acts normal to the axis of the screw).

- A 150-degree screw is more likely to slide within the barrel of the sideplate than a 135-degree screw based on experimental data. The analytical results indicate that the cause of this locking in the lower angle screws is the higher shearing force acting normal to the axis of the screw.

- The peak stress in the screw occurs between the fracture surface and the barrel of the sideplate.

- The peak stress in the screw is a function of the installation of the screw on the fracture surface, with screws installed lower on the fracture face having less stress in the screw.

- Screws installed lower on the fracture face have higher compressive contact stress due to a smaller area over which the axial component of the external loading can be applied.

- As the screw installation position moves upward on the fracture, the peak stress in the screw moves toward the fracture surface.

- Experimentally determined stiffness values are strongly dependent on the quality of the fracture reduction.

- The results of the deflection measurements at LVDT II for intact and fixated femurs indicate that the installation of the sideplate does not affect the bending stiffness of the femoral shaft.

- CT based cortical thickness values are not accurate in all cases based on comparison between manual and digital measurements.

- Three new two-dimensional finite element models of the proximal half of a human femur incorporating element thickness values based on equivalent moments of inertia were developed.

- A new three-dimensional finite element model of the proximal half of a femur with five areas for material properties was developed. The cortical thickness of this model was based on physical measurements at 6 cross sections with 10 points of thickness measurements per cross section.

- The maximum stress in the screw occurs distal to the fracture plane in both the 135- and 150-degree finite element models.

- Experimental and two-dimensional finite element results indicate that a 150-degree fixation is stiffer than a 135-degree fixation.

CHAPTER 11

RECOMMENDATIONS

This chapter will list recommendations for future research based on the findings of the current study. The list will be broken down into three sections. The sections will cover the experimental, analytical and finite element aspects of this study. Recommendations will be made for improvements of the current models and for new directions to take the research.

Experimental Recommendations

The first recommendation for any experimental study would be the use of fresh frozen whole femurs. The embalming process has a significant effect on the material properties of bone and therefore the results of the experimental tests performed on the bone. Also, the femurs in this test were almost too short for the installation of the 150-degree fixation device. Use of the entire femur would not only allow for better placement of the 150-degree fixation device, but would provide a more anatomical deflection of the femur under loading.

Additionally, the muscle forces acting on the femur should be included in the study. The addition of muscle forces to the experimental setup would provide more realistic results. However, until the magnitude of these forces can be determined, it may

be better to leave them out of any studies. It will become necessary to add these muscle forces at some time, as their addition will affect the stress profile in the femur.

A better system for measuring displacement needs to be developed. LVDT's are accurate in their measurements, but they are limited to measurements along one axis and are very difficult to place on the irregular geometry of the femur. Possibly, a high-resolution digital video capture system could be employed to record the experimental tests. The images from the camera could be studied frame by frame to determine the deflection profile of the femur.

Stress and strain data from the experimental tests should be gathered. Strain gages could be placed on the fixation device and on the surface of the femur. Also, pressure sensitive film could be placed on the fracture surface to record area of contact on the fracture surface. This type of data could be compared with the finite element and analytical predictions.

Other variables should be explored as well. Variables such as the coefficient of friction on the fracture surface would be useful for tuning the numerical models. The fracture gap size and the angle between the fracture surfaces should be recorded. There needs to be some way to quantify the quality of the fracture reduction. By quantifying the reduction, the data should provide more accurate comparisons with numerical predictions.

Lastly, the position of the screw on the fracture plane along with the screw angle should be explored. This study indicated that as the screw was placed in different positions on the fracture plane the location and magnitude of the maximum stresses changed. The effect of the screw position should be studied experimentally to confirm the numerical predictions.

Analytical Recommendations

More complex analytical models that include the crushing of the cancellous bone beneath the screw should be implemented. Also, analytical models that predict the contact pressure on the fracture surface could be developed. The value of the spring constant, ko, should be more accurately determined. This value was used when modeling the screw as a beam on an elastic foundation.

Optimization of the screw angle and position should be explored using the analytical equations. The optimization could be based on reducing stress in the screw, maximizing the stiffness of the fixation and maximizing contact on the fracture surface.

Finite Element Model Recommendations

Sensitivity tests should be performed on the models to determine their response to change in parameters such as element thickness, cortical thickness and material properties such as modulus of elasticity. Also, several new two-dimensional models should be developed that place the screw at different positions along the fracture plane to verify the predictions of the analytical models.

The three-dimensional fixated models should be completed and tested. Also, the sensitivity of the three-dimensional models should be determined. In addition, the finite element models should be extended to include the entire femur. Muscle forces should be included in the finite element simulations as well.

Optimization of the screw angle and position should also be performed using the finite element models. Also, different fracture conditions should be explored such as non parallel fracture surfaces, larger degrees of communition and effect of a non-planar fracture surface.

Finally, a parametric model should be developed that would allow for the input of key variables such as the material properties of the cortical bone and cancellous bone, the angle and location of the fracture and several bone geometry dimensions. This type of model could be used to individualize the finite element results to a particular patient and an optimization routine could be performed based on these variables that would predict the optimum size, angle and location of the fixation device for an individual fracture.

APPENDIX A

MANUAL MEASUREMENTS OF CORTICAL THICKNESS

APPENDIX A

MANUAL MEASUREMENTS OF CORTICAL THICKNESS

The data gathered during the manual measurements of the cortical thicknesses will be presented in this Appendix. These measurements were taken in an effort to make the finite element models more realistic. The data was taken from six cross sections of a femur. Ten data points, or cortical thickness numbers, were taken per cross section. The locations of the six cross sections are shown in **Figure A.1**. The data from the cross sections are shown in **Tables A.1** through **A.6**.

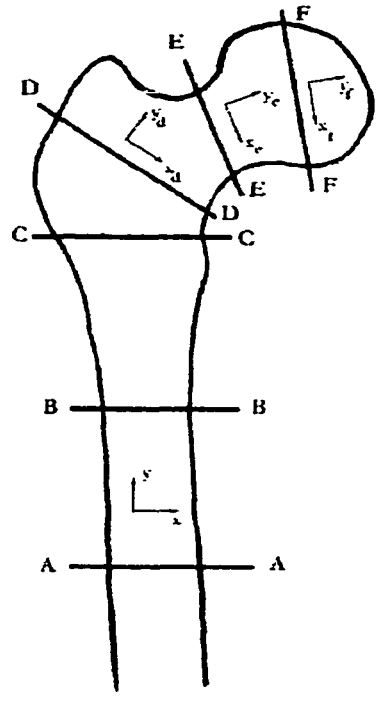

Figure A.1 - Locations of the cross sectional cuts, local coordinate systems shown.

Table A.1 - Cortical thickness data collected from section A-A.

Point Number	Thickness (64ths inch)	Point Number	Thickness (64ths inch)
1	12	**6**	17
2	13	**7**	15
3	18	**8**	18
4	16	**9**	17
5	17	**10**	14
6	17	**1**	12
Avg:	15.5	**Avg:**	15.5
Avg: (mm)	6.15	**Avg: (mm)**	6.15

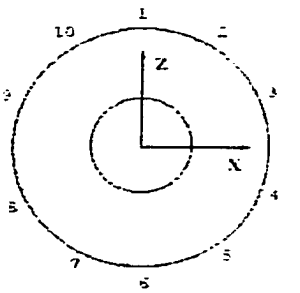

Table A.2 - Cortical thickness data collected from section B-B.

Point Number	Thickness (64ths inch)	Point Number	Thickness (64ths inch)
1	13	**6**	15
2	17	**7**	18
3	17	**8**	18
4	17	**9**	14
5	13	**10**	12
6	15	**1**	13
Avg:	15.3	**Avg:**	15
Avg: (mm)	6.07	**Avg: (mm)**	5.95

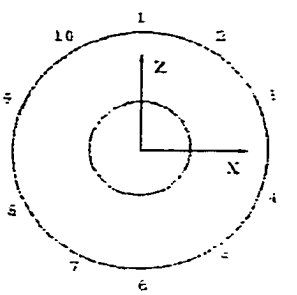

Table A.3 - Cortical thickness data collected from section C-C.

Point Number	Thickness (64ths inch)	Point Number	Thickness (64ths inch)
1	4	**6**	3
2	20	**7**	7
3	15	**8**	Na
4	8	**9**	10
5	3	**10**	8
6	3	**1**	4
Avg:	8.8	**Avg:**	6.4
Avg: (mm)	3.49	**Avg: (mm)**	2.54

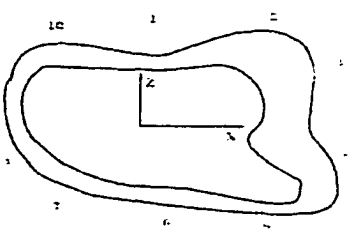

Table A.4 - Cortical thickness data collected from section D-D.

Point Number	Thickness (64ths inch)	Point Number	Thickness (64ths inch)
1	8	6	3
2	8	7	2
3	12	8	7
4	4	9	7
5	3	10	4
6	3	1	8
Avg:	6.3	Avg:	5.2
Avg: (mm)	2.5	Avg: (mm)	2.06

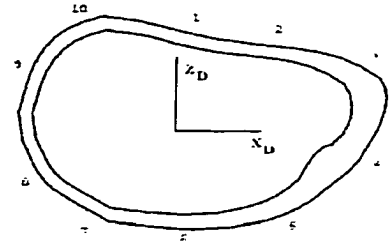

Table A.5 - Cortical thickness data collected from section E-E.

Point Number	Thickness (64ths inch)	Point Number	Thickness (64ths inch)
1	5	6	3
2	7	7	2
3	7	8	Na
4	8	9	4
5	6	10	4
6	3	1	5
Avg:	6	Avg:	3.6
Avg: (mm)	2.38	Avg: (mm)	1.43

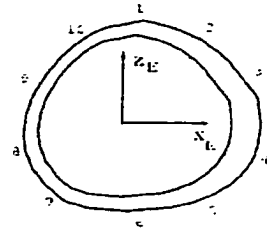

Table A.6 - Cortical thickness data collected from section F-F.

Point Number	Thickness (64ths inch)	Point Number	Thickness (64ths inch)
1	1	6	1
2	1	7	1
3	1	8	1
4	1	9	1
5	2	10	2
6	2	1	1
Avg:	1.3	Avg:	1.2
Avg: (mm)	0.52	Avg: (mm)	0.48

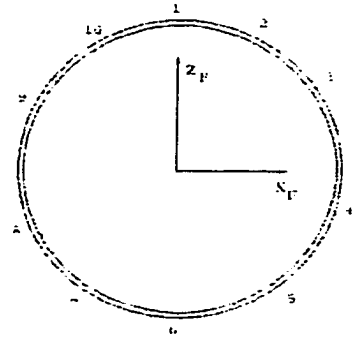

APPENDIX B

MATHCAD SOLUTIONS FOR ELEMENT THICKNESSES

APPENDIX B

MATHCAD SOLUTIONS FOR ELEMENT THICKNESSES

This section will contain the MathCad files used for calculating the element thicknesses at each of the six cross sections. These calculations are based on the assumption of an elliptical cross section. **Figure B.1** shows a reference diagram that depicts several of the measures used in the MathCad solutions.

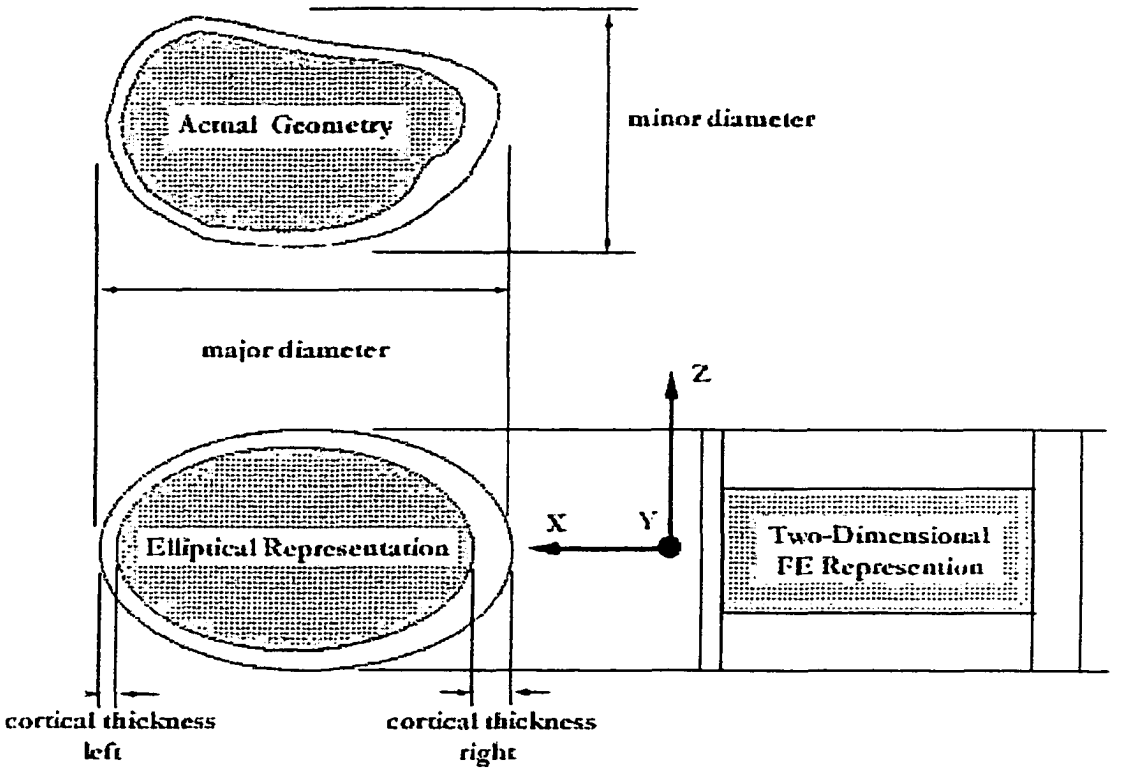

Figure B.1 - Reference diagram for the MathCad solutions for element thickness.

Section A-A, B-B and C-C

$rcortical := .0135 \cdot m$ radius of the cortical bone

$rcancellous := .00735 \cdot m$ radius of the cancellous bone

$Ishafta := \frac{\pi \cdot rcortical^4}{4}$ moments of inertia (based on circular cross sections)

$Ishaftb := \frac{\pi \cdot rcancellous^4}{4}$

$IshaftAA := Ishafta - Ishaftb$

$I2DAA := \frac{thicknessAA \cdot (2 \cdot rcortical)^3}{12}$ moment of inertia (based on rectangular cross sections)

$I2DAA := IshaftAA$

$thicknessAA := \frac{3}{2} \cdot \frac{I2DAA}{rcortical^3}$ equation for element thickness

$thicknessAA = 0.015 \cdot m$ element thickness at section AA

Section C-C, D-D and E-E

$o := 0.0035 \cdot m$

$n := 0.0025 \cdot m$

Average cortical thickness for the cross section, one on the left side and the other for the right side.

$a1 := 0.0123 \cdot m$ $\quad b1 := .0175 \cdot m$

$a2 := 0.0109 \cdot m$ $\quad b2 := .0145 \cdot m$

Definitions of major and minor diameters of the cortical and cancellous bone areas.

$Aouter := \pi \cdot a1 \cdot b1$

$Ainner := \pi \cdot a2 \cdot b2$

$yinner := b1 - (b2 + o)$

Calculation of the areas of the elliptical representaions of the outer and inner areas.
Y is the distance from the centroid of the inner area to the centroid of the whole.

$$Iouter := \frac{\pi \cdot a1 \cdot b1^3}{4}$$

Moment of inertia for the outer area.

$$Iinner := \frac{\pi \cdot a2 \cdot b2^3}{4} + Ainner \cdot yinner^2$$

Moment of inertia for the inner area.

$Icortical := (Iouter - Iinner)$

Moment of inertia for the cortical bone area.

$Icancellous := Iinner$

Moment of inertia for the cancellous bone.

$Icortical = 2.555 \cdot 10^{-8} \cdot m^4$

$Icancellous = 2.622 \cdot 10^{-8} \cdot m^4$

Section C-C, D-D and E-E Continued

$A1 = thicknesscortical \cdot o$

$A3 = thicknesscortical \cdot n$

$A2 = thicknesscancellous \cdot 2 \cdot b2$

Equations for the areas of the rectangular representations of the cortical and cancellous bones.

$$y1 := b1 - \frac{o}{2}$$

$$y3 := b1 - \frac{n}{2}$$

Distances between the centroid of the given areas and the centroid of the entire cross section.

$y2 := yinner$

$$Icortical2D = \frac{thicknesscortical \cdot n^3}{12} + A3 \cdot y3^2 + \left\{ \frac{thicknesscortical \cdot o^3}{12} + A1 \cdot y1^2 \right\}$$

Equations for the rectangular representation for the cortical bone.

$Icortical2D := Icortical$

$$thicknesscortical := \frac{-Icortical2D}{\left\{ \frac{-1}{12} \cdot n^3 - n \cdot y3^2 - \frac{1}{12} \cdot o^3 - o \cdot y1^2 \right\}}$$

$thicknesscortical = 0.017 \cdot m$

Equation for the cortical element thickness

$$Icancellous2D = \frac{thicknesscancellous \cdot h2^3}{12} + A2 \cdot y2^2$$

Equations for the rectangular representation of hte cancellous bone.

$Icancellous2D := Icancellous$

$$thicknesscancellous := \frac{-Icancellous2D}{\left[\frac{-1}{12} \cdot (2 \cdot b2)^3 - 2 \cdot b2 \cdot y2^2 \right]}$$

$thicknesscancellous = 0.013 \cdot m$

Equation for the cancellous element thickness

APPENDIX C

SAMPLES OF THE EXPERIMENTAL RESULTS

APPENDIX C

SAMPLES OF THE EXPERIMENTAL RESULTS

This section will contain some of the data collected during the experimental testing phase of the study. The data will be listed in **Tables C.1** through **C.3**. There will also be plots of the data shown in **Figures C.1** through **C.3**. The data listed here will be from one run of the intact femur, one run of the 135-degree fixation and one run of the 150-degree fixation.

Table C.1 - Experimental intact data.

Instron Displacement (mm)	Newtons	LVDT I (mm)	LVDT II (mm)
0	0	0	0
0.024	4.883	0	0.002
0.024	9.766	0	0.003
0.049	14.648	0	0.008
0.073	29.297	0	0.012
0.098	39.062	0	0.02
0.122	63.477	0	0.031
0.146	83.008	-0.003	0.045
0.146	107.422	-0.007	0.06
0.171	141.602	-0.012	0.079
0.195	170.898	-0.018	0.098
0.22	200.195	-0.023	0.118
0.244	224.609	-0.028	0.138
0.268	249.023	-0.032	0.155
0.293	263.672	-0.037	0.166
0.317	278.32	-0.038	0.177
0.317	297.852	-0.043	0.192
0.317	312.5	-0.048	0.208
0.366	346.68	-0.052	0.228
0.366	366.211	-0.057	0.251
0.391	400.391	-0.063	0.274
0.439	444.336	-0.071	0.303
0.415	473.633	-0.079	0.333

Table C.1 – Continued

0.439	507.812	-0.088	0.364
0.488	546.875	-0.097	0.398
0.488	581.055	-0.106	0.432
0.488	615.234	-0.116	0.469
0.537	649.414	-0.127	0.503
0.537	683.594	-0.137	0.542
0.586	727.539	-0.148	0.579
0.61	756.836	-0.161	0.619
0.635	791.016	-0.17	0.659
0.635	815.43	-0.182	0.7
0.684	854.492	-0.195	0.742
0.708	883.789	-0.207	0.783
0.708	913.086	-0.218	0.825
0.684	942.383	-0.232	0.867
0.708	971.68	-0.244	0.91
0.732	1005.859	-0.257	0.954
0.781	1040.039	-0.269	0.995
0.781	1069.336	-0.283	1.039
0.854	1113.281	-0.295	1.08
0.83	1137.695	-0.308	1.124
0.854	1176.758	-0.322	1.167
0.854	1206.055	-0.336	1.211
0.879	1245.117	-0.348	1.254
0.903	1279.297	-0.362	1.297
0.928	1318.359	-0.376	1.342
0.952	1352.539	-0.39	1.387

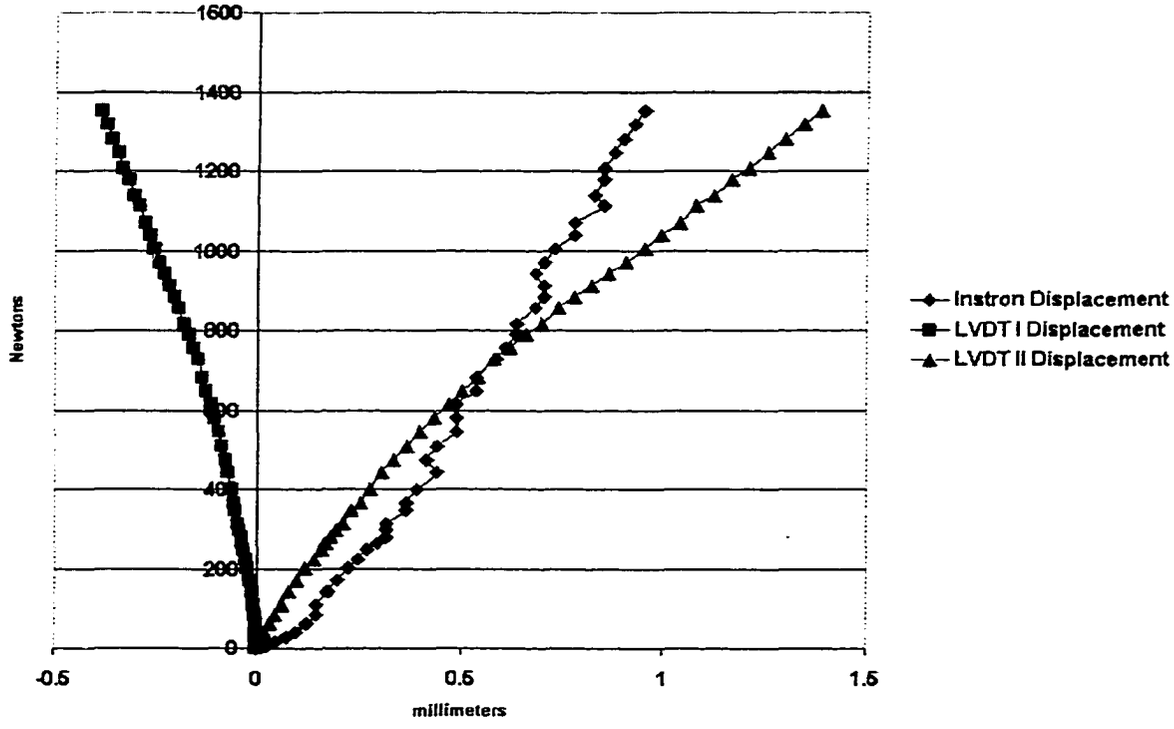

Figure C.1 - Intact data recorded during one of the experimental runs.

Table C.2 - Experimental 135-degree fixated data.

Instron Displacement (mm)	Newtons	LVDT I (mm)	LVDT II (mm)
0	0	0	0
0.024	4.883	0.002	0.002
0.049	14.648	0.002	0.003
0.049	24.414	0.002	0.008
0.073	39.062	0.003	0.014
0.097	53.711	0.003	0.022
0.122	73.242	0.003	0.031
0.146	92.773	0.005	0.042
0.171	117.187	0.006	0.053
0.195	136.719	0.009	0.068
0.195	161.133	0.011	0.081
0.219	185.547	0.014	0.095
0.244	205.078	0.017	0.108
0.268	229.492	0.02	0.119
0.293	244.141	0.02	0.133
0.317	253.906	0.022	0.143
0.342	258.789	0.022	0.147
0.342	268.555	0.022	0.158
0.366	283.203	0.026	0.166

Table C.2 - Continued

0.39	302.734	0.028	0.178
0.415	322.266	0.032	0.192
0.439	341.797	0.036	0.208
0.464	361.328	0.04	0.225
0.488	385.742	0.045	0.243
0.488	410.156	0.05	0.26
0.512	429.687	0.054	0.279
0.537	454.102	0.059	0.299
0.561	478.516	0.065	0.319
0.586	498.047	0.07	0.341
0.61	522.461	0.076	0.362
0.635	541.992	0.082	0.384
0.635	561.523	0.088	0.406
0.659	585.937	0.094	0.429
0.683	605.469	0.101	0.452
0.708	620.117	0.108	0.474
0.732	639.648	0.115	0.497
0.757	659.18	0.122	0.519
0.757	673.828	0.132	0.542
0.781	693.359	0.139	0.564
0.805	708.008	0.147	0.587
0.83	722.656	0.155	0.608
0.854	737.305	0.164	0.629
0.879	751.953	0.173	0.65
0.903	766.602	0.181	0.673
0.903	786.133	0.19	0.697
0.927	800.781	0.198	0.718
0.952	820.312	0.207	0.742
0.976	834.961	0.217	0.765
1.001	854.492	0.224	0.788
1.025	874.023	0.234	0.813
1.05	893.555	0.243	0.837
1.05	908.203	0.251	0.862
1.074	927.734	0.26	0.887
1.098	947.266	0.269	0.913
1.123	966.797	0.277	0.938
1.123	981.445	0.286	0.969
1.172	1005.85	0.293	0.991
1.196	1020.50	0.3	1.015
1.196	1040.03	0.31	1.042
1.22	1059.57	0.319	1.068
1.245	1074.21	0.328	1.094
1.269	1088.86	0.337	1.121
1.294	1103.51	0.345	1.147
1.318	1118.16	0.356	1.173

Table C.2 - Continued

1.318	1132.81	0.367	1.2
1.343	1147.46	0.376	1.226
1.367	1157.22	0.385	1.251
1.391	1171.87	0.398	1.276
1.416	1186.52	0.409	1.3
1.44	1196.28	0.419	1.325
1.465	1210.93	0.429	1.35
1.465	1220.70	0.44	1.375
1.489	1235.35	0.45	1.399
1.513	1245.11	0.463	1.423
1.538	1259.76	0.475	1.449
1.562	1269.53	0.486	1.474
1.587	1279.29	0.497	1.497
1.611	1289.06	0.508	1.522
1.611	1303.71	0.517	1.545
1.636	1313.47	0.528	1.568
1.66	1323.24	0.537	1.593
1.684	1333.00	0.549	1.618
1.709	1347.65	0.56	1.642
1.733	1357.42	0.57	1.667

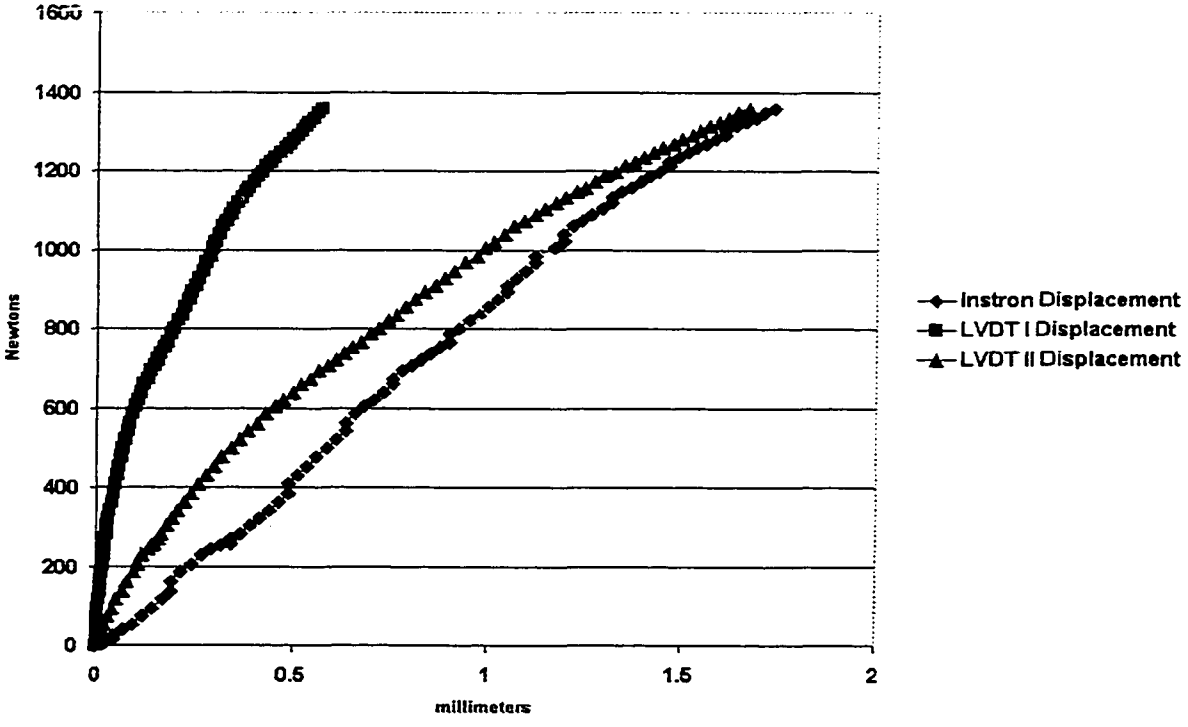

Figure C.2 - 135-degree fixation data recorded during one of the experimental runs.

Table C.3 - Experimental 150-degree fixated data.

Instron Displacement (mm)	Newtons	EXDET (mm)	EXDET (mm)
0	0	0	0
0.024	9.766	0.002	0.005
0.048	29.297	0.005	0.009
0.073	48.828	0.008	0.017
0.073	63.477	0.014	0.028
0.097	87.891	0.019	0.039
0.122	102.539	0.023	0.051
0.146	126.953	0.028	0.067
0.146	146.484	0.034	0.081
0.195	170.898	0.037	0.099
0.195	190.43	0.043	0.115
0.219	209.961	0.048	0.132
0.244	229.492	0.051	0.147
0.244	234.375	0.054	0.158
0.317	253.906	0.057	0.169
0.293	258.789	0.061	0.183
0.366	278.32	0.064	0.194
0.341	283.203	0.07	0.206
0.341	292.969	0.074	0.223
0.39	307.617	0.081	0.238
0.439	327.148	0.088	0.254
0.439	341.797	0.096	0.272
0.463	356.445	0.102	0.289
0.488	375.977	0.112	0.307
0.463	385.742	0.122	0.324
0.512	400.391	0.133	0.341
0.561	415.039	0.146	0.358
0.586	429.687	0.161	0.376
0.586	429.687	0.174	0.392
0.586	434.57	0.187	0.407
0.586	444.336	0.201	0.423
0.61	454.102	0.218	0.438
0.683	463.867	0.232	0.454
0.659	468.75	0.246	0.467
0.708	473.633	0.26	0.483
0.732	488.281	0.277	0.497
0.732	493.164	0.291	0.512
0.732	498.047	0.307	0.526
0.756	507.812	0.322	0.542
0.781	512.695	0.338	0.556
0.83	522.461	0.353	0.57
0.854	532.227	0.369	0.585
0.854	537.109	0.384	0.601
0.879	546.875	0.399	0.616

Table C.3 - Continued

0.903	551.758	0.415	0.63
0.903	561.523	0.43	0.644
0.976	576.172	0.446	0.659
0.976	581.055	0.461	0.673
1.025	595.703	0.477	0.689
1.001	590.82	0.491	0.704
1.025	605.469	0.505	0.72
1.025	610.352	0.52	0.735
1.049	620.117	0.537	0.751
1.123	634.766	0.553	0.765
1.123	639.648	0.57	0.779
1.123	649.414	0.584	0.794
1.147	659.18	0.599	0.81
1.147	668.945	0.613	0.825
1.171	683.594	0.63	0.842
1.196	698.242	0.641	0.859
1.22	712.891	0.653	0.876
1.245	727.539	0.664	0.893
1.269	751.953	0.675	0.913
1.342	781.25	0.684	0.932
1.294	795.898	0.695	0.952
1.318	820.312	0.703	0.974
1.367	844.727	0.714	0.994
1.367	864.258	0.723	1.014
1.44	888.672	0.732	1.034
1.416	903.32	0.742	1.057
1.464	927.734	0.751	1.077
1.464	947.266	0.762	1.099
1.513	971.68	0.771	1.121
1.513	991.211	0.78	1.142
1.562	1010.74	0.79	1.166
1.562	1030.27	0.8	1.189
1.562	1040.03	0.811	1.214
1.587	1069.33	0.821	1.238
1.635	1088.86	0.83	1.263
1.611	1103.51	0.839	1.289
1.66	1127.93	0.847	1.314
1.66	1137.69	0.856	1.339
1.684	1162.10	0.864	1.367
1.757	1186.52	0.872	1.393
1.709	1196.28	0.879	1.419
1.757	1225.58	0.887	1.447
1.782	1245.11	0.893	1.475
1.782	1259.76	0.898	1.501
1.855	1284.18	0.906	1.531

Table C.3 – Continued

1.831	1293.94	0.909	1.56
1.904	1318.35	0.915	1.59
1.88	1337.89	0.92	1.619
1.88	1347.65	0.924	1.648
1.88	1362.30	0.927	1.669

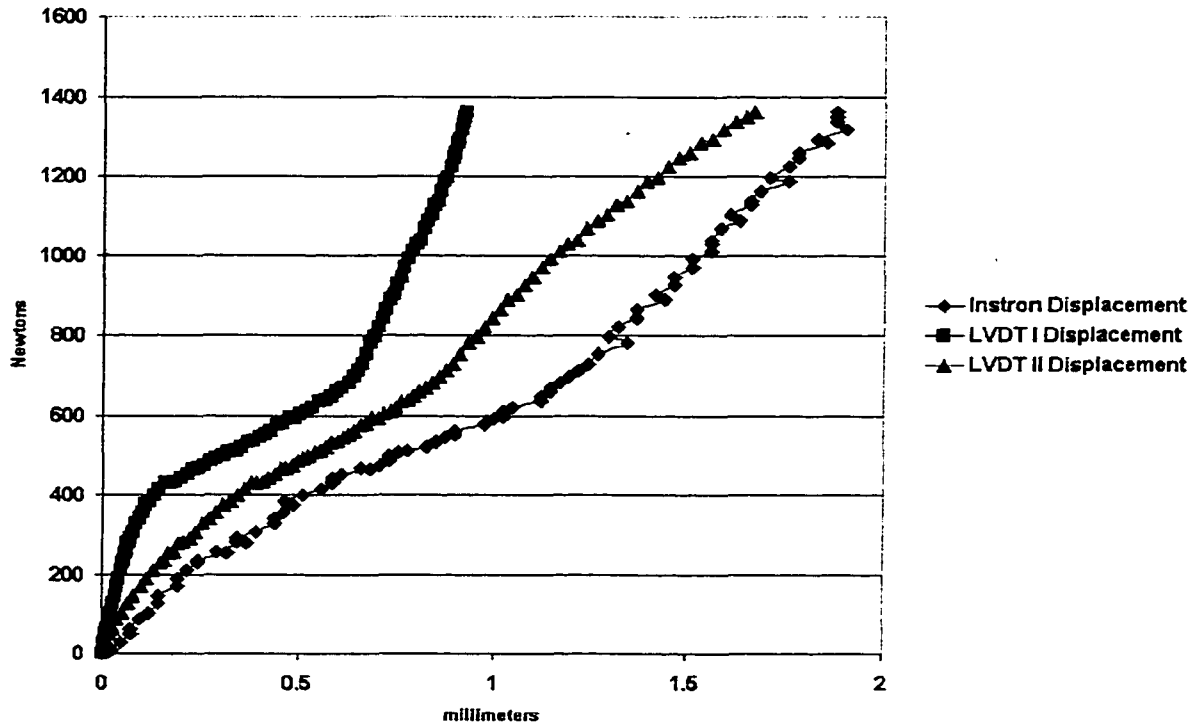

Figure C.3 - 150-degree fixation data recorded during one of the experimental runs.

APPENDIX D

MODELING THE SCREW AS A BEAM ON AN ELASTIC FOUNDATION

APPENDIX D

MODELING THE SCREW AS A BEAM ON AN ELASTIC FOUNDATION

Determination of ko from FEA analysis:

$disp := .65 \cdot mm \quad W := 1000 \cdot N \qquad bo := 5 \cdot mm$

$E := 300000000 Pa \qquad I := \frac{bo \cdot bo^3}{12}$

$\beta := \left(\frac{W}{2 \cdot E \cdot I \cdot disp}\right)^{\frac{1}{3}}$

$ko := \frac{\beta^4 \cdot 4 \cdot E \cdot I}{bo}$

$ko = 2.25541 \times 10^{11} \frac{kg}{m^2 s^2} \qquad \beta = 366.504\, m^{-1}$

Determination of β for the steel screw / bone combination:

$E := 190000000000 \cdot Pa \quad do := 7.22 \cdot mm \quad di := 3.28 \cdot mm$

$ko = 2.255 \times 10^{11} kg\, m^{-2} s^{-2} \qquad I := \frac{\pi}{64} \cdot \left(do^4 - di^4\right)$

$\beta := \left(\frac{do \cdot ko}{4 \cdot E \cdot I}\right)^{\frac{1}{4}}$

$\beta = 64.001\, m^{-1}$

Definition of the external force and the shear forces which cause bending:

$P := 1350 \cdot N$ **P is the externally applied loading to femur**

$V_{135} := P \cdot \sin\left(25 \cdot \frac{\pi}{180}\right) \qquad V_{150} := P \cdot \sin\left(10 \cdot \frac{\pi}{180}\right)$

$V_{135} = 570.535\, N \qquad V_{150} = 234.425\, N$

Determination of the Moment Arms for the Contact force, F, and the applied load, P:

$\theta_{135} := 25$ $\theta_{150} := 40$

$AC_{135}(x) := \frac{2}{3}\cdot x\cdot\cos\left(\theta_{135}\cdot\frac{\pi}{180}\right)$

$AC_{150}(x) := \frac{2}{3}\cdot x\cdot\cos\left(\theta_{150}\cdot\frac{\pi}{180}\right)$

$AB_{135}(x) := (x - 4.5\cdot mm)\cdot\cos\left(50\cdot\frac{\pi}{180}\right)$ $AB_{150}(x) := (x - 4.5\cdot mm)\cdot\cos\left(50\cdot\frac{\pi}{180}\right)$

$AC_{135}(9.47\cdot mm) = 5.722\times 10^{-3}\,m$ $AC_{150}(13.57\cdot mm) = 6.93\times 10^{-3}\,m$

$AB_{135}(9.47\cdot mm) = 3.195\times 10^{-3}\,m$ $AB_{150}(13.57\cdot mm) = 5.83\times 10^{-3}\,m$

Calculation of the concentrated moment applied to the screw at the fracture plane:

Sum Moments Around Point A (clockwise positive):

135 degrees

$F_{135}\cdot AC_{135}(x) + Mo_{135} - P\cdot AB_{135}(x) = 0$

$F_{135} := P\cdot\cos\left(25\cdot\frac{\pi}{180}\right)$

$M_{135}(x) := -F_{135}\cdot AC_{135}(x) + P\cdot AB_{135}(x)$

150 degrees

$F_{150}\cdot AC_{150} + Mo_{150} - P\cdot AB_{150} = 0$

$F_{150} := P\cdot\cos\left(10\cdot\frac{\pi}{180}\right)$

$M_{150}(x) := -F_{150}\cdot AC_{150}(x) + P\cdot AB_{150}(x)$

Computing the moment in the screw:

$M_{135total}(x,y,V) := M_{135}(x)\cdot e^{-\beta\cdot y}\cdot(\cos(\beta\cdot y) + \sin(\beta\cdot y)) + \frac{V}{\beta}\cdot e^{-\beta\cdot y}\cdot\sin(\beta\cdot y)$

$M_{150total}(x,y,V) := M_{150}(x)\cdot e^{-\beta\cdot y}\cdot(\cos(\beta\cdot y) + \sin(\beta\cdot y)) + \frac{V}{\beta}\cdot e^{-\beta\cdot y}\cdot\sin(\beta\cdot y)$

$y := 0\cdot mm, 0.25\cdot mm .. 35\cdot mm$

$$\frac{M_{135total}(35\cdot mm, y, V_{135})}{M_{150total}(35\cdot mm, y, V_{150})}$$

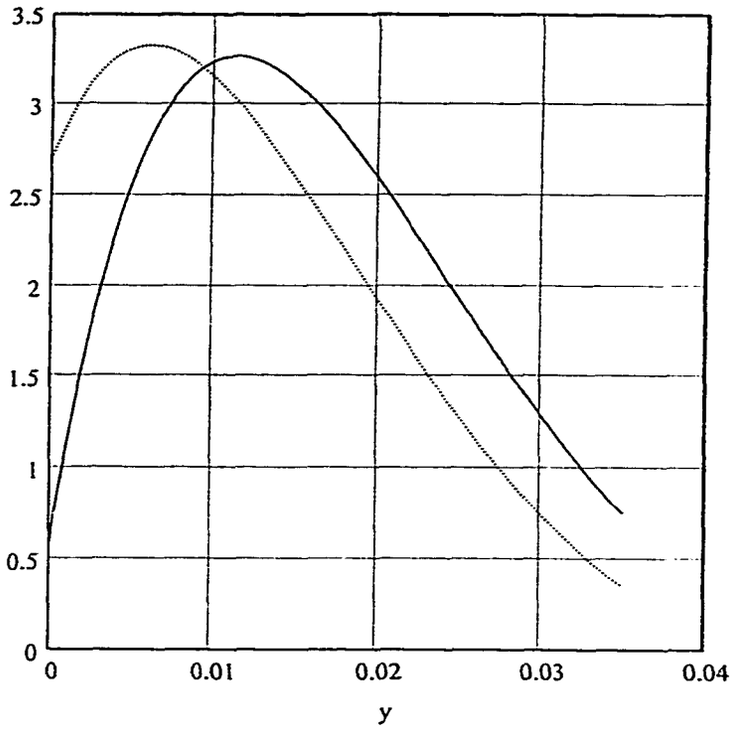

CALCULATION OF STRESSES:

135 degree screw:

$$\frac{M_{135total}(35\cdot mm, 11.3\cdot mm, V_{135})\cdot\frac{do}{2}}{I} = 9.239\times 10^{7}\,Pa$$

150 degree screw:

$$\frac{M_{150total}(35\cdot mm, 6.0\cdot mm, V_{135})\cdot\frac{do}{2}}{I} = 1.321\times 10^{8}\,Pa$$

$$x := \begin{pmatrix} 7 \\ 9 \\ 11 \\ 13 \\ 15 \\ 17 \\ 19 \\ 21 \\ 23 \\ 25 \\ 27 \\ 29 \\ 31 \\ 33 \\ 35 \end{pmatrix} \quad M135_{dist} := \begin{pmatrix} 19.8 \\ 18.8 \\ 18.0 \\ 17.3 \\ 16.5 \\ 16.0 \\ 15.3 \\ 14.8 \\ 14.0 \\ 13.5 \\ 13.0 \\ 12.5 \\ 12.3 \\ 11.8 \\ 11.3 \end{pmatrix} \cdot N \cdot m \quad M150_{dist} := \begin{pmatrix} 30.8 \\ 27.8 \\ 24.5 \\ 21.3 \\ 18.5 \\ 15.8 \\ 13.8 \\ 12.0 \\ 10.5 \\ 9.5 \\ 8.5 \\ 7.8 \\ 7.3 \\ 6.5 \\ 6.0 \end{pmatrix} \cdot N \cdot m$$

$$MaxStress_{135} := \begin{pmatrix} 3.774 \cdot 10^7 \\ 4.045 \times 10^7 \\ 4.337 \times 10^7 \\ 4.649 \times 10^7 \\ 4.98 \times 10^7 \\ 5.331 \times 10^7 \\ 5.701 \times 10^7 \\ 6.088 \times 10^7 \\ 6.492 \times 10^7 \\ 6.914 \times 10^7 \\ 7.351 \times 10^7 \\ 7.802 \times 10^7 \\ 8.268 \times 10^7 \\ 8.747 \times 10^7 \\ 9.239 \times 10^7 \end{pmatrix} \cdot Pa \quad MaxStress_{150} := \begin{pmatrix} 2.692 \times 10^7 \\ 3.349 \times 10^7 \\ 4.173 \times 10^7 \\ 5.066 \times 10^7 \\ 5.933 \times 10^7 \\ 6.783 \times 10^7 \\ 7.529 \times 10^7 \\ 8.233 \times 10^7 \\ 8.899 \times 10^7 \\ 9.583 \times 10^7 \\ 1.026 \times 10^8 \\ 1.098 \times 10^8 \\ 1.175 \times 10^8 \\ 1.244 \times 10^8 \\ 1.321 \times 10^8 \end{pmatrix} \cdot Pa$$

x = installation location along fracture face

M135dist = the distance (value of y) along the screw length
at which the moment of the 135 degree screw
is maximum

M150dist = the distance (value of y) along the screw length
at which the moment of the 135 degree screw
is maximum

MaxStress135 = maximum stress in screw for a given location of screw along the fracture face.

MaxStress150 = maximum stress in screw for a given location of screw along the fracture face.

PLOT OF MAXIMUM STRESS VERSUS SCREW INSTALLATION POSITION

$i := 0..11$

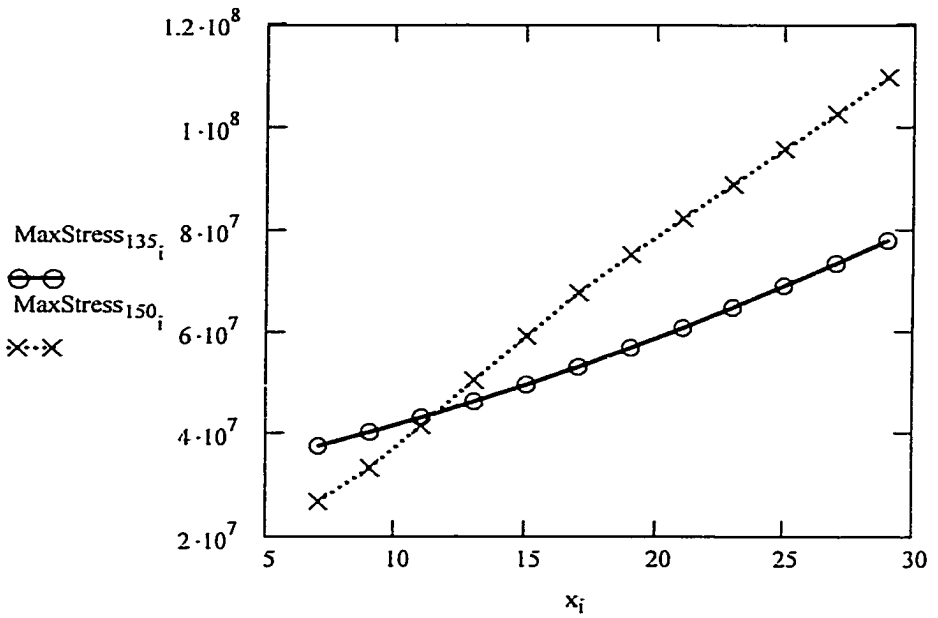

PLOT OF THE POSITION ALONG THE SCREW LENGTH AT WHICH THE PEAK STRESS OCCURS VERSUS THE SCREW INSTALLATION POSITION

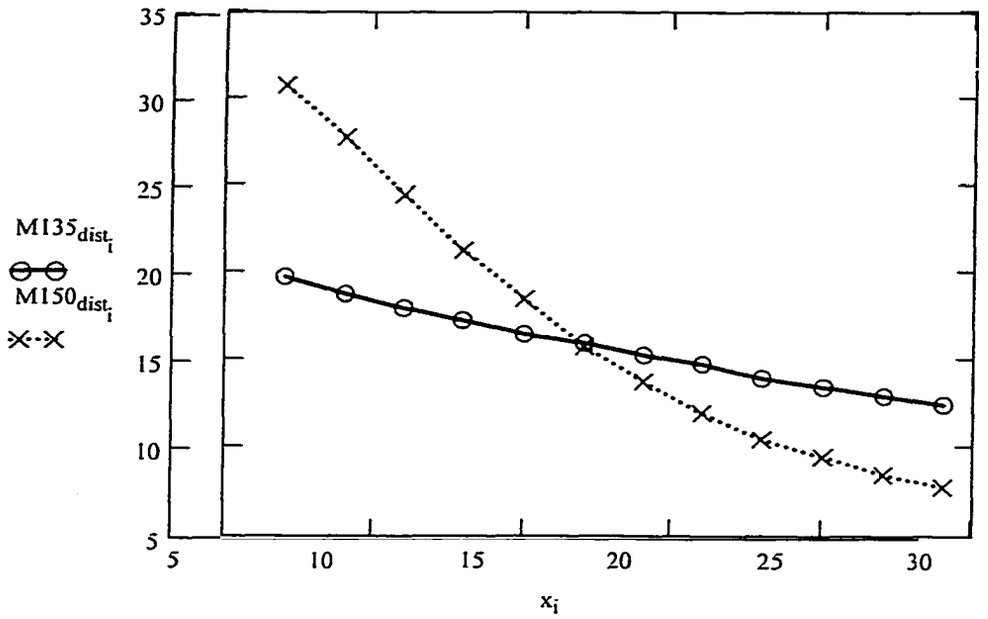

BIBLIOGRAPHY

1. **Albright, J.A.; Johnson, T.R.; Saha, S.** Principles of Internal Fixation. *Orthopedic Mechanics: Procedures and Devices.* Ghista, D.N., Roaf, R. editors. Academic Press, New York. 1978; 124-222.

2. **Bray, Timothy J.** Femoral Neck Fracture Fixation: Clinical Decision Making. *Clinical Orthopaedics and Related Research.* Lippincott-Raven Publishers. 1997; Number 339: 20-31.

3. **Boresi, Arthur P.; Schmidt, Richard J.; Sidebottom, Omar M.** Chapter 10: Beams on Elastic Foundations. "Advanced Mechanics of Materials." 5th edition, John Wiley and Sons, Inc. 1993; 404-424.

4. **Brekelmans, W.A.M.; Poort, H.W.; Sloof, T.J.J.H.;** A New Method to Analyze the Mechanical Behavior of Skeletal Parts. *Acta Orthopedica. Scandinavia.* 1972; Volume 43: 301-317.

5. **Carter, Dennis R.; Beaupre, Gary S.; Giori, Nicholas J.; Helms, Jill A.** Mechanobiology of Skeletal Regeneration. *Clinical Orthopaedics and Related Research.* Lippincott, Williams, and Wilkins 1998; Number 355S: S41-S55.

6. **Chapman, J.R.; Harrington, R.M.; Lee, K.M.; Anderson, P.A.; Tencer, A.F.; Kowalski, D.** Factors Affecting the Pullout Strength of Cancellous Bone Screws. *Journal of Biomechanical Engineering.* August 1996; Volume 118: 391-398.

7. **Chua, David; Jaglal, Susan B.; Schatzker, Joseph.** An Orthopedic Surgeon Survey on the Treatment of Displaced Femoral Neck Fracture: Opposing Views. *Canadian Journal of Surgery.* August 1997; Volume 40, Number 4: 271-277.

8. **Claes, L.E.; Heigele, C.A.; Neidlinger-Wilke, C.; Kaspar, D.;Seidl, W.; Margevicius, K.J.; Augat, P.** Effects of Mechanical Factors on the Fracture Healing Process. *Clinical Orthopaedics and Related Research.* 1998; Number 355S: S132-S147.

9. **Cristofolini, L.; Cappello, B.P.; McNamara, B.P.; Viceconti, M.** A Minimal Parametric Model of the Femur to Describe Axial Elastic Strain in Response to Loads. *Medical Engineering and Physics.* 1996; Volume 18, Number 6: 502-514.

10. **Cummings, S.R.; Rubin, S.M.; Black, D.** The Future of Hip Fractures in the United States: Numbers, Costs, and Potential Effects of Postmenopausal Estrogen. *Clinical Orthopedics.* 1990; Volume 252: 163-166.

11. **Davy, D.T.; Kotzar, G.M.; Brown, R.H.; Heiple, K.G.; Goldberg,** Telemetric Force Measurements Across the Hip After Total Hip Arthroplasty. *Journal of Bone and Joint Surgery.* 1988; Volume 70A: 45-50.

12. **Egol, Kenneth A.; Koval, Kenneth J.; Kummer, Frederick; Frankel, Victor H.** Stress Fractures of the Femoral Neck. *Clinical Orthopedics and Related Reasearch.* Lippencott-Raven Publications. 1998; Number 348: 72-78.

13. **Harty, Michael.** Anatomic Considerations. *Orthopedic Clinics of North America: Symposium on Surface Replacement Arthroplasty of the Hip.* October 1982; Volume 13, Number 4: 667-679.

14. **Hayes, W.C.; Snyder, B.; Levine, B.M.; Ramaswamy, S.** Stress-Morphology Reslationships in Trabecular Bone of the Patella. "Finite Elements in BioMechanics." Edited by Gallagher, R.H.; Simon, B.R.; Johnson, P.C.; Gross, J.F. John Wiley, NewYork. 1982; 223-268.

15. **Holmberg, S.; Kalen, R.; Thorngren, K.G.** Treatment and Outcome of Femoral Neck Fractures. *Clinical Orthopedics.* 1987; Volume 218: 42-52.

16. **Huiskes, R.; Janssen, J.D.; Sloof, T.J.** A Detailed Comparison of Experimental and theoretical Stress Analysis of a Human Femur. Mechanical Properties of Bone, Applied Mechanics Division, ASME. Editor: S.C. Cowin. New York, 1981; Volume 45: 211.

17. **Huiskes, R.; Garg, V.K.** On the Modelling of Long Bones in Structural Analysis. *Journal of Biomechanics.* 1982;Volume 15: 65-69.

18. **Huiskes, R.** Principles and Methods of Solid Biomechanics, Functional Behavior of Orthopedic Biomaterials. *Fundamentals in Structure-Property Relationships of Biomaterials.* Editor: D. F. Williams. Boca Raton, Florida: CRC Press. 1984; Volume 1: 51-97.

19. **Karastinos.** Unpublished Data. Resident Research. Louisiana State University Health Sciences Center. 2001.

20. **Kenwright, John; Gardner, Trevor.** Mechanical Influences on Tibial Fracture Healing. *Clinical Orthopaedics and Related Research.* Lippincott, Williams, and Wilkins 1998; Number 355S: S179-S190.

21. **Keyak, J.H.; Meagher, J.M.; Skinner, H.B.; Mote, C.D.** Automated Three-Dimensional Finite Element Modelling of Bone: A New Method. *Journal of Biomedical Engineering.* September 1990; Volume 12: 389-397.

22. **Keyak, J.H.; Fourkas, J.M.; Meagher, J.M.; Skinner, H.B.** Validation of an Automated Method of Three-Dimensional Finite Element Modelling of Bone. *Journal of Biomedical Engineering.* November 1993; Volume 15: 505-509.

23. **Koch, J.C.** The Laws of Bone Architecture. *American Journal of Anatomy.* 1917; Volume 21: 177-298.

24. **Kyle, R.F.; Wright, T.M.; Burstein, A.H.** Biomechanical Analysis of the Sliding Characteristics of Compression Hip Screw. *Journal of Bone and Joint Surgery.* December 1980; Volume 62-A, Number 8: 1308-1314.

25. **Lynn.** 14th Southern Bioengineering Conference. 1995.

26. **Merz, B.; Niederer, P.; Muller, R.; Ruegsegger, P.** Automated Finite Element Analysis of Excised Human Femora Based on Precision-QCT. *Journal of Biomechanical Engineering.* August 1996; Volume 118: 387-390.

27. **Meyer, H.** Die Architectur der Spongiosa. *Archiv F Anat Phys und Wissensch Medizin.* 1867; Volume 613: 615.

28. **Paul, J.P.** Forces Transmitted by Joints in the Human Body. *Proceedings of the Institution of Mechanical Engineers.* 1967; Volume 18: 8-15.

29. **Peacock, E.E.; Van Winkle, W. Jr.** "Surgery and Biology of Wound Repair." W.B. Saunders, Philadelphia, London and Toronto. 1970.

30. **Perren, S.M.; Cordey, J.; Baumgart, F.; Rahn, B.A.; Schatzker, J.** Technical and Biomechanical Aspects of Screws Used for Bone Surgery. *International Journal of Orthopedic Trauma.* 1992; Volume 2, Number 1: 31-48.

31. **Raaymakers, Ernst L.F.B.** Letter to the Editor: Hip Fracture. *The New England Journal of Medicine.* December 26, 1996; Volume 335, Number 26: 1996.

32. **Raftopoulos, D.D.; Qassem, W.** Three-Dimensional Curved Beam Stress Analysis of the Human Femur. *Journal of Biomedical Engineering.* October 1987; Volume 9: 356-366.

33. **Rhinelander, F.W.** Effects of Medullary Nailing on the Normal Blood Supply of the Diaphyseal Cortex. "A.A.O.S., Instructional Course Lectures." C.V. Mosby, St. Louis. 1973; Volume 16: 161.

34. **Rybicki, E.F.; Simonen, F.A.; Weis, E.B.** On the Mathematical Analysis of Stress in the Human Femur. *Journal of Biomechanics.* 1972; Volume 5: 203-215.

35. **Rybicki, E.F.; Simonen, F.A.** Mechanics of Oblique Fracture Fixation Using a Finite Element Model. *Journal of Biomechanics.* 1977; Volume 10: 141-148.

36. **Scholten, R.** Ueber die Berchnung der Mechanischen Beanspruchung in Knochenstrukturen Mittels fuer den Fluzeugbau entwickelter Rechenvarfahren. *Med. Othhop. Technik.* 1975, Volume 6: 130-138.

37. **Singh, M.; Nagrath, A.R.; Maini, P.S.** Changes in Trabecular Pattern of the Upper End of the Femur as an Index of Osteoporosis. *Journal of Bone and Joint Surgery.* 1970; Volume 52: 457-467.

38. **Taylor, M.E.; Tanner, K.E.; Freeman, M.A.R.; Yettram, A.L.** Stress and Strain Distribution within the Intact Femur: Compresion or Bending? *Medical Engineering and Physics.* 1996; Volume 18, Number 2: 122-131.

39. **Toridis, T.G.** Stress Analysis of the Femur. *Journal of Biomechanics.* 1969; Volume2: 163-174.

40. **Tronzo, R.G.** Hip Nails for All Occasions. *Orth. Clin. North America.* 1974; Volume 5: 479.

41. **UK National Osteoporosis Society.** Priorities for Prevention: Osteoporosis, a Decision Making Document for Diagnosis and Prevention. London: National Osteoporosis Society. 1994.

42. **Ullom-Minnich, P.** Prevention of Osteoporosis and Fractures. *American Family Physician.* 1999; Volume 60: 194-202.

43. **Wang, C.J.; Yettran, A.L.; Yao, M.S.; Procter, P.** Finite Element Analysis of a Gamma Nail within a Fractured Femur. *Medical Engineering and Physics.* 1998; Volume 20: 677-683.

44. **Weinrobe, M.; Stankewich, C.J.; Mueller, B.; Tencer, A.F.** Predicting the Mechanical Outcome of Femoral Neck Fractures Fixed with Cancellous Screws: An In Vivo Study. *Journal of Orthopaedic Trauma.* Lippincott-Raven Publishers, Philadelphia. 1998; Volume 12, Number 1: 27-37.

45. **Winkley, Geoff.** "Hip Fractures." http://www.emedicine.com/EMERG/topic198.htm. Scaletta, Tom editor.

46. **Wolff, J.** Uber die Innere Architectur der Knochen und ihre Bedeutung fur die Frage vom knochenwachtum. *Virchow's Arc F Path Anat u Phys.* 1870; Volume 50; 389.

47. **World Health Organisation Study Group.** Assessment of Fracture Risk and its Application to Screening for Postmenopausal Osteoporosis. Geneva: World Health Orginasation. Technical Report Number 843. 1994.

48. **Young, Warren C.** "Roark;s Formulas for Stress and Strain." 6th edition, McGraw-Hill, Inc. 1989.

49. **Zuckerman, Joseph D.** Current Concepts. *The New England Journal of Medicine.* June 1996; Volume 334, Number 23: 1519-1525.

50. **Zuckerman, Joseph D.; Rosenberg, Andrew D.** Letter to the Editor: Hip Fracture. *The New England Journal of Medicine.* December 26, 1996; Volume 335, Number 26: 1996.